N68-19240

TR-101-2

DESIGN OF STRAPDOWN GYROSCOPES FOR A DYNAMIC ENVIRONMENT

INTERIM SCIENTIFIC REPORT

15 January 1968

by Arthur Gelb and Arthur A. Sutherland, Jr.

Prepared under Contract No. NAS12-508 by

THE ANALYTIC SCIENCES CORPORATION
7 Lowell Avenue
Winchester, Massachusetts 01890

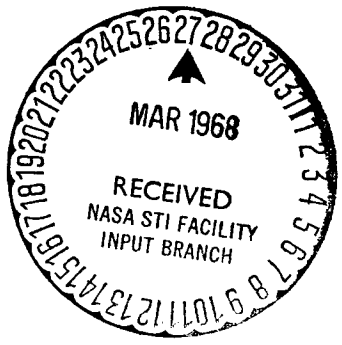

Electronics Research Center
NATIONAL AERONAUTICS AND SPACE ADMINISTRATION
Cambridge, Massachusetts

FOREWORD

It has been stated (Ref. 20) that the major obstacle to the realization of practical gimballess inertial reference equipment is the lack of inertial instruments specifically designed for this application. This report is directed to the design of single-degree-of-freedom integrating gyros and associated torquing loop parameters, specifically for the strapdown application. It contains the results of preliminary studies conducted to ascertain the basis for parameter design trade-offs in single-degree-of-freedom gyros for use in strapdown inertial reference systems.

This document is an Interim Scientific Report of research by The Analytic Sciences Corporation for Electronics Research Center, Cambridge, Massachusetts, under contract NAS 12-508. The work was performed by Drs. Arthur Gelb and Arthur A. Sutherland, Jr. of The Analytic Sciences Corporation. Prof. Wallace E. Vander Velde, M.I.T. Department of Aeronautics and Astronautics, consulted during the program.

ABSTRACT

A detailed error model is presented for the single-degree-of-freedom integrating gyro and the possibility of environmental vibrations generating sizeable constant drift rates in this instrument is demonstrated. A figure-of-merit relating gyro errors to the orientation error of the strapdown inertial reference system, independent of the transformation computations, is presented. An equation describing the behavior of this quantity as a function of the gyro histories is developed and exercised. Minimization of this figure-of-merit is a rational basis for the design of strapdown gyros.

The question of error compensation is treated, based on the use of information derived from the gyros under consideration, as well as from additional sensors. In this connection, a scheme for gyro monitoring is advanced. Two simplified strapdown gyro design examples are presented, in which the binary torqued rebalance loop is characterized using a quasi-linearization description and random vibrational motions are described through a simple approximation. In minimizing the figure-of-merit, the optimized gyro designs are shown to be mission (i.e., environment) dependent.

TABLE OF CONTENTS

TABLE OF CONTENTS (Cont.)

TABLE OF CONTENTS (Cont.)

SUMMARY

Strapdown inertial measurement units, in which the sensors are rigidly attached to the vehicle, offer many potential advantages over their gimballed counterparts. These include: less weight, lower power consumption, more flexible packaging, easier assembly and maintenance, as well as lower cost and improved reliability. On the other hand, in the strapdown system a greater burden is placed on the sensors and computational facilities. This report is oriented towards a major aspect of the sensor problem – reduction of strapdown system errors caused by gyros.

As a result of body mounting, vehicle rotational motions are transmitted directly to the gyros, forcing consideration of many error terms which are of little relative importance when stabilized platforms are used. The gyro float rebalance loop and coordinate transformation calculation required in strapdown systems also provide mechanisms for the generation of important gyro-caused system errors. All of these errors must be considered in the course of developing high accuracy strapdown inertial reference systems.

One question that arises is "What gyro and loop parameters are at the disposal of the designer, and how should they be chosen to optimize the performance of the single-degree-of-freedom integrating gyro subsystem?" These parameters include: damping coefficient, rotor and gimbal moments of inertia, rotor speed, maximum driving torque, loop sampling frequency, nonlinearity dead-band, and so on. They are not necessarily free for independent choice. Further, the error measure to be used in choosing these parameters is a matter which has not been adequately treated. In addition, the possibility for active compensation of gyro errors bears heavily on the best choice of gyro design parameters.

In addressing the problem of strapdown gyro design, this report first provides a comprehensive review of the most important single-degree-of-freedom strapdown gyro error sources. It is demonstrated that errors caused by the strapdown rotational environment can be considerably larger than those of principal interest when gimballed platforms are used. Continuous torqued, linear rebalance loops are discussed, and torquing error and loop bandwidth calculations are made. Binary and ternary pulse torqued rebalance loops are also treated, with torquing error, limit cycle behavior and loop bandwidth receiving special attention. It is shown that torquer dynamic characteristics, as well as static characteristics, need be carefully specified in an optimized gyro. In particular, for the binary-torqued rebalance loop studied, gyro bandwidth varies inversely as the square-root of the torquer time constant.

With the goal of optimizing gyro parameter design in mind, a connection is established between system errors and gyro loop errors. This figure-of-merit relates the performance of gyros to the accuracy of a strapdown inertial reference system, independent of the details of the transformation computation, thereby providing a generalized measure of the effectiveness of strapdown gyros. It allows the calculation of system attitude error build-up by direct manipulation of time series of gyro errors and vehicle motions without requiring a simulation of the transformation matrix calculations. Minimization of this figure-of-merit is one rational basis for the design of strapdown gyros.

Several schemes for compensating motion-induced gyro errors are considered, including: self-compensation through the use of the three gyro outputs, use of special angular motion sensors, a new form of gyro monitoring, and gyro rebalance loop dynamic compensation, with the advantages and disadvantages of each technique discussed. The rebalance loop limit cycle is shown to be a potential source of large error, and removal of limit cycles

from the output of pulse torqued gyros is treated. Using approximations developed during the course of the Phase I effort, two design examples are presented. They illustrate an approach to the determination of the optimum set of single-degree-of-feeedom gyro physical parameters. In addition, they permit evaluation of the effects of various compensation schemes on the optimum choice of parameters.

Foremost among the conclusions drawn in this report is that a practical limit exists on the error reduction obtainable solely through gyro parameter manipulation; active compensation, using external sensors and/or information available in the strapdown gyro triad, appears necessary for most missions. Thus, active error compensation must be considered integral to the strapdown single-degree-of-freedom gyro design problem, with such compensation chosen to favor those errors which cannot be reduced by gyro parameter manipulation. An equally important conclusion is that the presence of motion-induced errors precludes use of the static testing procedures common for platform gyros. Strapdown gyros must be subjected to dynamic testing.

1. INTRODUCTION

1.1 GYROSCOPES

Gyroscopes are angular motion sensors. They are commonly based on the use of a spinning member, the rotor, as the sensing element.* All gyroscopes can be classified under two major groups: single-degree-of-freedom gyros and two-degree-of-freedom gyros. The two-degree-of-freedom gyro senses angular motion directly, by measuring the displacement of the rotor spin axis relative to the case. The rotor may be mounted in mechanical gimbals, or may be supported by electric or magnetic fields as in the electrostatically suspended vacuum gyro and cryogenic gyro.

In the case of the single-degree-of-freedom gyro the spinning rotor is mounted in a gimbal which allows it only one degree-of-freedom relative to the case. See Fig. 1.1-1. The equation of motion of an "ideal" single-degree-of-freedom gyro can be determined by equating reaction torques about the output axis to the "applied" gyroscopic precession torque which results from case motion about the input axis, viz:

$$I_{oo} \ddot{\alpha}_o + C \dot{\alpha}_o + K \alpha_o = H \omega_i \qquad (1.1\text{-}1)$$

where

α_o = gimbal-to-case angle about the output axis

I_{oo} = rotor plus gimbal moment of inertia (dyne-cm/rad/sec^2)

*Notable exceptions are the laser gyro and tuning fork gyro, among others.

C = viscous damping coefficient (dyne-cm/rad/sec)

K = spring constant (dyne-cm/rad)

H = rotor angular momentum

ω_i = angular rate of the case about input axis

As indicated by Eq. (1.1-1), in the absence of motion about other axes, a constant value of ω_i results in the following steady-state value of α_o:

$$\alpha_o = \frac{H}{K} \omega_i$$

Hence, this gyro is referred to as a rate gyro, as the gimbal angle is a direct measure of case rate. In the situation where K = 0, we get a steady-state gimbal angle rate,

$$\dot{\alpha}_o = \frac{H}{C} \omega_i$$

Thus, gimbal angle is related directly to the integral of the input rate, and this gyro is therefore called a rate integrating gyro. By mounting the gyro rotor in an enclosure which serves as the gimbal and floating the whole assembly in a fluid of appropriate density, the gyro output axis bearings are unloaded and thus some uncertainty torques are minimized. This configuration, called the floated rate integrating gyro, is extensively used for very high accuracy applications such as inertial navigation.

In gimballed platform applications, the gyro float angle, α_o, is continuously nulled by platform gimbal servo action. In strapdown system applications, the gyro float angle is nulled by the application of a torque generated by passing an electric current through the windings of an output axis torquer. The current, which may be continuous (analog) or a series of pulses (digital), is derived from a measurement of the float angle. The closed loop comprised of float dynamics, float angle pick-off, torquing electronics

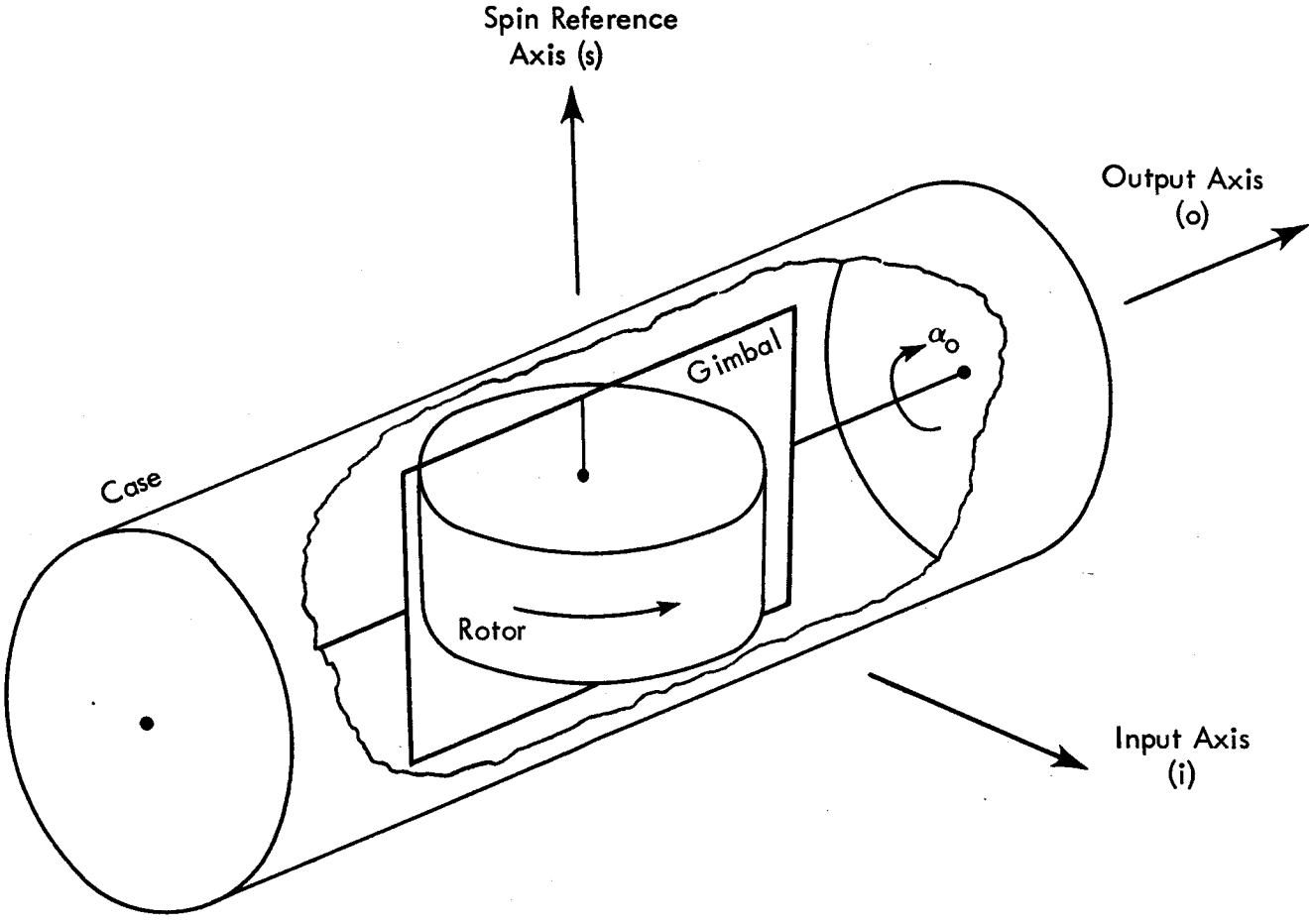

Figure 1.1-1. Single-Degree-of-Freedom Gyro

and output axis torquer is called the rebalance loop. The rebalance current is taken as a measure of input rate (for continuous torqued gyros) or incremental input angle (for pulse torqued gyros). Figure 1.1-2 shows a general schematic diagram of a strapdown gyro rebalance loop.

1.2 STRAPDOWN GYRO DESIGN

Strapdown single-degree-of-freedom gyros display many different kinds of errors. There are those which would be found in a gimballed system application, where the gyro is isolated from vehicle rotational motions. But there also exists a whole new class of errors specifically due to the interaction of the strapdown gyro with its rotational environment, as well as others due to both the rebalance loop mechanization and the computational process which operates on the gyro output signals. To draw proper conclusions relative to strapdown gyro design, it is necessary to realize that certain kinds of gyro errors will be more important than others, as their effects are viewed in the strapdown system output error. What is needed is a system level performance measure for the gyro-originated errors. Furthermore, the possibilities for error compensation should be accounted for in the design of strapdown gyros, so that gyro design parameters can be chosen to favor those errors which cannot be well compensated. Elements of the design problem are illustrated in Fig. 1.2-1.

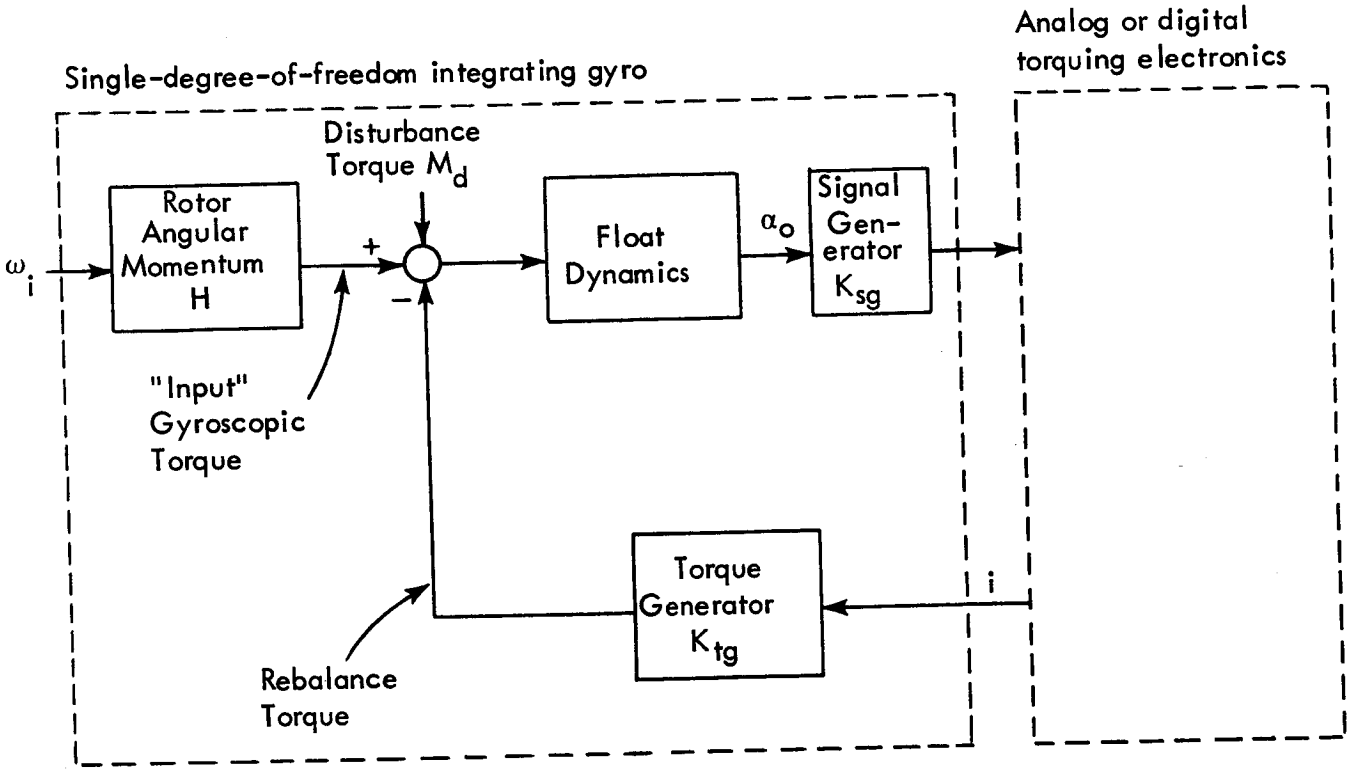

Figure 1.1-2. Strapdown Gyro Rebalance Loop Schematic.

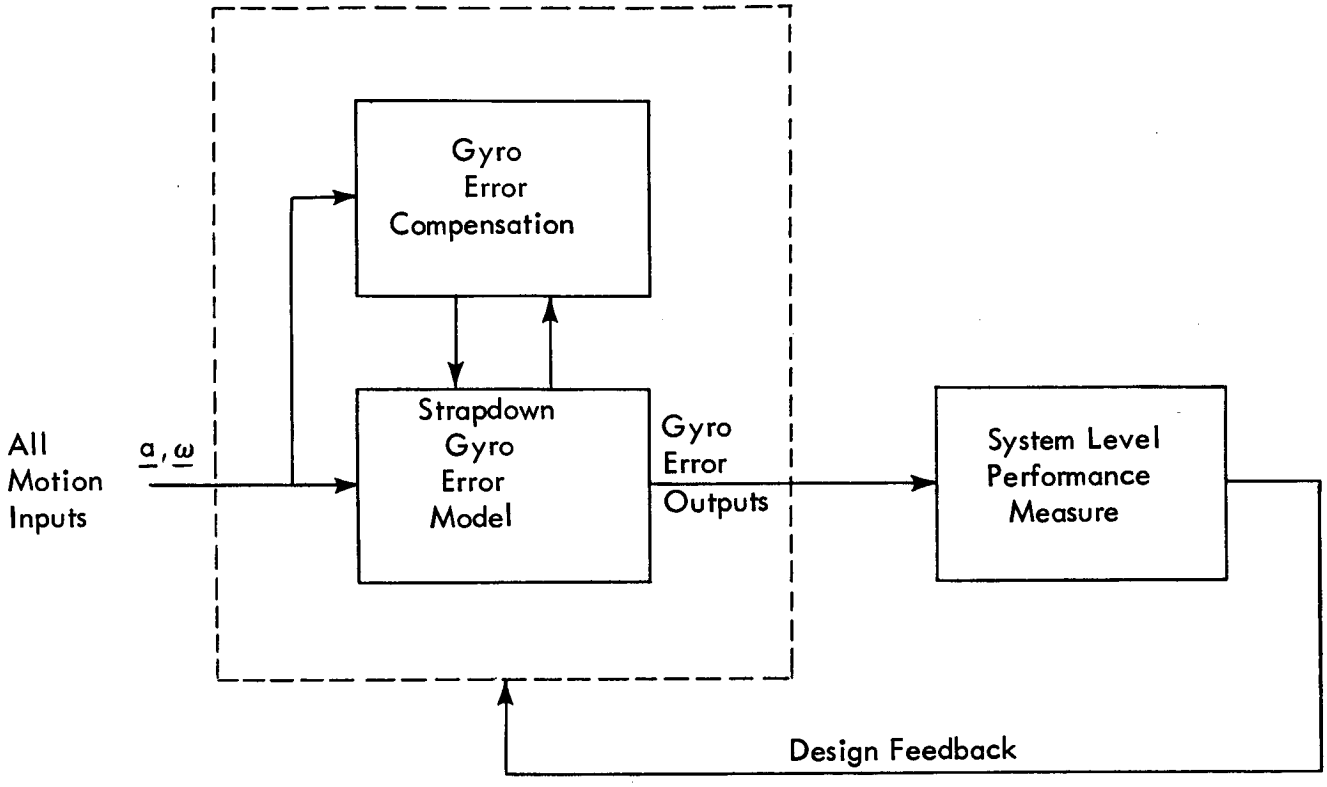

Figure 1.2-1 Strapdown Gyro Design Problem

2. STRAPDOWN SINGLE-DEGREE-OF-FREEDOM GYRO ERROR MODEL

2.1 GYRO ERROR MODEL

Gyro drift rate results from unwanted torques on the float. For reference purposes the various types of torques are displayed in Fig. 2.1-1. The nomenclature used in this figure as well as in subsequent sections is presented below. In each case the subscripts o, i, s refer to output, input and spin axes, respectively.

a_o, a_i, a_s = case linear accelerations

$\omega_o, \omega_i, \omega_s$ = case angular rates

$\dot{\omega}_o, \dot{\omega}_i, \dot{\omega}_s$ = case angular accelerations

$\alpha_o, \alpha_i, \alpha_s$ = gimbal-to-case angular misalignments

β_o, β_i = rotor-to-gimbal angular misalignments

I_{oo}, I_{ii}, I_{ss} = float moments of inertia (including gimbal and rotor components)

$I_{oo_r}, I_{ii_r}, I_{ss_r}$ = rotor moments of inertia

$I_{os_g}, I_{oi_g}, I_{si_g}$ = gimbal products of inertia

Ω_s = rotor spin rate relative to the gimbal

$H = I_{ss_r} \Omega_s$

We now proceed to a discussion of the various torques and their origins.

2.2 ANGULAR MOTION TORQUES

The torques due to rigid body rotational motion are derived in Appendix A, the result of which is presented below for convenience:

$$
\begin{aligned}
[\underline{M}_f]_{o'} = {} & I_{oo}(\ddot{\alpha}_o + \dot{\omega}_o) + (I_{ii} - I_{ss})\omega_s\omega_i - H\omega_i \\
& + I_{os_g}[\dot{\omega}_s - \omega_o\omega_i] \\
& + I_{oi_g}[\dot{\omega}_i + \omega_o\omega_s] \\
& + I_{si_g}[\omega_s^2 - \omega_i^2] \\
& + \alpha_o[(I_{ss} - I_{ii})(\omega_s^2 - \omega_i^2) + H\omega_s] \\
& + \alpha_s[-(I_{ss} - I_{ii})\omega_o\omega_s - H\omega_o - I_{oo}\dot{\omega}_i] \\
& + \alpha_i[(I_{ss} - I_{ii})\omega_o\omega_i + I_{oo}\dot{\omega}_s] \\
& + \beta_o[(I_{ss_r} - I_{ii_r})(\omega_s^2 - \omega_i^2) + H\omega_s] \\
& + \beta_i[(I_{ss_r} - I_{oo_r})(-\dot{\omega}_s + \omega_o\omega_i) - I_{ss_r}\dot{\Omega}_s] \qquad (2.2\text{-}1)
\end{aligned}
$$

In the strapdown system mechanization, gyro float angle off null is interpreted in terms of case motion about the input axis. Thus, terms other than $-H\omega_i$ on the right hand side of Eq. (2.2-1) must be regarded as error torques. The first term, $I_{oo}\ddot{\alpha}_o$, is the inertial reaction corresponding to gimbal-to-case angular acceleration. In combination with float viscous damping torque, $C\dot{\alpha}_o$, it is responsible for the basic gyro time constant, and appears in the "ideal" gyro model of Eq. (1.1-1). Other entries, such as rebalance loop applied torque and random error torques, complete the description of float torques.

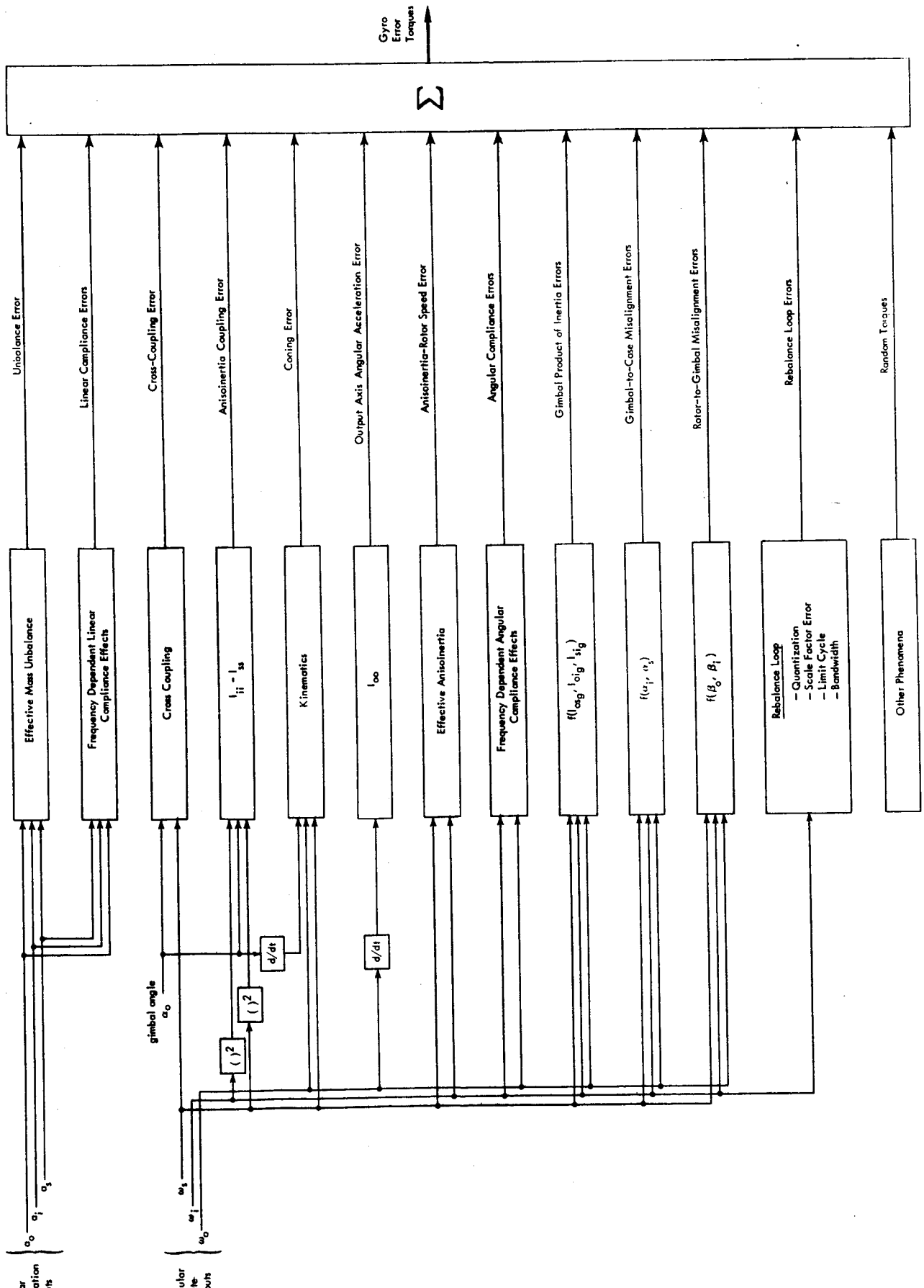

Figure 2.1-1. Strapdown Single-Degree-of-Freedom Gyro Error Torques

2.2.1 Output Axis Acceleration

This term results from case motion about the output axis. It is given by

$$\begin{matrix}\text{output axis angular} \\ \text{acceleration torque}\end{matrix} = I_{oo}\dot{\omega}_o \qquad (2.2\text{-}2)$$

and is one of the larger error contributors in strapdown system mechanizations (see Sec. 3.3). Several schemes for compensation of this error are discussed in Chapter 4.

2.2.2 Cross-Coupling

Cross-coupling error torques are due to float angles off null. The cross-coupling terms in Eq. (2.2-1) are:

$$\begin{matrix}\text{cross-coupling} \\ \text{torques}\end{matrix} = \alpha_o[(I_{ss}-I_{ii})(\omega_s^2-\omega_i^2)+H\omega_s] \qquad (2.2\text{-}3)$$

The first term is commonly called anisoinertia coupling. The second term is often referred to as cross-coupling, and results from a portion of the case rate about the spin reference axis being applied along the actual gimbal input axis.

It is easily demonstrated that the cross-coupling term can result in a rectified gyro float torque. Consider the following case input rates:

$$\begin{aligned}\omega_i &= W_i \sin wt \\ \omega_o &= W_i \sin (wt + \gamma_o) \\ \omega_s &= W_s \sin (wt + \gamma_s)\end{aligned} \qquad (2.2\text{-}4)$$

Presuming that the dominant torques acting on the float are given by

$$\begin{matrix}\text{dominant} \\ \text{float torques}\end{matrix} \cong I_{oo}\dot{\omega}_o - H\omega_i$$

it can be seen that for a linear, continuous rebalance loop the steady-state float angle response can (approximately) be expressed as a combination of sinusoids, each at frequency w. Thus, writing the float angle as the linear rebalance loop response to the dominant float torques yields

$$\alpha_o(t) \cong W_i L_1(w) \sin(wt + \lambda_1(w)) + w\, W_o L_2(w) \sin(wt + \lambda_2(w)) \qquad (2.2\text{-}5)$$

where

$$L_1(w) = \frac{H}{\sqrt{(K_{sg}K_{tg}K_1 - I_{oo}w^2)^2 + (Cw)^2}}$$

$$\lambda_1(w) = -\tan^{-1}\frac{Cw}{K_{sg}K_{tg}K_1 - I_{oo}w^2}$$

and

$$L_2(w) = \frac{I_{oo}}{H} L_1(w)$$

$$\lambda_2(w) = \lambda_1(w) + \frac{\pi}{2}$$

and K_1 represents the gain of linear torquing electronics in Fig. 1.1-2.

The second term in Eq. (2.2-5), proportional to w, is the float response to output axis angular acceleration. From Eqs. (2.2-5) and (2.2-3) it can be seen that the cross-coupling term results in a non-zero average value

(i. e. , rectified) torque. It is given by

$$\begin{matrix}\text{average cross-}\\ \text{coupling torque}\end{matrix} = \frac{HW_s}{2}\left[W_i L_1(w)\cos\left(\lambda_1(w)-\gamma_s\right] + w\, W_o L_2(w)\cos\left(\lambda_2(w)-\gamma_s\right)\right]$$

The first term in this equation is called spin-output rectification, and the second is called spin-input rectification.

2. 2. 3 Anisoinertia-Rotor Speed Loop

Conventionally, the anisoinertia torque has been taken as the term $(I_{ii}-I_{ss})\,\omega_s\omega_i$ appearing in Eq. (2. 2-1). But proper consideration of this term requires simultaneous treatment of rotor speed errors. This is shown in the following.

The rotor is driven by a hysteresis synchronous motor. When rotating in synchronism, the torque applied to the rotor is proportional to the phase difference between the rotor and the rotating field. This leads to the simplified rotor speed error model illustrated in Fig. 2. 2-1, where ω_s is the input and $\delta\Omega$ is the output. In Laplace transform notation, we get (friction and windage torques, which are relatively small, are neglected):

$$\delta\Omega(s) = -\frac{s^2}{s^2 + K_h/I_{ss_r}}\,\omega_s(s) \qquad (2.2\text{-}6)$$

Considering the "ideal" gyroscopic torque to be $-H\omega_i$, or, equivalently, $-I_{ss}\,\Omega_s\omega_i$, it can be seen that a rotor speed error leads to the following error torque:

$$\begin{matrix}\text{rotor speed}\\ \text{error torque}\end{matrix} = -\,I_{ss_r}\,\delta\Omega\,\omega_i$$

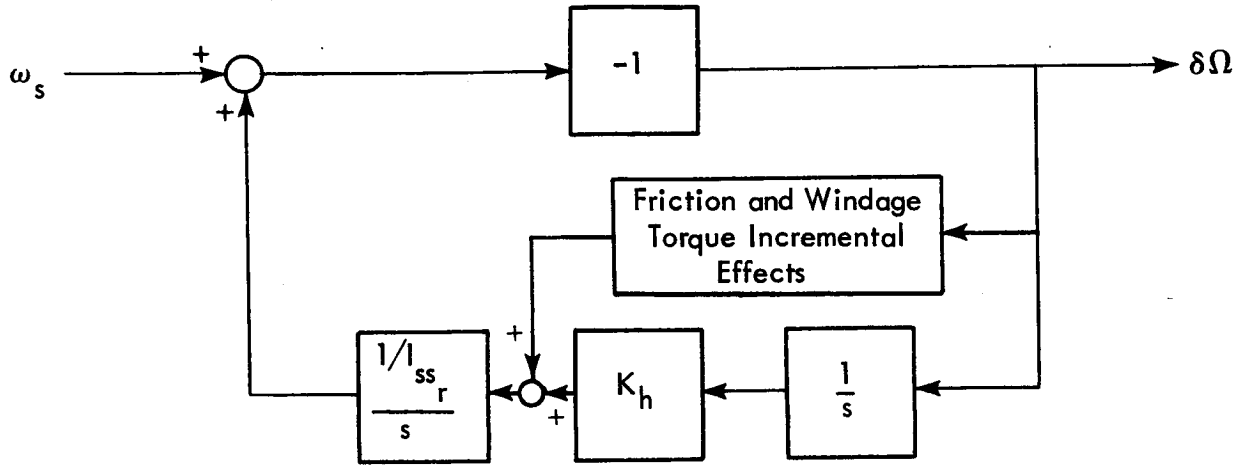

ω_s = angular velocity of case about spin reference axis

$\delta\Omega$ = change in rotor speed relative to the gimbal

K_h = torque constant (hysteresis synchronous motor), dyne-cm/rad

Figure 2.2-1. Error Model of Rotor Speed Control Loop.

Thus, the effective anisoinertia error torque can be written as

$$\begin{matrix}\text{effective}\\ \text{anisoinertia}\\ \text{error torque}\end{matrix} = (I_{ii}-I_{ss})\,\omega_s\omega_i - I_{ss_r}\,\delta\Omega\,\omega_i \qquad (2.2\text{-}7)$$

The importance of the additional term can be seen by considering two limiting cases. First, assume ω_s to be slowly varying that $\delta\Omega \cong 0$ at all times. From Eq. (2.2-7) we get

$$\begin{matrix}\text{anisoinertia}\\ \text{error torque}\end{matrix} = (I_{ii} - I_{ss})\,\omega_s\omega_i \qquad (2.2\text{-}8)$$

Eliminating this term thus becomes a matter of setting I_{ii} and I_{ss} equal. Since

$$I_{ii} = I_{ii_g} + I_{ii_r} \quad \text{and} \quad I_{ss} = I_{ss_g} + I_{ss_r} \qquad (2.2\text{-}9)$$

an inertially asymmetric rotor leads to the requirement for an inertially asymmetric gimbal.

Next, consider the situation where ω_s is varying so rapidly that the speed control loop can not follow it at all. That is, $\delta\Omega \cong -\omega_s$. From Eq. (2.2-7) we now get

$$\begin{matrix}\text{anisoinertia}\\ \text{error torque}\end{matrix} = (I_{ii} - I_{ss})\,\omega_s\omega_i + I_{ss_r}\,\omega_s\,\omega_i$$

$$= (I_{ii} - I_{ss_g})\,\omega_s\,\omega_i \qquad (2.2\text{-}10)$$

Eliminating this error torque places <u>different</u> requirements on gimbal and rotor inertias. This effect can be argued physically by observing that the

gyro rotor is essentially uncoupled (about the spin axis) from the rest of the instrument when high angular rates occur about the spin axis. As a result of this uncoupling, the inertia of the rotor about the spin axis does not contribute to float error torques.

Of course, the changing effective anisoinertia term is a problem when attempts are made to reduce gyro error torques. For the input rates described in Eq. (2.2-4), it is readily shown that Eqs. (2.2-6) and (2.2-7) yield a rectified torque term given by:

$$\text{average effective anisoinertia torque} = \left[I_{ii} - I_{ss_g} + I_{ss_r} \left(\frac{K_h/I_{ss_r}}{w^2 - K_h/I_{ss_r}} \right) \right] \frac{W_s W_i}{2} \cos \gamma_s \qquad (2.2\text{-}11)$$

The frequency sensitive nature of this term is apparent.

2.2.4 Gimbal Products of Inertia

While they are probably small relative to other torques on an instantaneous basis, gimbal product of inertia terms can nevertheless be responsible for rectified float torques as well. The product of inertia terms are, from Eq. (2.2-1),

$$\text{gimbal product of inertia torques} = I_{os_g} [\dot{\omega}_s - \omega_o \omega_i] + I_{si_g} [\omega_s^2 - \omega_i^2] + I_{oi_g} [\dot{\omega}_i + \omega_o \omega_s] \qquad (2.2\text{-}12)$$

When subjected to the case angular rates described by Eq. (2.2-4), the non-zero average value of the gimbal product of inertia torques is

$$\begin{aligned}\text{average gimbal product of inertia torque} &= \frac{1}{2}\left[-I_{os_g} W_o W_i \cos\gamma_o\right. \\ &\left. + I_{si_g}(W_s^2 - W_i^2) + I_{oi_g} W_o W_s \cos(\gamma_o - \gamma_s)\right] \end{aligned} \quad (2.2\text{-}13)$$

2.2.5 Gimbal and Rotor Misalignment

We have already discussed the error torques due to gimbal-to-case misalignment about the output axis (α_o). There are also important torques due to gimbal-to-case misalignments about the spin and input axes, as well as rotor-to-gimbal misalignments about the input and output axes. Rotor-to-gimbal misalignment about the spin axis is of no significance. The pertinent error torques are, from Eq. (2.2-1),

$$\begin{aligned}\text{gimbal-to-case misalignment torques} &= \alpha_s\left[-(I_{ss} - I_{ii})\,\omega_o\omega_s - H\,\omega_o - I_{oo}\,\dot{\omega}_i\right] \\ &+ \alpha_i\left[(I_{ss} - I_{ii})\,\omega_o\omega_i + I_{oo}\,\dot{\omega}_s\right] \end{aligned} \quad (2.2\text{-}14)$$

and

$$\begin{aligned}\text{rotor-to-gimbal misalignment torques} &= \beta_o\left[(I_{ss_r} - I_{ii_r})\;(\omega_s^2 - \omega_i^2) + H\,\omega_s\right] \\ &+ \beta_i\left[(I_{ss_r} - I_{oo_r})\;(-\dot{\omega}_s + \omega_o\omega_i) - I_{ss_r}\,\dot{\Omega}_s\right] \end{aligned} \quad (2.2\text{-}15)$$

where the misalignment angles are all treated as small and constant. The terms in these equations are similar in origin to others already discussed.

There are anisoinertia terms, cross-coupling terms, anisoinertia coupling terms, case angular-acceleration terms due to cross-coupling, and rotor speed error terms. In the presence of constant angular rates or accelerations for long durations, these terms can be quite significant.

When subjected to the case angular rates described by Eq. (2. 2-4), the non-zero average value of the misalignment terms is as follows:

$$\begin{aligned}\text{average value of misalignment torques} = & -\frac{\alpha_s}{2}(I_{ss}-I_{ii})\,W_o W_s \cos(\gamma_o-\gamma_s) \\ & +\frac{\alpha_i}{2}(I_{ss}-I_{ii})\,W_o W_i \cos\gamma_o \\ & +\frac{\beta_o}{2}(I_{ss_r}-I_{ii_r})\,(W_s^2-W_i^2) \\ & +\frac{\beta_i}{2}(I_{ss_r}-I_{oo_r})\,W_o W_i \cos\gamma_o \end{aligned} \qquad (2.2\text{-}16)$$

These terms can be expected to be small.

Suspension System Design - The gimbal and rotor misalignment errors have, in addition to a constant portion resulting from imperfect gyro construction, time varying characteristics which result from radial and axial suspension system compliance. These additional contributions are generated by gyroscopic torques due to output axis angular rates and inertia torques caused by angular accelerations. They can provide motion-induced error torques over and above those shown in Eq. (2. 2-16) for constant misalignment. When designing suspension systems for the rotor and gimbals these errors must be computed and sufficient stiffness provided to keep them within acceptable limits.

2.2.6 Coning Errors

Gyro errors result when the sensor outputs are used to represent quantities which they only approximate. An example already treated is the cross-coupling error of a single-degree-of-freedom gyro. This error arises because the torque on the float is assumed to be caused by the angular rate about a case-fixed axis while it is actually the result of the rate about a slightly displaced gimbal-fixed axis.

A gyro error of similar origin arises in the gimballed platform use of a single-degree-of-freedom rate integrating gyro. If angular vibrations are applied to the inertial system at a frequency higher than the bandwidth of the motion isolation system (gimbal servo loops), the platform experiences oscillatory angular motion. In that case the gyro input axis changes spacial orientation and the integral of inertial angular rate about this sensor-fixed axis does not necessarily represent the rotation angle about its nominal direction.

Coning errors take their name from the fact that the motion commonly used to demonstrate them is one in which the gyro input axis describes a cone in space. It has been demonstrated (Ref. 1) that such a "coning" motion is generated and the gyro periodically returns to its original spacial orientation only under certain circumstances. This motion is described by one angular vibration about a space fixed axis perpendicular to the axis of the cone and another about an axis fixed in the gyro, essentially orthogonal to the first vibration and to the gyro input axis. If we consider only small amplitude vibrations, the angular rate of the gyro case relative to inertial space for this motion can be written as

$$\underline{\omega}_{IC} \cong \begin{bmatrix} \dot{\nu} \\ \dot{\eta} \\ \eta\dot{\nu} \end{bmatrix}$$

where

$$\nu = A_i \sin wt$$

describes vibration about the space-fixed axis and

$$\eta = A_2 \sin(wt + \psi)$$

describes vibration about the axis fixed in the gyro. The vector $\underline{\omega}_{IC}$ is resolved in the gyro case coordinates. The inertial angular rate about the gyro input axis, $\eta\dot{\nu}$, integrated over one period of vibration, indicates an apparent reorientation angle:

$$\rho = \pi A_1 A_2 \sin\psi \qquad (2.2\text{-}17)$$

But this is an error because we know the motion prescribed causes no net reorientation over one vibration period. The error results from integrating the angular rate projection along the gyro input axis while it describes a cone and using the result to imply a rotation about some axis which is assumed fixed in space.

2.2.7 Rotational Compliance

The gyro model employed in previous sections implicitly assumes one rotational degree-of-freedom about the spin axis, and that the rotor is otherwise rigidly connected to the float structure. Similarly, one rotational degree of freedom was assumed about the output axis and that the float is otherwise rigidly connected to the case. In a real gyroscope, however, there does exist finite compliance between the rotor and the float as well as between the float and the case. These additional degrees of freedom are responsible for high frequency resonant phenomena in the gyroscope. A discussion of

suitable spring-mass models for the compliance effects can be found in Ref. 1. For our present purposes it is sufficient to recognize the existence of these terms, and to note that the resonant frequencies involved bracket the structural natural frequency given by:

$$(\omega_n)_r = \sqrt{\frac{K}{I_{ii_r}}}$$

where K is the spring constant between the rotor and gimbal about the input (output) axis, in dyne-cm/rad. This frequency is typically on the order of 400 or more Hz. The potential effect of rotational compliance on limit cycle frequencies is discussed in Appendix F.

2.2.8 Rotor Dynamic Unbalance

A disturbance torque about the gyro output axis can result if the rotor does not have perfect dynamic balance. This effect occurs only at the rotor spin frequency and is independent of the environment. However, it does have some bearing on compensation schemes within the gyro loop. The torque enters the loop as a disturbance at rotor spin frequency and care must be taken not to provide a high gain at that frequency when placing compensation in the rebalance loop. Rotor dynamic imbalance in two gyros is a potential source of system coning error.

2.3 LINEAR ACCELERATION TORQUES

Gyro torques produced by linear case accelerations occur in gimballed as well as strapdown systems. For purposes of discussion, these terms are grouped under the headings of Mass Unbalance and Linear Compliance.

2.3.1 Mass Unbalance

Mass unbalance torque is caused by a displacement between the output axis and the float center of mass. If we call δ_s and δ_i the displacement components along the spin and input axes, respectively, then the output axis mass unbalance torque can be written as (see Fig. 2.3-1)

$$\begin{aligned} \text{mass unbalance torque} &= m(\underline{\delta} \times \underline{a}) \cdot \hat{o} \\ &= m(\delta_s a_i - \delta_i a_s) \end{aligned} \qquad (2.3\text{-}1)$$

where $\hat{o}$ is a unit vector along the output axis

$$\underline{\delta} = \begin{bmatrix} \delta_o \\ \delta_s \\ \delta_i \end{bmatrix} \quad \text{and} \quad \underline{a} = \begin{bmatrix} a_o \\ a_s \\ a_i \end{bmatrix}$$

There exists another torque which, although not a mass unbalance term, is proportional to the first power of acceleration along the output axis. Hence, it is included in this section. It is attributed to damping fluid thermal convection currents resulting from a temperature gradient and an acceleration field along the output axis. For uniformity with Eq. (2.3-1) this term can be written in the form

$$\text{thermal convection torque} = m\,\delta_o a_o \qquad (2.3\text{-}2)$$

2. 3. 2 Linear Compliance

Consider the linear compliance matrix

$$[K] = \begin{bmatrix} K_{oo} & K_{os} & K_{oi} \\ K_{so} & K_{ss} & K_{si} \\ K_{io} & K_{is} & K_{ii} \end{bmatrix} \tag{2. 3-3}$$

where the first and second subscripts denote the directions of deflection and applied specific force, respectively. The linear compliance coefficients account for the net effect of both rotor and gimbal deflection. Terms with the same subscripts are called direct-compliances, while terms with different subscripts are called cross-compliances. It follows from the definition of the compliance matrix that, for slowly varying inputs,

$$\underline{\delta} = m\,[K]\,\underline{a} \tag{2. 3-4}$$

As in the case of mass unbalance, we compute the linear compliance torque about the float output axis in the form

$$\begin{aligned} \text{linear compliance torque} &= m(\underline{\delta} \times \underline{a}) \cdot \hat{o} \\ &= m^2[K_{so}a_o a_i + K_{si}\,a_i^2 + (K_{ss}-K_{ii})\,a_i a_s \\ &\quad - K_{io}a_o a_s - K_{is}a_s^2] \end{aligned} \tag{2. 3-5}$$

The quantity $(K_{ss}-K_{ii})\,a_i a_s$, similar in form to the anisoinertia terms of Section 2. 2, is called the anisoelastic torque. Observe that each of the terms in Eq. (2. 3-5) can produce a non-zero average value torque for identical frequency inputs.

It is to be noted that, for high frequency vibration inputs, the dynamic counterpart to Eq. (2.3-4) must be employed. In this spring-mass linear compliance system, resonance phenomena are, of course, encountered. Discussion of these phenomena can be found in Ref. 2.

Finally, there exists a float torque which cannot be described in terms of rotation or acceleration. It is the random torque responsible for the drift rate which is a limiting factor in cruise type gimballed platform systems. As we shall see, it can be quite small in comparison with other error terms in strapdown single-degree-of-freedom gyros.

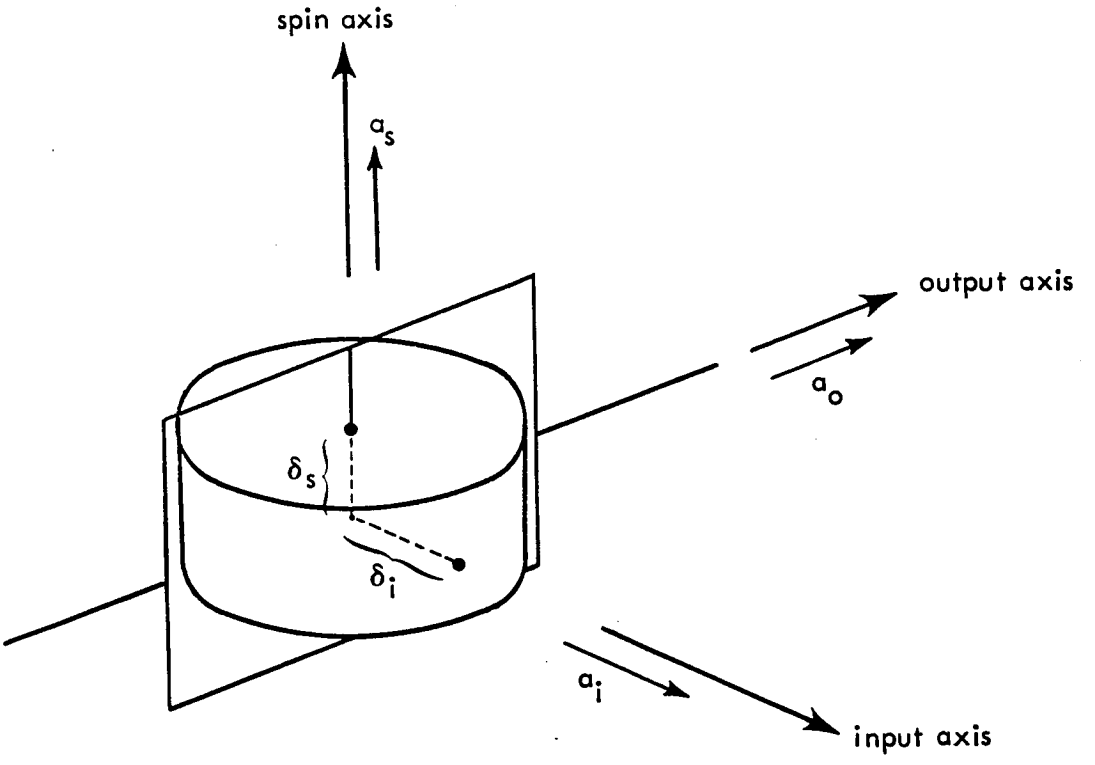

Figure 2.3-1. Mass Unbalance Terms for the Float Assembly

2.4 REBALANCE LOOP ERRORS

In holding the gyro float angle close to null the rebalance loop generates information which represents input angular velocity. One important aspect of strapdown gyro design is to provide a torquing system which has the required accuracy throughout the range of input rates anticipated. Required dynamic range can be defined in terms of input rate (ω_i) and allowable error rate (ω_e) as

$$\text{required dynamic range} \triangleq \frac{\text{allowable error rate, } \omega_e \left(\frac{\text{deg}}{\text{hr}}\right)}{\text{input rate, } \omega_i \left(\frac{\text{deg}}{\text{sec}}\right)} \times \frac{1}{3600} \left(\frac{\text{hr}}{\text{sec}}\right) \qquad (2.4\text{-}1)$$

This relationship has been plotted in Fig. 2.4-1. Estimates as to the operational accuracy of analog and digital torquing systems are better than 100 PPM and 10 PPM, respectively. As an illustration of the severity of the problem, consider the case where an input rate of 3 deg/sec is to be measured within an error corresponding to 0.01 deg/hr. The required dynamic range is better than 1 PPM.

Aspects of rebalance loop design including: configuration, limit cycle considerations, loop bandwidth and torquer scale factor error are discussed in the following sections. While floatation damping is assumed, all results apply to the case of non-floated, electric-network-stabilized single-axis gyros as well.

2.4.1 Rebalance Loop Configurations

Analog Torquing - Analog torquing may provide an attractive rebalance loop configuration for the lower accuracy strapdown system applications. As a result of analog torquing, float angle off null can be kept quite small, thus minimizing cross-coupling torques.

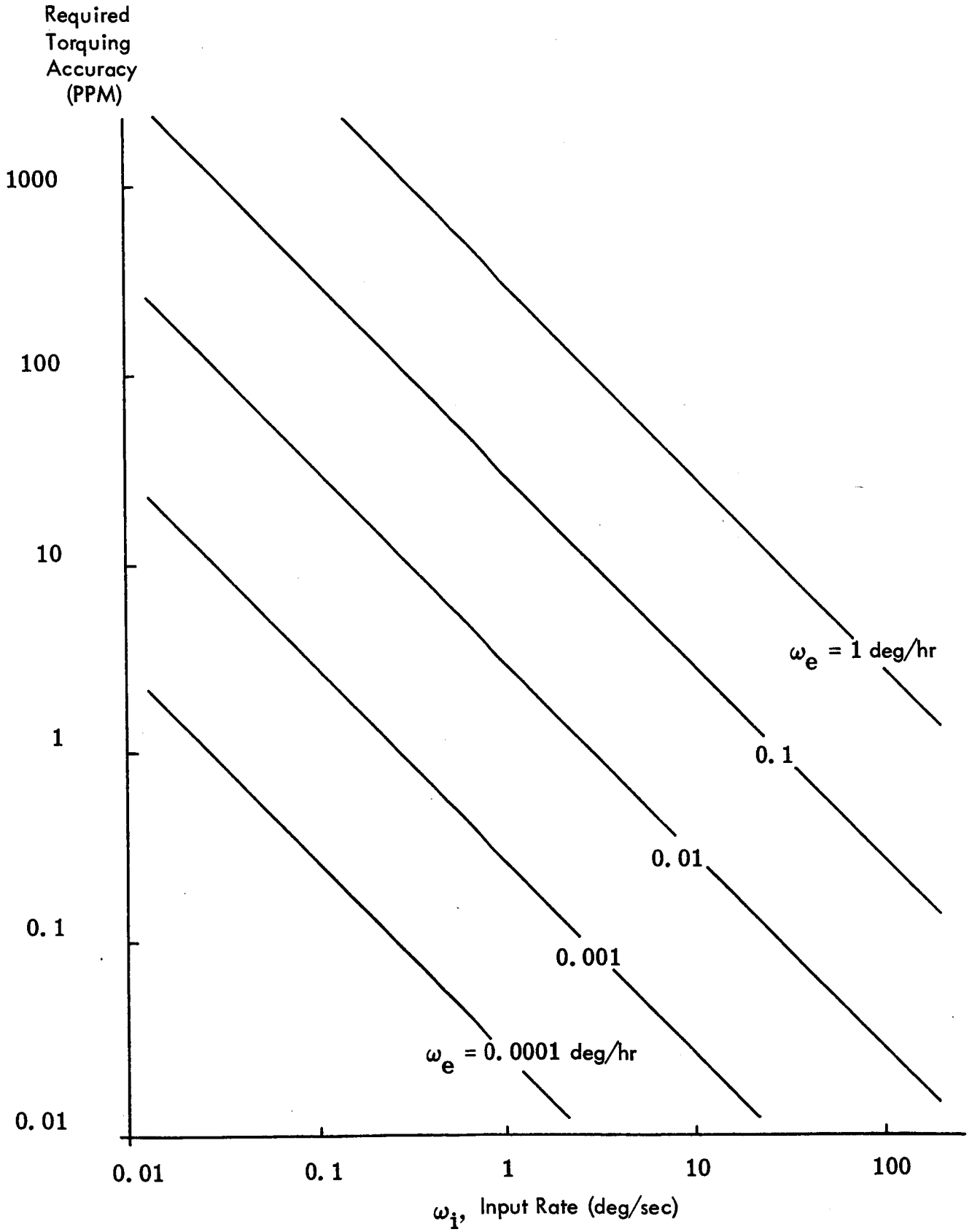

Figure 2.4-1 Required Torquing Accuracy vs. Input Rate

Figure 2.4-2(a) illustrates a linear, continuous torqued loop. The output, which is an indication of ω_i, can be processed through a delta-modulator read-out, thus providing an incremental angle suitable for input to a digital computer. A different but interesting possibility is to simply quantize the angular rate information for digital computer input. This may be better for use with a low speed general purpose digital computer and a high order integration algorithm. Finally, the possibility of using the output directly in an analog computation scheme may hold promise for certain low accuracy strapdown system applications.

Digital Torquing - In pulse-rebalanced loop configurations, the gyro torquer current is provided in the form of a series of pulses. The pulse waveform may be rectangular, sine, or any other shape desired. The integrated or average torque over a given time interval is proportional to the sum of current pulses over that time interval. Ideally, each current pulse represents a change in angular orientation about the input axis. This can be seen by first writing the equation of torque balance for the float. For a floated, rate integrating gyro, we get

$$I_{oo}\ddot{\alpha}_o + C\dot{\alpha}_o = H\omega_i - iK_{tg} + M_d \qquad (2.4\text{-}2)$$

where iK_{tg} represents the torque generator moment applied about the gyro output axis, and M_d denotes the disturbance torque portion of Eq. (2.2-1). Rearranging terms in Eq. (2.4-2) and integrating over the duration of one current pulse (say, from t to t + Δt) yields

$$\frac{K_{tg}}{H}\int_t^{t+\Delta t} i\,dt = \Delta\theta + \int_t^{t+\Delta t}\frac{M_d(t)}{H}\,dt - \frac{I_{oo}}{H}\left[\dot{\alpha}_o(t+\Delta t) - \dot{\alpha}_o(t)\right] - \frac{C}{H}\left[\alpha_o(t+\Delta t) - \alpha_o(t)\right] \qquad (2.4\text{-}3)$$

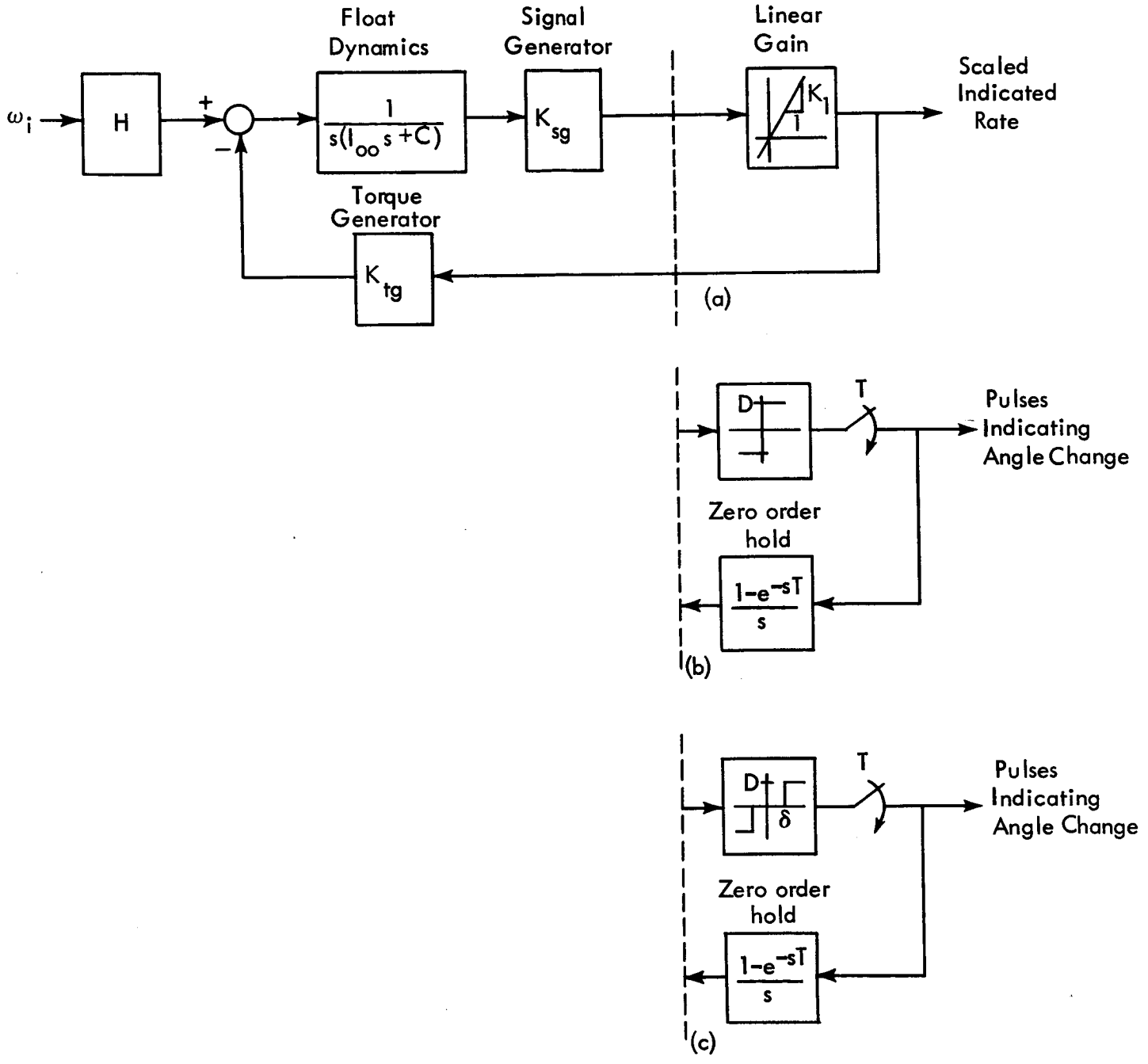

Figure 2.4-2. Rebalance Loop Configurations.

where

$$\Delta\theta = \int_{t}^{t+\Delta t} \omega_i(t)\, dt \qquad (2.4\text{-}4)$$

Now it can be argued that, since the average float position is at null or a constant off null, the expected value of the last two terms in Eq. (2.4-3) is zero. In any event, they have bounded magnitude and represent rotational information temporarily stored in the dynamics of the float. Also, the average drift rate M_d/H is presumably zero (any known torques having been calibrated). This leads to the interpretation of a (scaled) pulse of current in terms of an incremental rotation about the gyro input axis.

Two pulse torque modes are commonly considered - binary torquing and ternary torquing. In binary, or two-state torquing, the sign of the torque depends upon the sign of the gyro float angle at the last sampling time. Ternary torquing, which requires more complex electronics, provides for three torquing levels. These are plus, minus or zero, depending upon the sign and magnitude of the float angle.

Pulse torquing is used both with electromagnetic (i.e., Microsyn) and permanent magnet torquers. Due to the torque-current squared relationship Microsyn torquers require the application of constant waveform current pulses so that the instrument can be calibrated for pulses of consistent shape. Other disadvantages include side-loading and residual magnetic torque errors. The permanent magnet torquer is a linear torquer-current device, and does not suffer from side-loading or residual magnetic effects. But permanent magnet torquers suffer errors due to scale factor stability problems and rotor flex leads, as well as AC sensitivities (i.e. torque generator reaction torque).

Figure 2.4-2 illustrates two pulse rebalanced loop configurations. The sampling is periodic and the sampling rate is chosen on the basis of the desired information quantum and the maximum gyro case rate. In each case

the loop output is $\Delta\theta$, a discrete angle. The torque generators are fed from a constant current source, with the current switched between two opposing windings to produce torque of different signs, or switched to a dummy load or off to produce zero torque. The torque generator acts as a zero-order hold in the feedback path. Figure 2.4-3 provides additional details of the electrical functions performed. It illustrates the torquing electronics functions left unspecified in Fig. 1.1-2 for the case of pulse rebalance gyros.

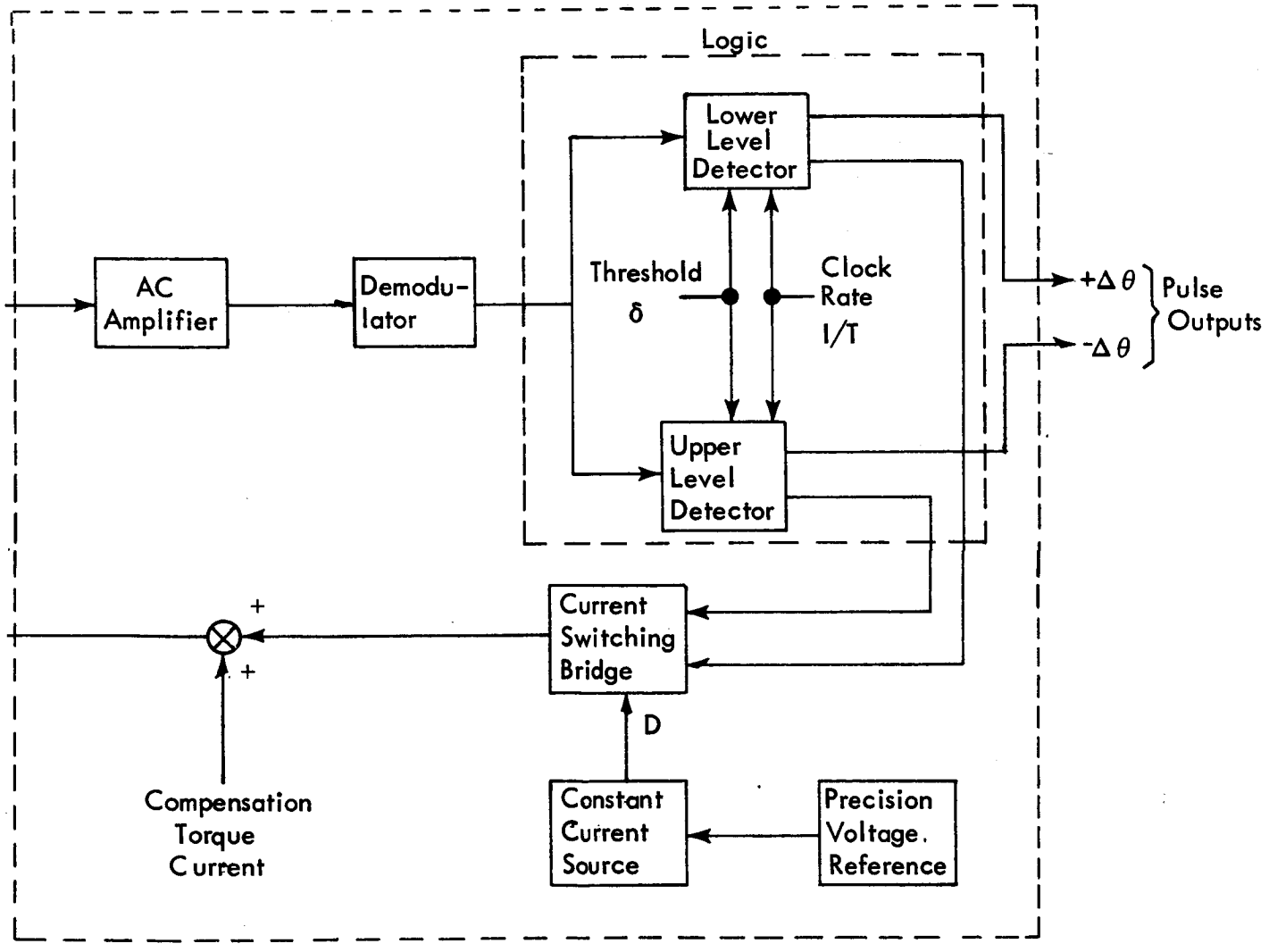

Figure 2.4-3 Pulse Torquing Electronics

Binary torqued loops always display a limit cycle, which is a self-sustained oscillation, even in the absence of an input. The limit cycle may assume a variety of modes, depending upon the ratio of float time constant to sampling time. The limit cycle is undesirable because instrument cross-coupling errors are directly proportional to the amplitude of the limit cycle if there are coherent body oscillations. Furthermore, any portion of the limit cycle which propagates into the coordinate transformation updating algorithm can cause a burn-out error condition during boost of a space vehicle. Finally, since torque is applied all the time, the balance between plus and minus torque levels is especially critical.

Ternary torquing (or "pulse-on-demand" torquing) can circumvent the no-input limit cycle mode, but still will result in various mode shapes in the presence of an input. The most severe case is a one-half maximum rate input, in which case all loop operation centers about the switching boundary of the loop nonlinearity. This is analogous to a binary torquing condition, but with half the drive level. Thus, moding errors are always less in ternary torqued systems than in binary torqued systems for gyros of the same dynamic properties. On the other hand, the average float offset angle, which gives rise to cross-coupling errors in the presence of a monotonic input, is generally larger than in the case of binary torquing due to the dead zone in the torquing logic. Also, it is more difficult to maintain the calibration of the switching circuitry to three standard conditions than two.

Figure 2.4-4 illustrates moding behavior for binary and ternary systems in response to the same constant input rate. The ternary system output is arranged to give no "wrong way" pulses, this being the desirable output format. Notice that instantaneous deviations from the average torque are smallest in the case of ternary torquing.

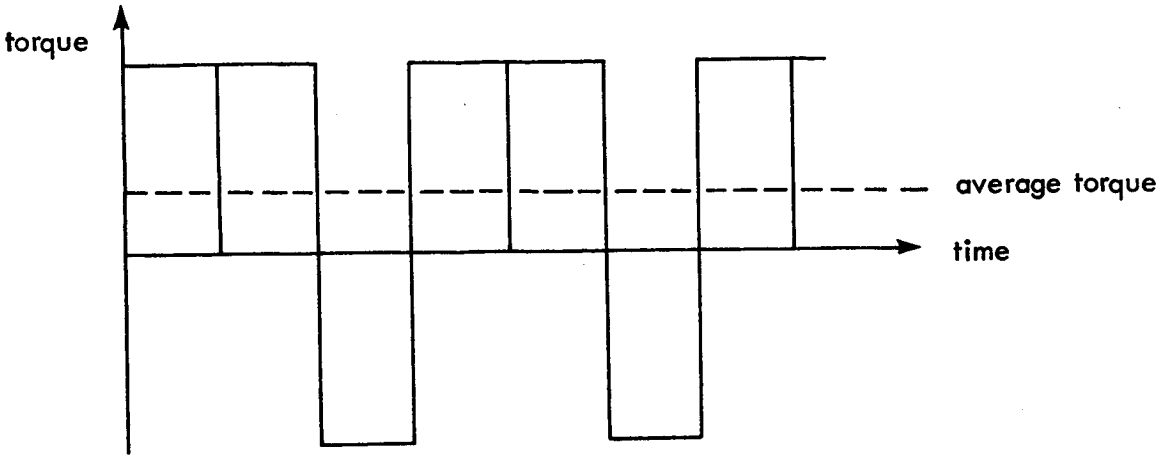

Binary Torquing (Two Level)

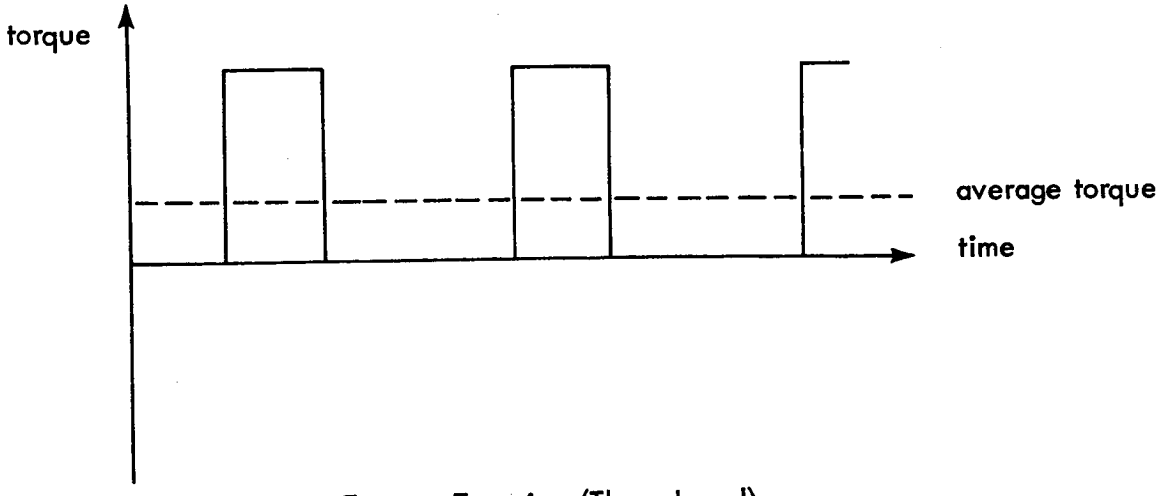

Ternary Torquing (Three Level)

Figure 2.4-4. Typical Moding Patterns Yielding the Same Average Torque

2.4.2 Limit Cycle Calculations

The amplitudes and frequencies of limit cycles in nonlinear systems are readily computed by the describing function method (Refs. 3, 4).

In the describing function method, one assumes the existence of a loop limit cycle and then tests to determine conditions under which it will maintain itself. In a periodic regime, the loop nonlinearity output will be some form of square-wave. If there is sufficient low-pass filtering between the nonlinearity output and its input the filtered square wave, upon arriving at the nonlinearity input, closely approximates a single sinusoid. In that event, there is no need to consider nonlinearity output higher harmonics in the first place. Thus, the describing function gain ($N_A(A)$) of the nonlinearity is defined as the complex ratio of nonlinearity output first harmonic to the corresponding input first harmonic. In the case of memoryless (i.e., single-valued) nonlinearities such as binary and ternary elements, the describing function gain is a real number. Appendix B contains describing function calculations for the nonlinearities of interest; some useful results are repeated below.

binary element: $$N_A(A) = \frac{4D}{\pi A} \qquad \text{for all } A \tag{2.4-5}$$

ternary element: $$N_A(A) = \frac{4D}{\pi A}\sqrt{1 - \left(\frac{\delta}{A}\right)^2} \qquad \text{for } A \geq \delta$$

$$= 0 \qquad \text{for } A < \delta \tag{2.4-6}$$

In the following examples it is assumed that the rebalance loop sampling frequency is sufficiently high that delays due to sampling can be neglected in limit cycle calculations. The effect of sampling delays is discussed in detail in Appendix E.

Example 1 - Consider the binary torqued rebalance loop illustrated in Fig. 2.4-5(a). The describing function condition for a loop limit cycle is

$$N_A(A)\, H(j\omega_\ell) = -1 \qquad (2.4\text{-}7)$$

where $H(j\omega_\ell)$ is the open-loop linear elements transfer function (sampling ignored), evaluated at the limit cycle frequency ω_ℓ rad/sec, viz:

$$H(j\omega_\ell) = \frac{K_{sg}K_{tg}/C}{j\omega_\ell(\tau_f j\omega_\ell + 1)(\tau_{tg} j\omega_\ell + 1)} \qquad (2.4\text{-}8)$$

where $\tau_f = I_{oo}/C$ is the float time constant and τ_{tg} is the torquer time constant. Inserting Eqs. (2.4-8) and (2.4-5) into Eq. (2.4-7) yields the following magnitude and angle conditions required for a solution:

magnitude condition: ($|N|\,|H| = 1$)
$$\frac{4D}{\pi A}\,\frac{K_{sg}K_{tg}}{C}\,\frac{1}{\omega_\ell\sqrt{\tau_f^2\omega_\ell^2+1}\,\sqrt{\tau_{tg}^2\omega_\ell^2+1}} = 1 \qquad (2.4\text{-}9)$$

angle condition: ($\measuredangle N + \measuredangle H = -\pi$)
$$-\frac{\pi}{2} - \tan^{-1}\tau_f\omega_\ell - \tan^{-1}\tau_{tg}\omega_\ell = -\pi \qquad (2.4\text{-}10)$$

Using the trigonometric identity

$$\tan^{-1} x + \tan^{-1} y = \tan^{-1}\left(\frac{x+y}{1-xy}\right)$$

Eq. (2.4-10) can be solved for ω_ℓ. There results

$$\omega_\ell = \sqrt{\frac{1}{\tau_f \tau_{tg}}} \text{ rad/sec} \qquad (2.4\text{-}11)$$

Inserting this result into Eq. (2.4-9) yields

$$A = \frac{4D}{\pi} \frac{K_{sg}K_{tg}}{C} \frac{\tau_f \tau_{tg}}{\tau_f + \tau_{tg}} \text{ volts} \qquad (2.4\text{-}12)$$

This solution corresponds to a stable limit cycle.

If $\tau_f = 1 \times 10^{-3}$ sec and $\tau_{tg} = 0.1\ \tau_f$, then Eq. (2.4-11) yields $\omega_\ell = 3.18 \times 10^3$ rad/sec = 500 cps. If loop sampling frequency is in excess of 5,000 cps, for example, sample and hold operations contribute very small phase lag and can be neglected.

Example 2 – For the ternary torqued rebalance loop of Fig. 2.4-5(b), a condition under which limit cycling will not occur is readily established. For a limit cycle to occur, the associated frequency would have to be given by Eq. (2.4-11), since the present describing function is, as before, non-phase shifting. This allows the evaluation $|H(j\omega_\ell)|$ as

$$|H(j\omega_\ell)| = \frac{K_{sg}K_{tg}}{C} \frac{\tau_f \tau_{tg}}{\tau_f + \tau_{tg}} \qquad (2.4\text{-}13)$$

If the maximum value of $N_A(A)$ is such that it, multiplied by $|H(j\omega_\ell)|$, is less than unity, Eq. (2.4-7) will not be satisfied and limit cycling will not occur. From Eq. (2.4-6) the maximum value of N_A occurs when:

$$\frac{d}{dA}\left(\frac{4D}{\pi A}\sqrt{1-\left(\frac{\delta}{A}\right)^2}\right) = 0$$

which yields $A = \sqrt{2}\delta$ and, correspondingly,

$$N_A(A)\Big|_{max} = \frac{2D}{\pi\delta} \qquad (2.4\text{-}14)$$

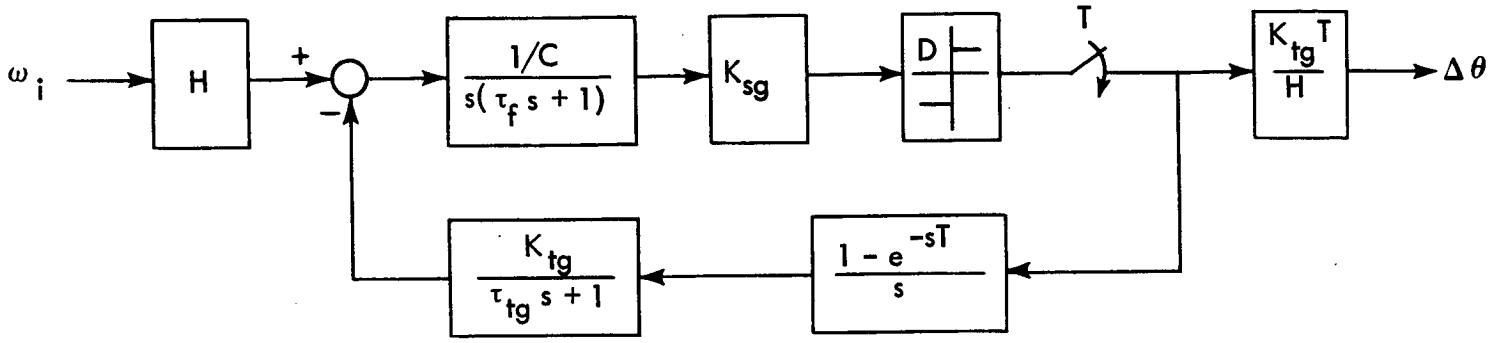

(a) Binary Torqued

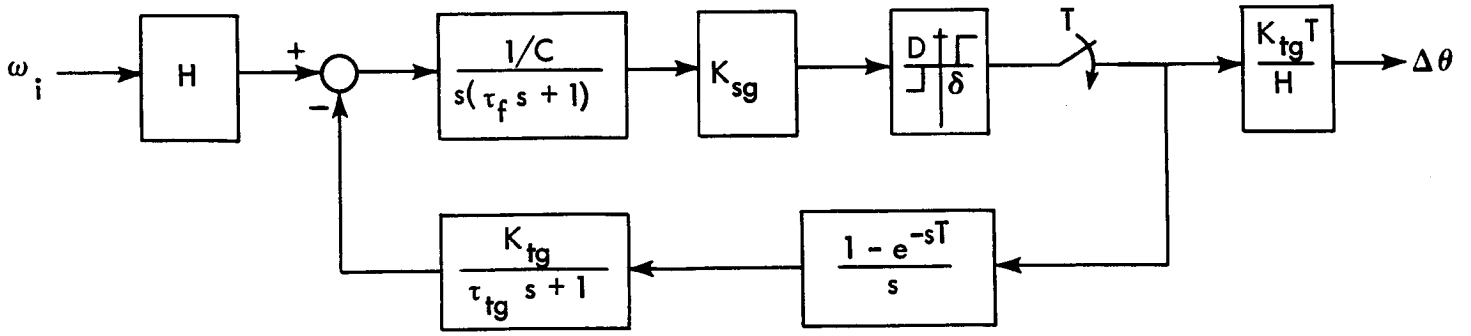

(b) Ternary Torqued

Figure 2.4-5. Example Pulse Rebalance Loop Configurations

Thus, a limit cycle will not occur if

$$\frac{2D}{\pi\delta}\ \frac{K_{sg}K_{tg}}{C}\ \frac{\tau_f\tau_{tg}}{\tau_f+\tau_{tg}} < 1 \qquad (2.4\text{-}15)$$

2.4.3 Loop Bandwidth Calculations

Consider the linear, continuous torqued rebalance loop shown in Fig. 2.4-6. The gain K_1 has units of milliamp/millivolt and represents the operation of linear conversion of signal generator voltage output to torque generator current input. As a good approximation in this linear system, torquer dynamics have been omitted. $\hat{\omega}_i$ denotes the continuous output, which is an estimate of the input rate ω_i. The second-order transfer function from ω_i to $\hat{\omega}_i$ can be written as follows:

$$\frac{\hat{\omega}_i}{\omega_i}(s) = \frac{K_{sg}K_{tg}K_1/I_{oo}}{s^2 + (C/I_{oo})\,s + (K_{sg}K_{tg}K_1/I_{oo})}$$

$$= \frac{\omega_n^2}{s^2 + 2\zeta\,\omega_n\,s + \omega_n^2} \qquad (2.4\text{-}16)$$

where the natural frequency and damping ratio are given as

$$\omega_n = \sqrt{K_{sg}K_{tg}K_1/I_{oo}} \quad \text{rad/sec} \qquad (2.4\text{-}17)$$

$$\zeta = \frac{C}{2\sqrt{I_{oo}K_{sg}K_{tg}K_1}} \qquad (2.4\text{-}18)$$

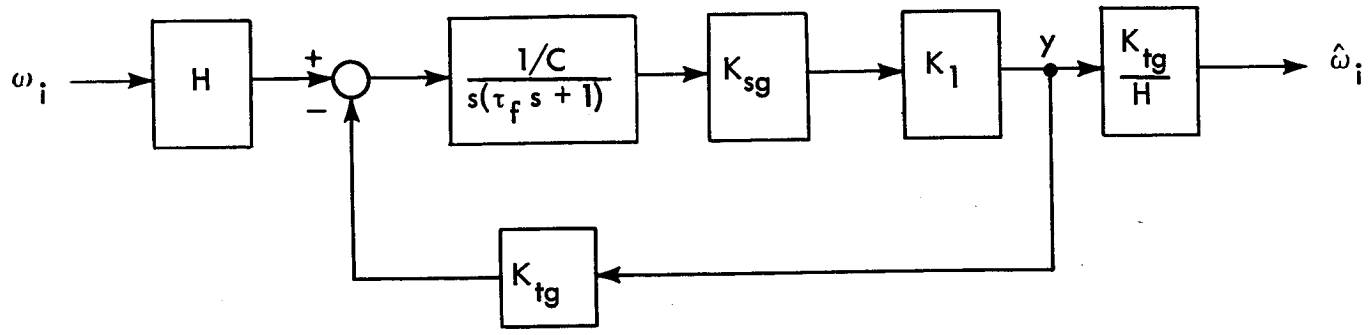

Figure 2.4-6. Example Analog Rebalance Loop Configuration.

For a second-order system, bandwidth, defined as the frequency at which the closed-loop amplitude transfer equals $1/\sqrt{2}$, can be calculated directly in terms of ζ and ω_n. The result is (Ref. 5)

$$\omega_{BW} = \omega_n \sqrt{1 - 2\zeta^2 + \sqrt{2-4\zeta^2 + 4\zeta^4}} \qquad (2.4\text{-}19)$$

Assuming the following loop parameters

$I_{oo} = 250$ gm-cm^2, $C = 1 \times 10^5$ dyne-cm-sec

$K_{sg} = 20$ mv/mrad, $K_{tg} = 1,200$ dyne-cm/ma

$K_1 = 1,000$ ma/mv

we get

$$\omega_n = 314 \text{ rad/sec} = 50 \text{ cps}, \quad \zeta = 0.64$$

and

$$\omega_{BW} = 345 \text{ rad/sec} = 55 \text{ cps}$$

Now consider the limit cycling, binary torqued loop of Fig. 2.4-5(a). The problem in computing bandwidth for this loop is one of specifying the equivalent nonlinearity gain to signals of interest, assuming once again that dynamics of the sample and hold operations can be ignored. In the case of slowly varying input signals (relative to the limit cycle period), the signal appearing at the input to the nonlinearity can be modeled as a sinusoid (the limit cycle) plus a bias (response to the input signal). The gain to the bias, defined as the ratio of nonlinearity output dc amplitude to nonlinearity input dc amplitude (the bias, B), has been called the dual input describing function (Ref. 6). It is denoted $N_B(A, B)$.

The calculation of $N_B(A, B)$ for a binary nonlinearity, Appendix B, reveals that

$$N_B(A, B) = \frac{2D}{\pi B} \sin^{-1}\left(\frac{B}{A}\right) \qquad (2.4\text{-}20)$$

In the limit of small B/A this becomes

$$N_B(A, 0) = \frac{2D}{\pi A} \qquad (2.4\text{-}21)$$

A very important result of recent research in describing function theory suggests that "the gain of the nonlinearity to a small signal in the presence of other signals is the same regardless of the shape of the small signal," (Ref. 3). This means that the use of $N_B(A, 0)$ to represent the nonlinearity gain to information passing through the rebalance loop can be justified on the basis of "smallness" as well as "slowness."

To compute the bandwidth of the limit cycling loop we can use the results of the linear system calculation, Eqs. (2.4-17), (2.4-18) and (2.4-19), with K_1 replaced by $N_B(A, 0)$. Neglecting the torquer dynamic lag in the feedback path causes no important error at this point in the calculation. From Eqs. (2.4-21) and (2.4-12) we get

$$N_B(A, 0) = \frac{C}{2K_{sg}K_{tg}} \frac{\tau_f + \tau_{tg}}{\tau_f \tau_{tg}} = K_1 \qquad (2.4\text{-}22)$$

Equations (2.4-17) and (2.4-18) now yield

$$\omega_n = \frac{1}{\tau_f} \sqrt{\frac{\tau_f + \tau_{tg}}{2\tau_{tg}}} \text{ rad/sec} \qquad (2.4\text{-}23)$$

$$\zeta = \sqrt{\frac{\tau_{tg}}{2(\tau_f + \tau_{tg})}} \qquad (2.4\text{-}24)$$

Note that a very interesting phenomenon has occurred. Both ω_n and ζ are independent of all of the loop gains (K_{sg}, K_{tg}, D)! It is this very behavior which is capitalized upon the design of certain adaptive control systems. Figure 2.4-7 describes ω_n and ζ as functions of the ratio τ_f/τ_{tg}.

Utilizing the gyro parameters values employed in earlier portions of this section, we can compute

$$\omega_n = 1,500 \text{ rad/sec} = 240 \text{ cps}, \quad \zeta = 0.135$$

and

$$\omega_{BW} = 2,300 \text{ rad/sec} = 365 \text{ cps}$$

Of course, these results are only valid for sufficiently high sampling frequencies. Nevertheless, comparison of these results with those obtained for the corresponding analog torqued rebalance loop shows a very important facet of pulse rebalanced loop behavior. See Fig. 2.4-8. The effect of changing the float time constant while holding τ_{tg} fixed is illustrated in Fig. 2.4-9. The arrow indicates the direction of increasing damping if I_{oo} is assumed fixed.

Consideration of the sinusoidal response of a nominally non-limit-cycling ternary torqued rebalance loop is involved with questions of limit cycle induction, amplitude-sensitive responses and jump resonance phenomena. Under these circumstances the interpretation of bandwidth, per se, has limited meaning. Thus, it is not pursued any further here. Finally, it is recalled that the gyro rebalance loops shown in Fig. 2.4-5 contain convenient simplifications of the rotor-gimbal dynamics and nonlinear characteristics. In particular, angular compliance and switching hysteresis effects have been ignored. Appendix F treats the influence of angular compliance on limit cycles in some detail. A preliminary conclusion is that these additional dynamics should be considered in any thorough limit cycle investigation for gyros with

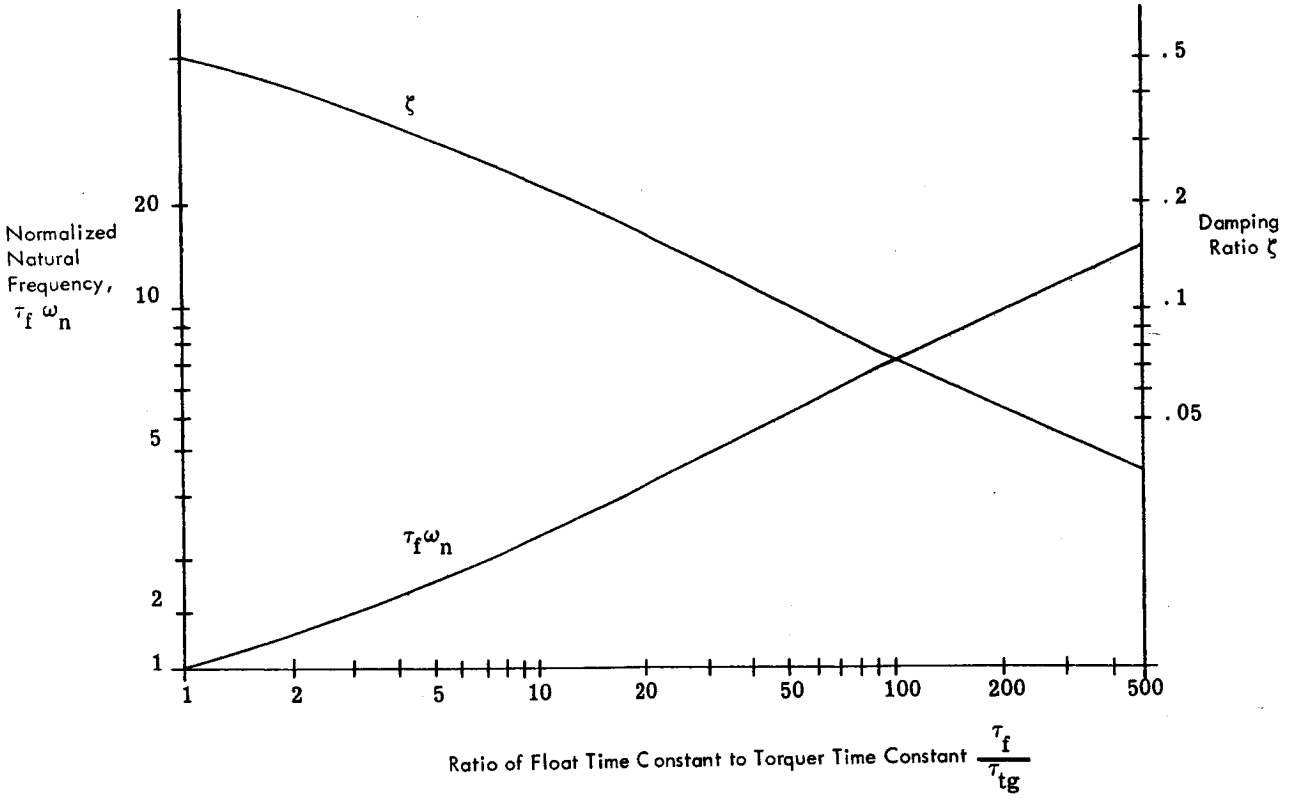

Figure 2.4-7 Binary Torqued Rebalance Loop ζ And $\tau_f\omega_n$ As Functions Of $\frac{\tau_f}{\tau_{tg}}$

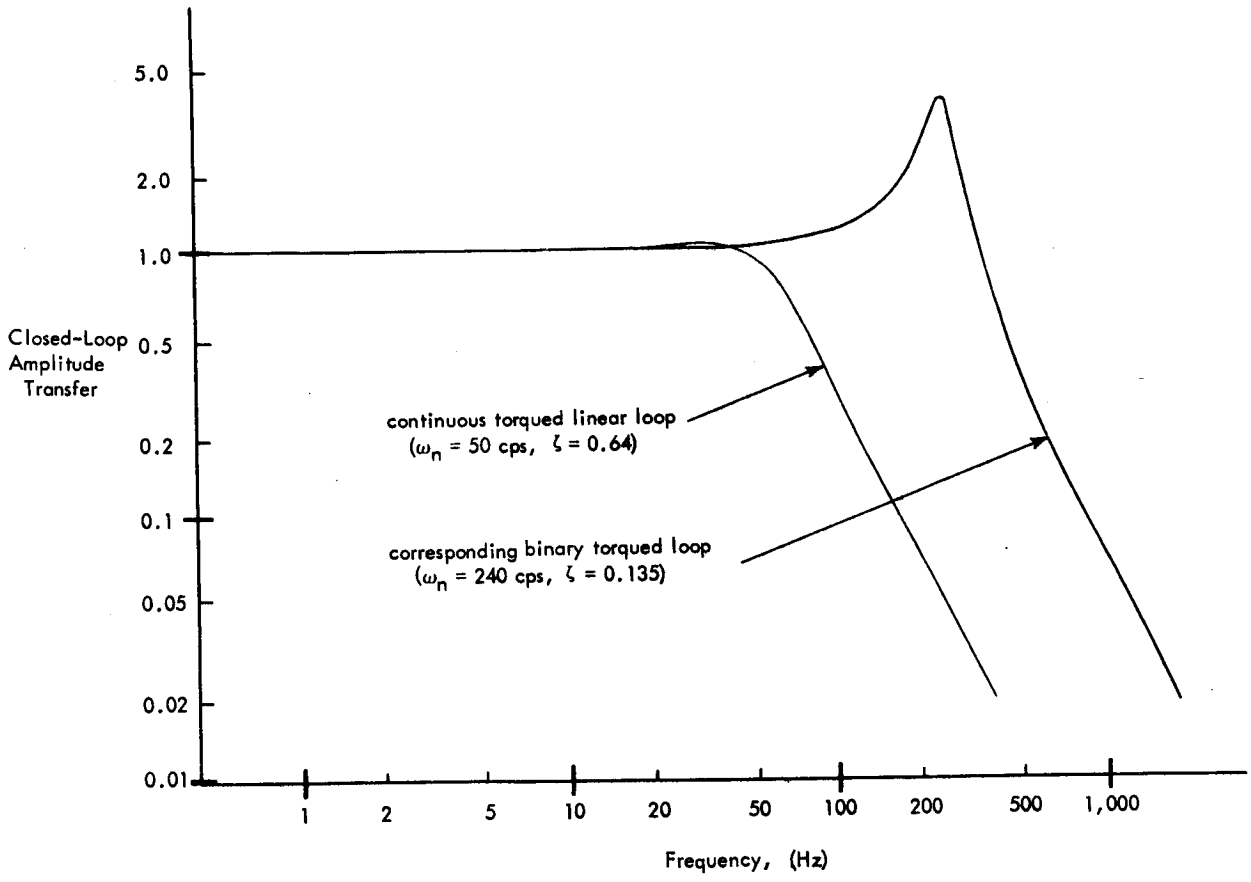

Figure 2.4-8. Frequency Response Characteristics for Example Rebalance Loop

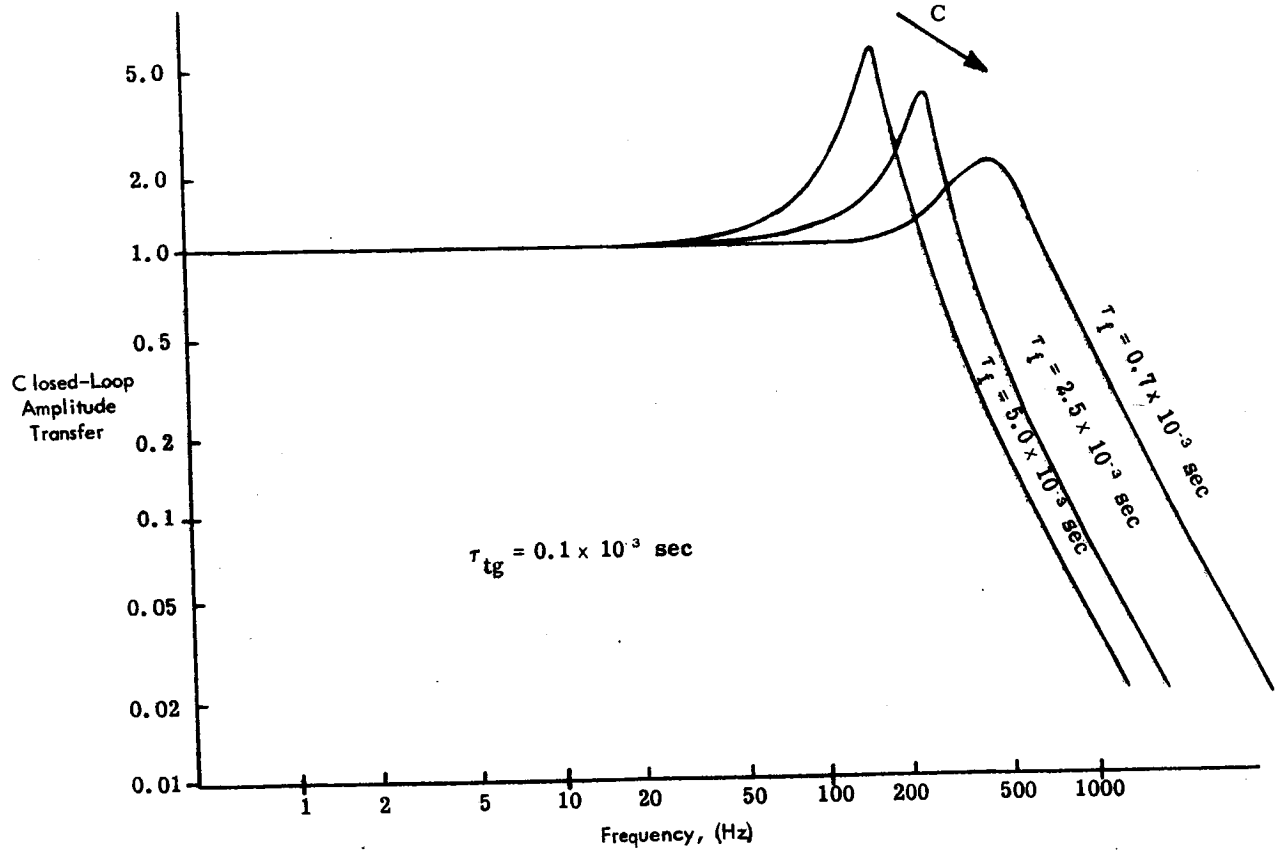

Figure 2.4-9 Effect of Varying C on Loop Frequency Response

typical physical parameters. Hysteresis in the nonlinear element arises from detection threshold in the signal generator, ac amplifier and demodulator in combination. It provides some amplitude-dependent phase lag to the describing function but is not considered significant in limit cycle analysis of representative gyros (see Appendix E).

2.4.4 Torquing Errors

Analog torquing errors can be classified in terms of three dominant parts:

bias
scale factor
nonlinearity

A bias torque, M_b, results in a steady state drift rate given by

$$\begin{matrix}\text{torquer bias} \\ \text{drift rate}\end{matrix} = \frac{M_b}{H} \text{ deg/hr} \qquad (2.4\text{-}25)$$

In the case of a torquer scale factor error, η, the actual torquer gain is $K_{tg}(1 + \eta)$ as compared to the value K_{tg} which is believed to exist. The resulting error is

$$\begin{matrix}\text{torquer scale} \\ \text{factor error}\end{matrix} = \eta\omega_i \text{ deg/hr} \qquad (2.4\text{-}26)$$

To see the effect of torquer nonlinearity, let us consider the situation where the torquer input-output characteristic is piecewise-linear, with a slope change at the origin. That is,

$$y = K_{tg}^{+} x \quad \text{for } x \geq 0$$

$$= K_{tg}^{-} x \quad \text{for } x < 0$$

where K_{tg}^{+} and K_{tg}^{-} are slightly different from the nominal value K_{tg}. If this nonlinearity is in the feedback path of the system in Fig. 2.4-6, the amplitude response (A) at station y due to a sinusoidal input $\omega_i = W_i \sin wt$ is

$$A = \frac{H}{K_{tg}} \; W_i \; \frac{K_1 K_{sg} K_{tg}/I_{oo}}{\sqrt{(K_1 K_{sg} K_{tg}/I_{oo} - w^2)^2 + (w\,C/I_{oo})^2}}$$

where the effect of the nonlinearity has been neglected owing to its small influence on A.

Now we make the observation that, for the rebalance loop of Fig. 2.4-6 to be in a steady state, the waveform at station y must contain a bias if $K_{tg}^{+} \neq K_{tg}^{-}$. This follows from the fact that if there is no bias at y, there will be a bias at the output of the torque generator due to the asymmetric torquer characteristic. But this would cause the float to have an average motion in one direction, hence the system would not be in a steady state. Therefore a bias must exist at y.

The bias at y is readily computed using the appropriate dual input describing function calculated in Appendix B. As the nonlinearity output bias must be zero, we simply set the quantity $BN_B(A, B)$ equal to zero. For small B/A, Eq. (B-9) yields

$$BN_B(A, B) \cong B \left(\frac{K_{tg}^{+} + K_{tg}^{-}}{2} \right) + A \left(\frac{K_{tg}^{+} - K_{tg}^{-}}{\pi} \right) = 0$$

or

$$B \cong - \frac{2}{\pi} \left(\frac{K_{tg}^{+} - K_{tg}^{-}}{K_{tg}^{+} + K_{tg}^{-}} \right) A \qquad (2.4\text{-}27)$$

and BK_{tg}/H is the drift rate term due to torquer nonlinearity. In the special case where

$$K_{tg}^{+} = K_{tg}(1 + \epsilon_{tg}) \quad \text{and} \quad K_{tg}^{-} = K_{tg}(1 - \epsilon_{tg})$$

the drift rate term becomes

$$\begin{matrix}\text{torquer nonlinearity} \\ \text{drift rate}\end{matrix} = -\frac{2\epsilon_{tg}}{\pi} \quad \frac{K_{tg}}{H} \quad A \qquad (2.4\text{-}28)$$

For input frequencies within the bandpass of the rebalance loop we get $A \cong HW_i/K_{tg}$ and hence the drift rate is equal to $-2\epsilon_{tg}W_i/\pi$ deg/hr.

In the case of binary torquing we can model the torquing error in terms of a general plus-pulse weight and a general minus-pulse weight – each of which differs a bit from standard. Taking the standard pulse weight as the incremental angle $\Delta\theta$ and general plus- and minus-pulse weights as $\Delta\theta(1 + \eta_b^{+})$ and $-\Delta\theta(1 + \eta_b^{+})$, respectively, for a pulse duration of T sec the drift rate becomes

$$\begin{matrix}\text{binary torqued} \\ \text{limit cycle error} \\ \text{(small input case)}\end{matrix} = \frac{\Delta\theta}{2T}\,(\eta_b^{+} - \eta_b^{-}) \text{ deg/hr} \qquad (2.4\text{-}29)$$

This expression is valid for small inputs, which do not materially affect the limit cycle waveform. For large, monotonic inputs, the binary rebalance loop pulse train must assume a non-zero average value corresponding to the input rate. The resulting moding pattern will be periodic, with n^{+} positive pulses and n^{-} negative pulses during a time interval $(n^{+} + n^{-})T$ such that

$$\left(\frac{n^{+} - n^{-}}{n^{+} + n^{-}}\right) \quad \frac{\Delta\theta}{T} = \omega_i$$

for rational $\omega_i/(\Delta\theta/T)$. The corresponding rate error is

$$\left(\frac{n^+\eta_b^+ - n^-\eta_b^-}{n^+ + n^-}\right)\frac{\Delta\theta}{T}$$

which can be rewritten as

$$\text{binary torqued moding pattern error (large input case)} = \left(\frac{\eta_b^+ - \eta_b^-}{2}\right)\frac{\Delta\theta}{T} + \left(\frac{\eta_b^+ + \eta_b^-}{2}\right)\omega_i \text{ deg/hr} \qquad (2.4\text{-}30)$$

In the case where $\eta_b^+ = \eta_b^- = \eta_b$, this reduces to $\eta_b\omega_i$ deg/hr.

For ternary torquing we can model the error as due to an error in plus-pulse weight, an error in minus-pulse weight, and an error in the zero level. Drift in the absence of an input is due to errors in the zero torque level:

$$\text{ternary torqued calibration error (no inputs)} = \eta_b^o\left(\frac{\Delta\theta}{T}\right) \qquad (2.4\text{-}31)$$

Again, the expression is approximately valid for small inputs. If we consider ratios of $\omega_i/(\Delta\theta/T)$ of the nature 1/q where q is an integer (other rational ratios do not provide unique moding without specification of gyro dynamics) the error rate with ternary torquing is:

$$\text{ternary torqued moding error (large inputs with rational } \omega_i/(\Delta\theta/T)) = \eta_b^o(\Delta\theta/T) + (\eta_b^* - \eta_b^o)\omega_i \qquad (2.4\text{-}32)$$

The quantity η_b^* represents η_b^+ or η_b^- depending on whether ω_i is positive or negative. Figure 2.4-10 is a plot of the errors described by Eqs. (2.4-30) and (2.4-32). Of course the errors indicated are only correct for rational

values of $\omega_i/(\Delta\theta/T)$ with binary switching and ratios with characteristic $1/q$ for ternary switching.

It is to be noted that in the case of both binary and ternary torquing the major issue is that of the stability of the pulse weights.

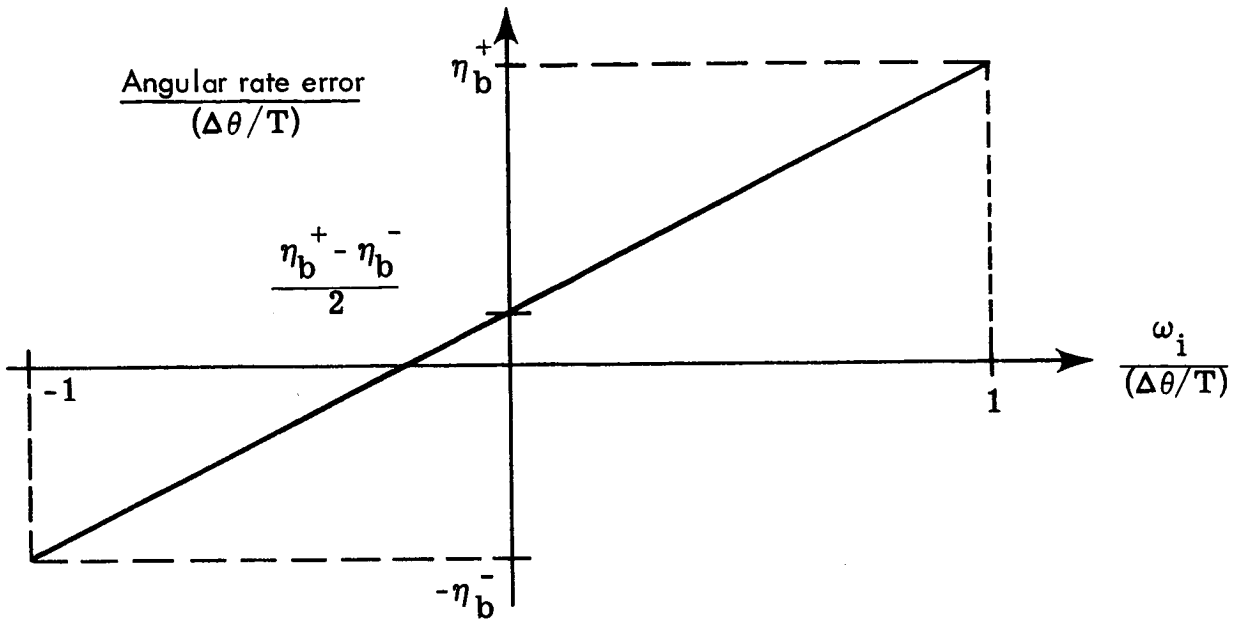

(a) binary torquing

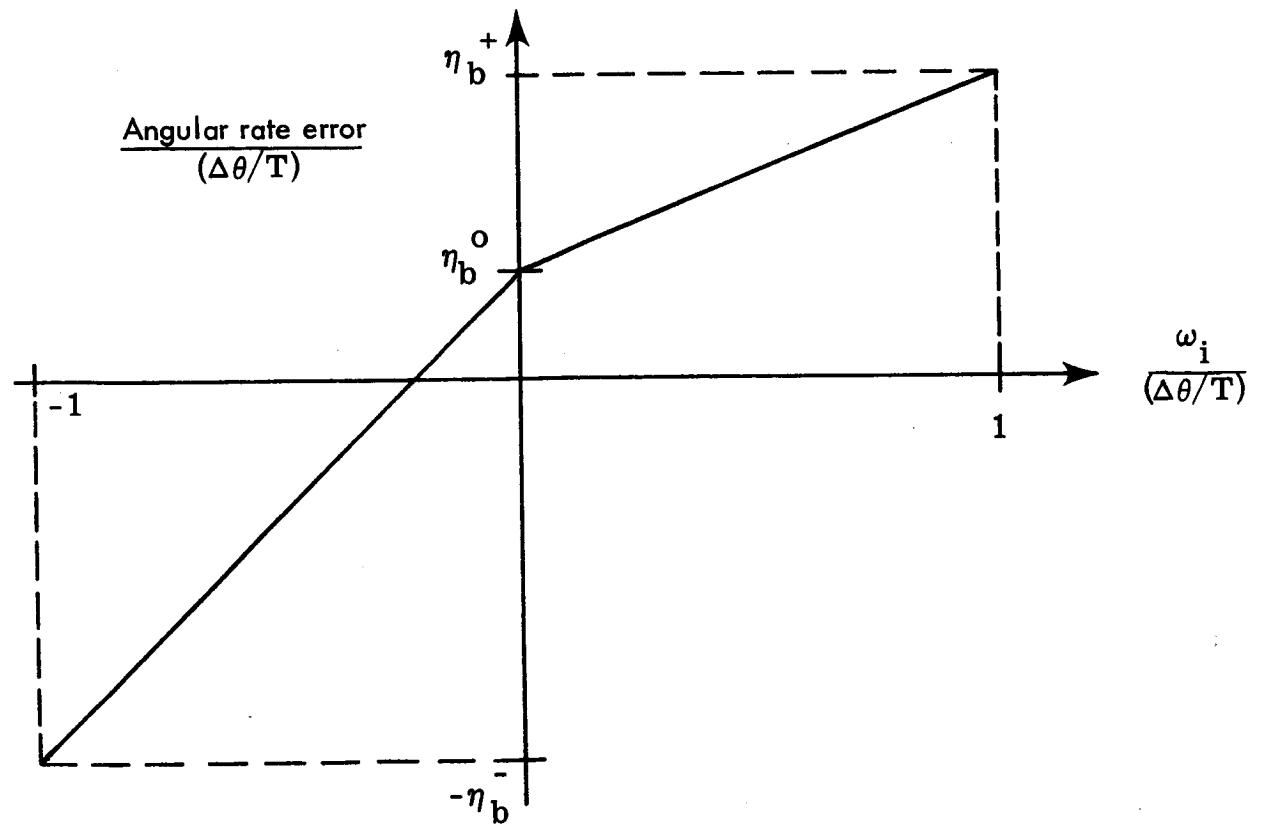

(b) ternary torquing

Figure 2.4-10 Torquer Scale Factor Errors

2.5 TYPICAL GYRO ERRORS

Environmental disturbances acting on a single-degree-of-freedom gyro are capable of generating constant torques, as shown in previous sections. The maximum amplitude of the resultant constant drift rate is calculated in this section for several of these effects. Angular-motion-induced drift rates are emphasized because these are unique to strapdown gyros. Table 2.5-1 displays the range of values assumed by important coefficients in a group of nine typical single-degree-of-freedom floated gyros intended for strapdown system usage.

Example - for purposes of comparison, the following representative group of parameters is chosen:*

$H = 2 \times 10^5$ gm-cm^2/sec, $\quad I_{oi_g} = I_{os_g} = 1.50$ gm-cm^2

$I_{oo} = 250$ gm-cm^2, $\quad I_{si_g} = 0.30$ gm-cm^2

$I_{ss_r} = 80$ gm-cm^2,

$I_{ii_r} = I_{oo_r} = 50$ gm-cm^2 $\quad \frac{I_{ss}-I_{ii}}{H} = 4$(deg/hr)/(rad/sec)^2

$$L_2(w) = \frac{I_{oo}}{H} L_1(w)$$

$L_1(w) = 2.0 \times 10^{-3} \frac{\text{rad}}{\text{rad/sec}}$, a measure of rebalance loop stiffness

$$\frac{m\delta_i}{H} \text{ or } \frac{m\delta_s}{H} = 5 \times 10^{-2} \frac{\text{deg/hr}}{g},$$

$$\frac{m^2}{H}(K_{ss} - K_{ii}) = 10^{-2} \frac{\text{deg/hr}}{g^2},$$

Torquer nonlinearity = $\epsilon_{tg} = 0.01\%$

Misalignment angles = ± 5 sec

*Note that these parameters are provided here for the purpose of illustration only. They are not necessarily identical with those given in preceding or subsequent examples.

TABLE 2.5-1

RANGE OF TYPICAL VALUES OF GYRO PARAMETERS

Parameter	Symbol	Units	Typical Range	
			Minimum	Maximum
Rotor Angular Momentum	H	$\frac{\text{gm-cm}^2}{\text{sec}}$	5×10^4	3×10^6
Float Output Axis Moment of Inertia	I_{oo}	gm-cm^2	100	250
Linear Damping Coefficient	C	dyne-cm-sec	6×10^4	8×10^5
Float Time Constant	τ_f	msec	0.25	6.0
Rotor Spin Axis Moment of Inertia	I_{ss_r}	gm-cm^2	40	140
Anisoinertia Error Coefficient	$\frac{I_{ss}-I_{ii}}{H}$	$\frac{\text{deg/hr}}{(\text{rad/sec})^2}$	4	30
Uncertainty in Float Mass Unbalance	$\frac{m\delta_i}{H}$, $\frac{m\delta_s}{H}$	$\frac{\text{deg/hr}}{g}$	5×10^{-3}	3.3×10^{-1}
Anisoelastic Error Coefficient	$\frac{m^2}{H}(K_{ss}-K_{ii})$	$\frac{\text{deg/hr}}{g^2}$	4×10^{-3}	1×10^{-1}
Torquer Scale Factor Error	η	%	1×10^{-2}	5×10^{-2}
Torquer Time Constant	τ_{tg}	μ sec	25	100
Misalignment Angles	$\alpha_i, \alpha_s, \beta_o, \beta_i$	$\widehat{\text{sec}}$	1	15
Torquer Sensitivity	K_{tg}	$\frac{\text{deg/hr}}{\text{ma}}$	75	1200
Signal Generator Sensitivity	K_{sg}	volt/rad	5	40

The vehicle is assumed to be subject to a one g specific force and to experience angular vibration described by Eq. (2.2-4) with

$$W_i = W_o = W_s = 0.2 \text{ rad/sec}$$

$$w = 10 \text{ rad/sec}$$

The vibrations are representative of those anticipated in a typical boost vehicle. The peak constant gyro drift rates (assuming the worst combinations of misalignment, λ_1, λ_2, γ_o and γ_s and specific force orientation) in a single gyro are presented in Table 2.5-2. The drift rates shown are calculated by dividing the constant error torque for each effect by the rotor angular momentum.

It should be noted that the anisoinertia error coefficient chosen in this example was at the low end of the range presented. This was done to illustrate the fact that choosing rotor and gimbal inertias to minimize drift rate when the rotor is coupled to the gimbal by the rotor speed regulation loop causes excessive drift rates when the rotor is uncoupled.

It can be seen from Table 2.5-2 that the strapdown rotational environment produces gyro drift rates which are large compared to the random drift rates and acceleration-caused gyro errors that are characteristic of gimballed platform systems. Although they may be small, the misalignment caused drift rate errors in a strapdown system are greater than in a gimballed platform because of the severe angular rates that can occur about the cross axes.

TABLE 2.5-2

MAXIMUM CONSTANT GYRO DRIFT RATE
FOR THE EXAMPLE

Error Terms	Constant Drift Rate (deg/hr)
Spin-Input Cross Coupling	8.00
Spin-Output Cross-Coupling	0.10
Anisoinertia (Rotor Coupled)	0.08
Anisoinertia (Rotor Uncoupled)	1.52
Float Mass Unbalance	0.05
Anisoelasticity	0.01
Torquer Nonlinearity	2.60
Misalignment*	0.50
Gimbal Products of Inertia	0.084
Pseudo-Coning due to Output Axis Effect**	5.00

* Computed on the basis of 0.05 rad/sec constant angular rates.

** See Appendix D.

PRECEDING PAGE BLANK NOT FILMED.

3. RELATIONSHIP BETWEEN STRAPDOWN SYSTEM ERRORS AND GYRO ERRORS

A measure of the quality of any inertial system, gimballed or strapdown, is some weighted combination of its attitude, position and velocity indication capabilities, depending on the mission involved. This chapter deals with a relationship between the individual gyro errors and the attitude indication accuracy of a strapdown inertial reference system.

3.1 A FIGURE-OF-MERIT

Figure 3.1-1 is a schematic representation of a strapdown system. The navigation computations are the same as for gimballed inertial systems. The unique feature of strapdown systems is the coordinate transformation which resolves the acceleration vector $\underline{a}_b$ from body axes into stabilized axes. The gyros measure inertial rotation rate in body axes, $\underline{\omega}_b$. These indications are then used to calculate system attitude in the form of a coordinate transformation matrix, C. Inevitably, errors $\underline{\Delta a}_b$ and $\underline{\Delta\omega}_b$ occur in the measured vectors $\underline{a}_b$ and $\underline{\omega}_b$. Furthermore, as a result of $\underline{\Delta\omega}_b$, an error will occur in the transformation matrix C, which we designate ΔC. We take as a measure of gyro performance at the system level, the figure-of-merit

$$J = \frac{1}{2} \text{tr} \, (\Delta C^T \, \Delta C) \qquad (3.1\text{-}1)$$

where the notation $\text{tr}(\Delta C^T \Delta C)$ is the trace of the matrix $\Delta C^T \Delta C$, which is the sum of its diagonal elements. Appendix C demonstrates that

$$J = \varphi_x^2 + \varphi_y^2 + \varphi_z^2$$

where the quantities φ_x, φ_y and φ_z represent small angle misalignments between the true reference coordinate system and the computed reference axes. Figure 3.1-2 illustrates these relations. The quantity J is a measure of the total system attitude error; the direction of the error vector is irretrievably lost in the process of reducing the figure-of-merit to a scalar quantity. When the acceleration vector, measured in body coordinates, is transformed into the reference frame, an error arises due to ΔC. Appendix C shows that minimizing J minimizes the upper bound on the length of that error vector. Thus, our goal is to minimize J.

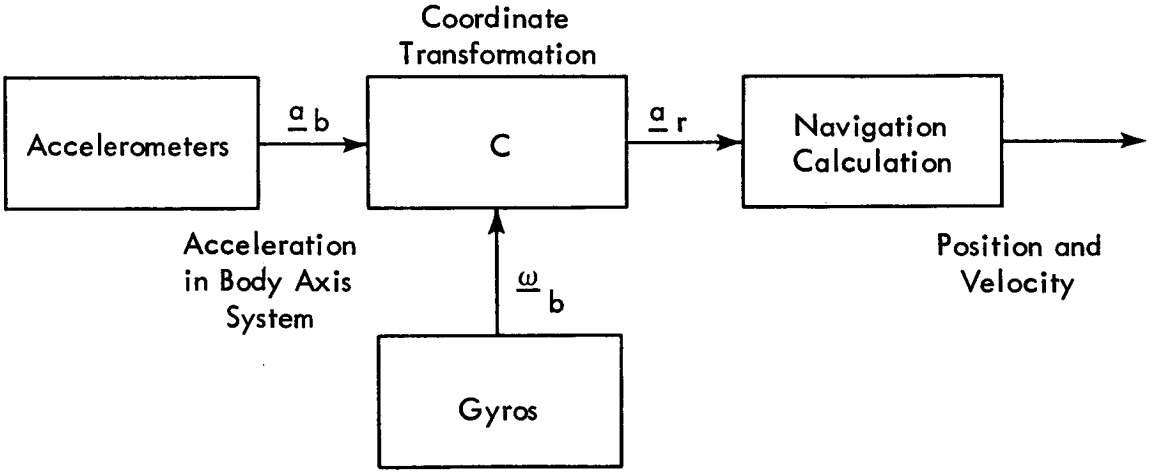

Figure 3.1-1. Strapdown Inertial Navigator.

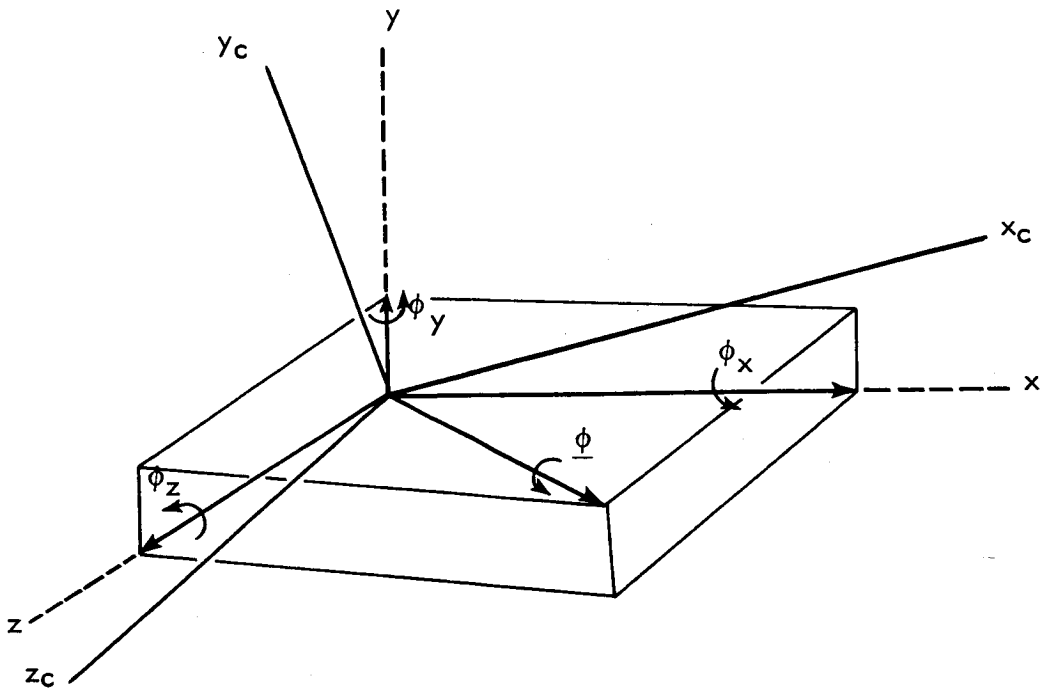

x, y, z = true coordinates

x_c, y_c, z_c = computer indicated coordinates

$\underline{\phi}$ = error rotation, from true to computed coordinates

Figure 3.1-2 Small Orientation Errors.

3.2 SYSTEM ERROR GROWTH

In order to evaluate the effect of gyro errors on system attitude error, growth of the figure-of-merit, J, must be related to the behavior of errors at the input to the transformation matrix calculation. This is done in considerably detail in Ref. 19 and the results are discussed in Appendix D herein. The relations used are conceived to be independent of the computation algorithm used to update the transformation matrix C.

3.2.1 Effect of Individual Gyro Errors

The system attitude error, as reflected in the figure-of-merit, behaves as the integral of individual gyro errors. This is discussed in Appendix D. For example, a constant error in angular rate indication by a single gyro produces a system attitude error which grows linearly with time; for this form of contribution to system attitude error, gyro drift rate is identical to system drift rate. Such behavior is not surprising and only reflects the growth of gimballed platform errors under similar circumstances. Since sizeable constant error torques are generated in single-degree-of-freedom gyros by environmental angular motion, this effect is a principal contributor to strapdown system errors.

3.2.2 Effect of Errors From Gyro Pairs

The major system attitude drift rate arising from errors in several gyros appears when two angular motion sensors generate errors which are oscillatory in nature, of the same frequency, and have a $\frac{\pi}{2}$ phase difference. Considered separately, gyro errors of this nature do not contribute growing

system attitude errors but when combined in the direction cosine matrix calculations a constant system drift rate is generated (see Appendix D). This important system error is generated because the erroneous gyro outputs are interpreted as true oscillatory angular motion about two orthogonal body axes. Motion of this kind produces a constant angular rate about a third axis, space-fixed and essentially orthogonal to the pair of body axes. The direction cosine matrix calculations imply such a vehicle motion from the incorrect gyro outputs. In terms of sinusoidal oscillatory angular rate errors a' and b' coming from a pair of gyros with input axes perpendicular, the constant system drift rate can be expressed as

$$\begin{matrix}\text{constant system} \\ \text{drift rate}\end{matrix} = \frac{a'b'}{2\nu} \sin \psi \qquad (3.2\text{-}1)$$

where ν is the frequency of the oscillations and ψ is the relative phase between them. Equation (3.2-1) expresses the major system drift rate generated by the combination of gyro errors in the system computer as it maintains an indication of the sensor package attitude. Errors of this type are frequently called "pseudo-coning" drift rates because the gyro errors causing them fool the computer into believing that the sensor package is undergoing a coning motion.

It is important to note that pseudo-coning errors can be generated by an oscillatory error from a single gyro if the sensor package is also experiencing true oscillatory motion about an axis monitored by another gyro. This combination generates one of the major system drift rates when single-degree-of-freedom gyros are used in strapdown systems. A detailed illustration is deferred until the next section but the mechanism for error growth is the same as that discussed above. The combination of properly phased true vehicle oscillation (accurately measured by the appropriate gyro) and false angular motion cause the computer to indicate a constant rate about a third axis.

3.3 SYSTEM DRIFT RATE DUE TO OUTPUT AXIS ANGULAR ACCELERATION ERRORS

When an oscillatory angular environment exists, output axis angular acceleration errors cause the major system "pseudo-coning" drift rate. When the gyros are arranged in an orthogonal triad, an angular oscillation about the input axis of one gyro can produce output axis angular acceleration errors in a second gyro. Furthermore, if the motion frequency is within the gyro bandwidth, the true oscillation and the oscillatory error have a relative phase which produces the maximum pseudo-coning drift rate.

Output Axis Error Pseudo-Coning Drift Rate from Three Gyros - Consider the error generated in the single-degree-of-freedom gyro, gyro ① of Fig. 3.3-1, by angular acceleration about the output axis. Assume the gyro triad experiences angular motion described by the vector ω shown, where the orientation of this vector has a uniform probability in three-dimensional space. Also assume that the gyros measuring the angular rates about the body-fixed axes x and z are error-free. The error torque about the output axis of gyro ① is given by

$$M_d = I_{oo}\,\dot{\omega}_z$$

$$= AI_{oo}\,\nu \sin\phi \cos\nu t \qquad (3.3\text{-}1)$$

If gyro ① has a unity transmission characteristic, this torque generates an error in the indication of body angular rate along the y or input axis of

$$e_{\omega_{b_y}} = -\frac{AI_{oo}\nu}{H} \sin\phi \cos\nu t \qquad (3.3\text{-}2)$$

The error-free gyro, measuring the component of angular rate along the z axis, indicates

$$\omega_z = A \sin\phi \sin\nu t \qquad (3.3\text{-}3)$$

small angular displacement of body axis

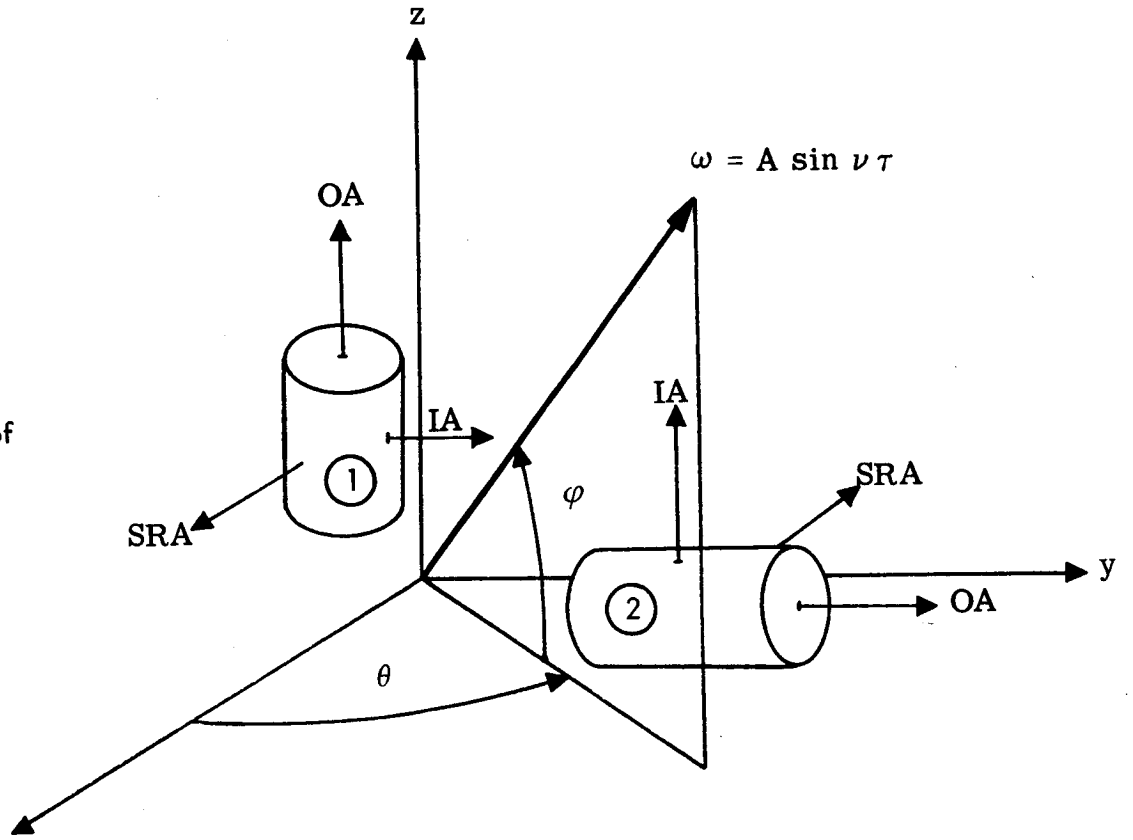

system attitude drift rate due to output axis angular acceleration error averaged over all (equally probable) orientations of ω is:

$$\frac{-A^2 I_{oo}}{3H} \cos^2 \nu\tau \qquad \text{For Gyro } (1)$$

$$\frac{A^2 I_{oo}}{3H} \cos^2 \nu\tau \qquad \text{For Gyro } (2)$$

Figure 3.3-1. A Pseudo-Coning System Attitude Error

Due to the motion ω_z, the body axes are rotated relative to a set of axes fixed in inertial space by an angle (assumed small) given by

$$\theta_z = \int \omega_z \, dt$$

$$= -\frac{A}{\nu} \sin \phi \cos \nu t \qquad (3.3\text{-}4)$$

The projection of $e_{\omega_{y_b}}$ on the stationary (inertially fixed) x axis is

$$e_{\omega_{x_I}} = -e_{\omega_{b_y}} \theta_z \qquad (3.3\text{-}5)$$

The probability density function, $p(\phi, \theta)$ for the two angles describing the orientation of the ω vector is

$$p(\phi, \theta) = \frac{\cos \phi}{4\pi} ; \quad -\frac{\pi}{2} \leq \phi \leq \frac{\pi}{2} , \quad 0 \leq \theta \leq 2\pi$$

The average projection of the false angular rate on the stationary x axis (over all orientations of the angular rate vector) is

$$-\frac{A^2 I_{oo}}{3H} \cos^2 \nu t$$

The projection contains a secular component of $-A^2 I_{oo}/6H$. This is a constant system attitude drift rate due to pseudo-coning (see Appendix D).

If an identical (not error-free) gyro, gyro ② in Fig. 3.3-1, is oriented to measure body angular rates about the z axis, the projections of the output axis angular acceleration errors on the stationary x axis from gyros

① and ② cancel. However, no such cancellation can be arranged for the pseudo-coning drift rate generated in the third gyro of the triad. It can be seen that output axis angular acceleration gyro errors cause a pseudo-coning system drift rate that has a non-zero ensemble average value. This is unique among the system drift rates generated by angular motion and results from the fact that the two oscillatory angular rates (true motion and the gyro error) which are rectified in the cosine matrix calculation result from motion about the same vehicle axis. Consequently, they always have the same correlation. Using the numbers supplied in Section 2.5 the output axis pseudo-coning error generated by oscillatory motion is 5.0 deg/hr about each vehicle axis.

3.4 CONSTANT SYSTEM ATTITUDE DRIFT RATE AS A FUNCTION OF ANGULAR OSCILLATION FREQUENCY

If angular oscillations with unity amplitude are assumed about all three axes of a single-degree-of-freedom gyro triad, constant system drift rates can be computed and the results are easily related to angular motion with different amplitudes. The constant system drift rates calculated here are those generated by one gyro (of course in the case of pseudo-coning drift rate the appropriate pair of gyros is assumed).

Unless otherwise stated, the gyro physical parameters are those presented in the example of Section 2.5. Two additional parameters, the linear damping coefficient, C, and the torque generator time constant, τ_{tg}, must be specified. Equations (2.4-23) and (2.4-24) together with the relation

$$\tau_f = \frac{I_{oo}}{C}$$

permit calculation of the natural frequency and damping ratio of the linearized model of a binary pulse torqued gyro. Lags due to the sampling nature of the gyro loop are ignored.

The constant system drift rates generated by each gyro (or gyro pair if appropriate) are computed as a function of oscillation frequency when the angular motion components are all assumed to have the same phase. The constant portion of the pseudo-coning effect due to output axis angular acceleration is dominant, followed by the anisoinertia error generated when the oscillation frequency is above the natural frequency of the wheel speed regulation loop. The anisoinertia drift rate is not plotted because it is not frequency dependent except in the vicinity of the regulation loop resonance. When the rotor inertia is coupled to the float about the spin axis (low oscillation frequency) the drift rate per gyro is negative 2 degrees per hour. For oscillations above the wheel speed regulation loop natural frequency the rotor and float are not coupled and the drift rate is 39 degrees/hour per gyro. (It should be remembered that the numbers quoted here are for angular oscillations about each axis with an amplitude of one radian per second. Since these drift rate magnitudes vary as the square of the amplitude, error growth decreases rapidly with angular rate magnitude.) In order to permit a more meaningful comparison, the pseudo-coning error is assumed to be reduced by compensation to one tenth its uncompensated value. Other error sources which generate significant frequency dependent system attitude drift rates are spin-input and spin-output cross coupling.

Figure 3.4-1 is a plot of the constant system drift rates computed for each gyro. Three values of the damping coefficient are illustrated to demonstrate the fact that the system errors are highly dependent on the gyro parameters assumed. The effect of three gyros is obtained by multiplying the ordinates shown by $\sqrt{3}$. It is emphasized that a sizeable additional drift rate resulting from anisoinertia effects is not shown. It would add almost 40 degrees/hour to the plot over most of the frequency range illustrated. Also, the pseudo-coning error is assumed compensated as described above. The shape of the curve in Fig. 3.4-1 is directly related to the transmission characteristics calculated for the chosen gyro parameters through describing function

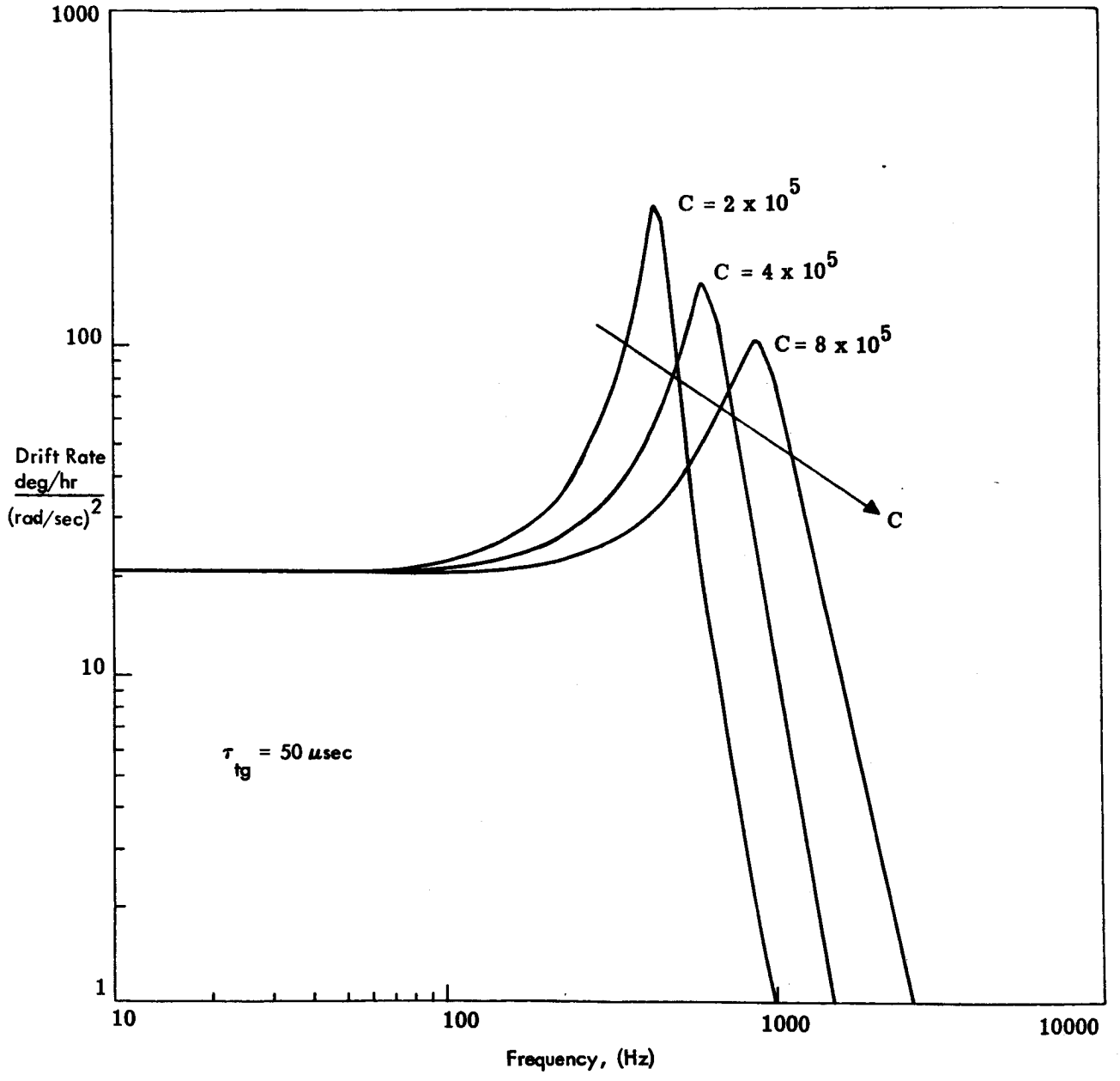

Figure 3.4-1 Constant Attitude Drift Rate Resulting From Errors in a Single Gyro (In-Phase Motion)

analysis. The drift rates reach high peaks near the gyro natural frequencies. The amplitude of the peaks is large because the damping ratios calculated for the gyro loops are very low and the errors depend on the amplitude transmission characteristics of the sensors.

Figure 3.4-2 is a plot of the constant system drift rates computed for a gyro experiencing angular rate oscillations with amplitudes of 1 rad/sec and a relative phase of $\pi/2$ radians. The only effects that generate constant gyro errors in this case are spin-input and spin-output crosscoupling. The calculations are made assuming the oscillations about the input and output axes are in phase and lead the oscillation about the spin axis by one quarter period. The dominant contribution is made by spin-input crosscoupling and is largest at frequencies near the gyro natural frequency. Because the parameters selected provide low damping ratios, the amplitude in this region is large. Calculation of a strapdown system drift rate using Fig. 3.4-2 is not straightforward because the relative phase between oscillations described above cannot be experienced by all three strapdown gyros simultaneously. Scaling the results for different oscillation amplitudes is accomplished in the same manner as for the conditions represented in Fig. 3.4-1.

When the co-spectral and quadrature spectral densities* are known for random angular rates about vehicle axes, Figs. 3.4-1 and 3.4-2 can be used to determine the RMS system drift rate generated by a triad containing this particular gyro. Of course, anisoinertia errors must be added because they are not shown in the figures. The procedure is to divide the appropriate spectral densities into sufficiently small segments, multiply by the ordinate shown in Fig. 3.4-1 or 3.4-2 at the center frequency of each segment and add the results.

*See Ref. 13, p. 33.

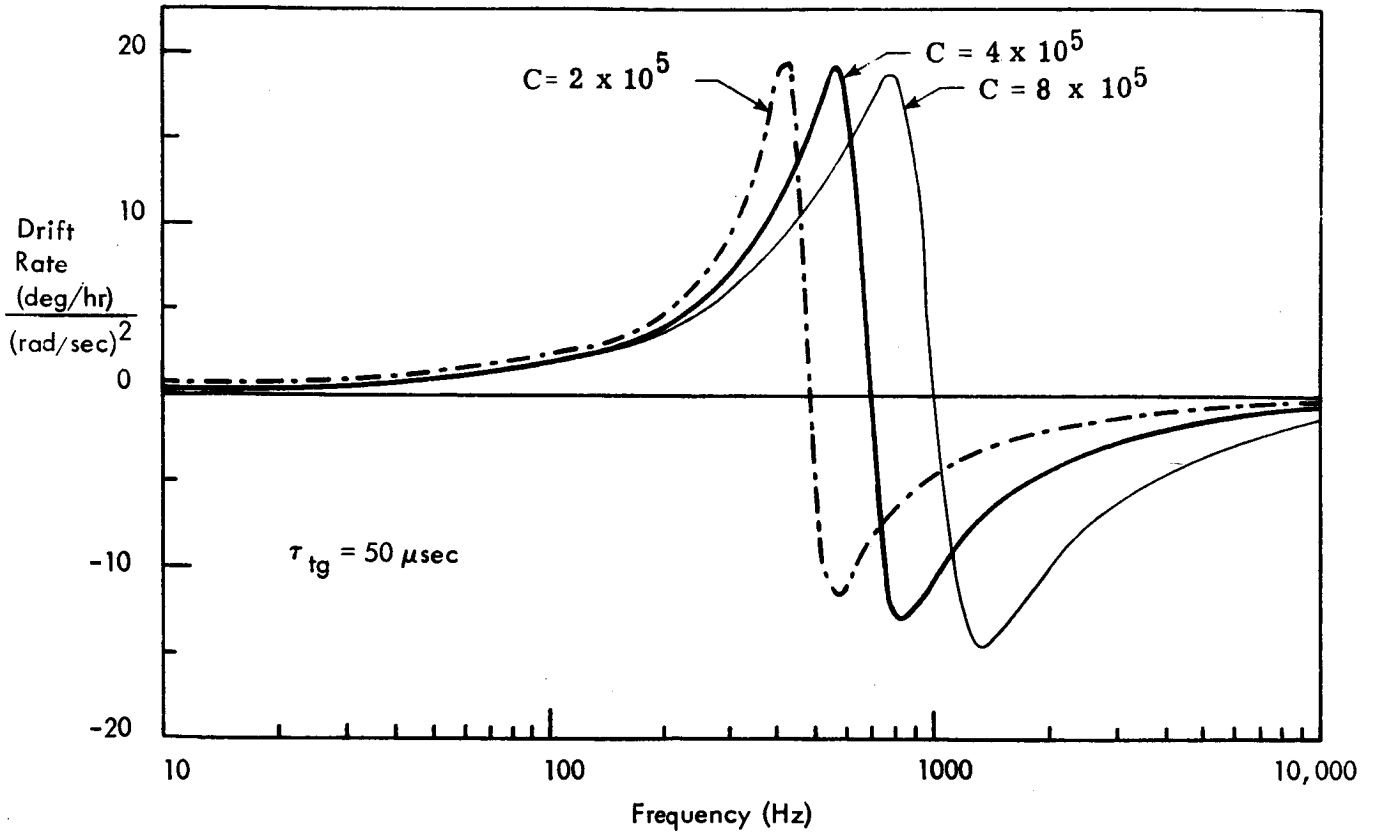

Figure 3.4-2 Constant Gyro Drift Rate Resulting From Angular Motion With $\pi/2$ Phase Difference

PRECEDING PAGE BLANK NOT FILMED.

4. COMPENSATION OF GYRO ERRORS

4.1 MOTION INDUCED ERRORS

System drift rates due to motion-induced gyro errors are a serious problem in strapdown inertial systems. Several methods for reducing these errors by measuring the motion environment and applying counter torques as corrections to the single-degree-of-freedom gyro are treated (see Fig. 4.0-1).

4.1.1 Compensation Without Additional Measurements

It is possible to infer all the motion information that is needed to compute the major error torques on single-degree-of-freedom gyros directly from the gyro outputs themselves. In some cases, such as the recovery of angular acceleration information from the output of a pulse torqued gyro, considerable filtering is required. However, under the assumption that all derivatives and necessary integrals of angular rates can be recovered accurately, outputs from the essential inertial sensors can be used to compute error torques and corrective torques can be applied. This is an attractive approach for reducing strapdown system drift rate. Unfortunately, this scheme closes new information loops containing two or more of the strapdown gyros. Chapter 4 of Ref. 19 demonstrates that when output axis angular acceleration errors are compensated in the manner described above the system is stable for a reasonable set of gyro parameters. However, when crosscoupling errors are compensated using motion information from the three essential gyros only (and also measuring float angles) stability is best established by a detailed simulation. If more than one kind of gyro error is to be compensated in this way, stability analysis is further complicated. The approach described offers considerable advantages over others in terms of reliability and system weight

and power requirements. However, in the absence of simulation results indicating stability and accuracy we will concentrate on other means for reducing motion generated gyro errors.

Another technique proposed (Ref. 16) uses signals and instruments already available without generating closed loops. The electrical suspension systems of single-degree-of-freedom gyros provide the forces and torques necessary to cause the gimbal-rotor combination to follow case (and therefore vehicle) motions. If one set of restraint devices provides forces only in the plane containing the gyro input and output axes, the difference between restraint forces on the two ends of the gimbal can be used to deduce angular acceleration about the gyro spin reference axis. Thus one gyro's suspension system can be used to indicate angular acceleration about the output axis of another gyro. This technique relies heavily on the absence of cross-compliance in the suspension system.

4.1.2 External Measurement Devices

Motion-induced gyro errors can be compensated through the use of additional motion sensing devices. Two approaches are discussed below: the use of three additional gyros paired with the essential sensors of the strapdown gyro triad and use of specially designed sensors to measure the pertinent motion parameters.

Redundant Sensors - The use of three additional gyros, paired with members of the primary gyro triad, permits significant reduction of motion-induced errors through simple averaging of the outputs. Figure 4.1-1 illustrates this scheme. Initially, it is assumed that the gyros paired have identical physical parameters and they offer identical transmission characteristics between moments applied to the gimbals and the point at which their outputs are averaged. Also their initial states at the start of motion are assumed to be the same. Each gyro pair has nominal input axes aligned parallel to provide redundant measurement of angular motion about that axis. Their outputs are averaged and, with the proper relative orientation of spin reference axes, certain gyro errors are cancelled or statistically reduced by the averaging process.

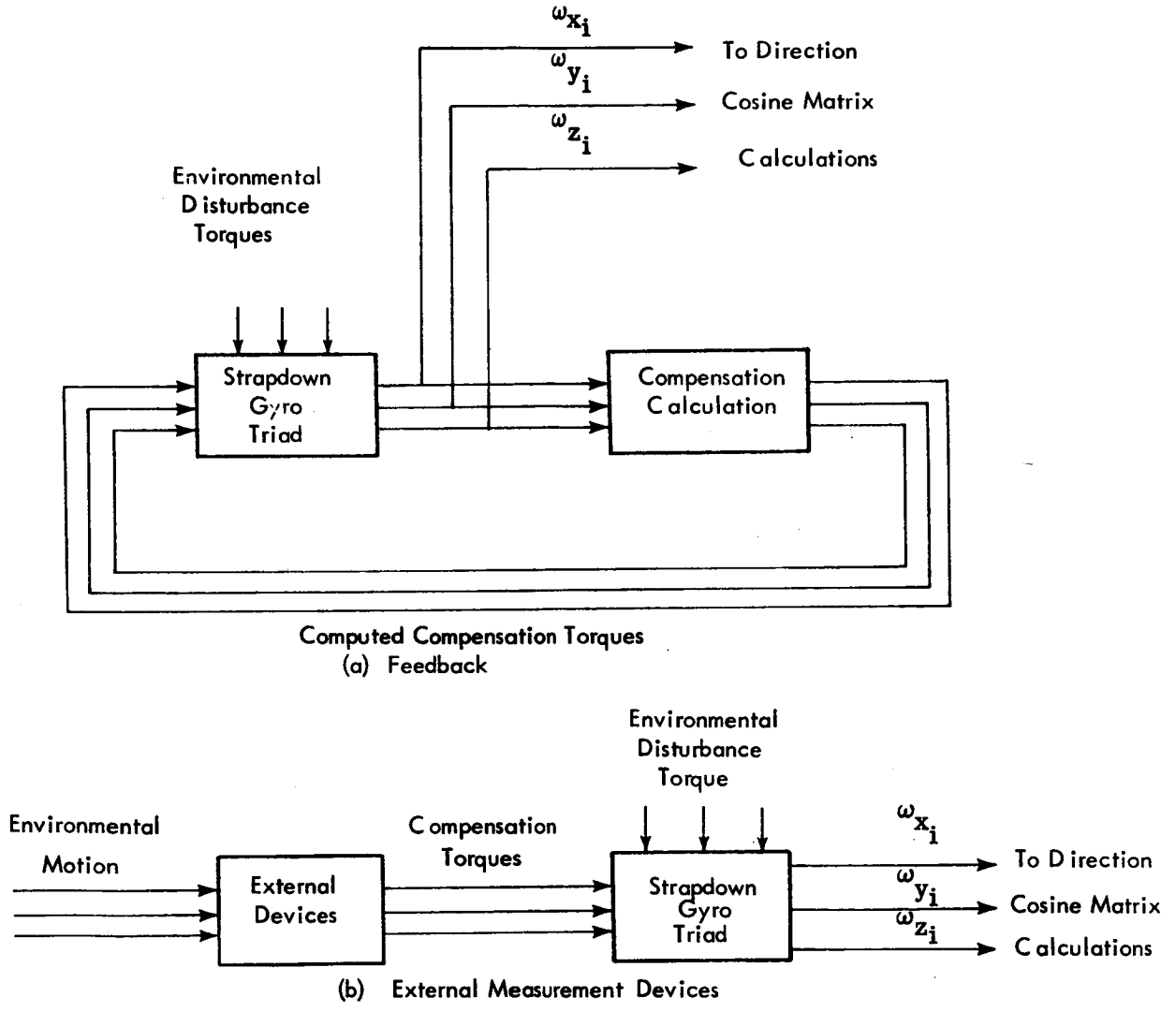

Figure 4.0-1 Two Schemes for Reducing Gyro Errors Through the Application of Counter-Torques

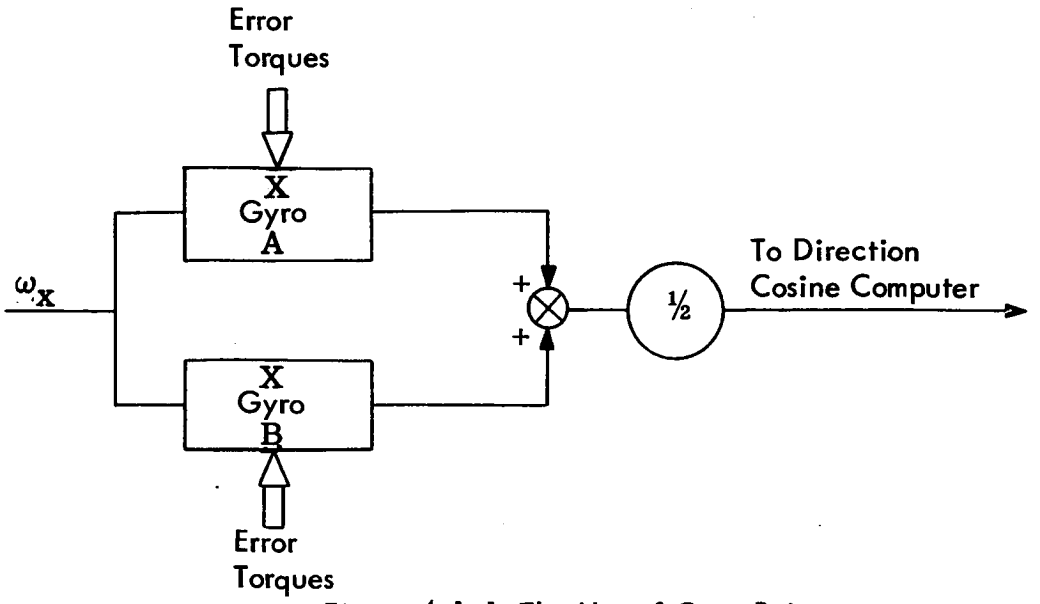

Figure 4.1-1 The Use of Gyro Pairs

It was demonstrated in Section 2.5 (Table 2.5-2) that gyro errors generated by interaction between the gyro motion environment and necessary physical characteristics of the gyro can be much larger than those produced by imperfect construction and operation. It is in reducing these errors that the pairing of identical gyros has its greatest value. If the two sensors are oriented as shown in Fig. 4.1-2, output averaging provides cancellation of several important angular motion induced gyro errors. For example, consider spin-input cross-coupling errors. An angular rate about IA will cause the gimbals of the two gyros to rotate through the same angle but in opposite directions. A simultaneous angular rate about one of the gyros' spin reference axes (remember they are both experiencing the same vehicle motion) provides a positive error torque on one gyro and a negative torque of equal magnitude on the other. When the effects of the two error torques appear at the outputs of the identical gyros and are added they cancel. In a similar manner, the errors due to anisoinertia-rotor-speed loop effects, output axis angular acceleration and anisoinertia cross-coupling, for that portion of gimbal angle which results from output axis angular acceleration, are removed. Assuming perfect cancellations, the use of three identical gyro pairs with their outputs

averaged reduces the RSS error due to oscillatory motion provided by the sources outlined in Table 2.5-2 from 9.9 deg/hr to 2.6 deg/hr. The latter drift rate is almost entirely a result of torquer nonlinearity.

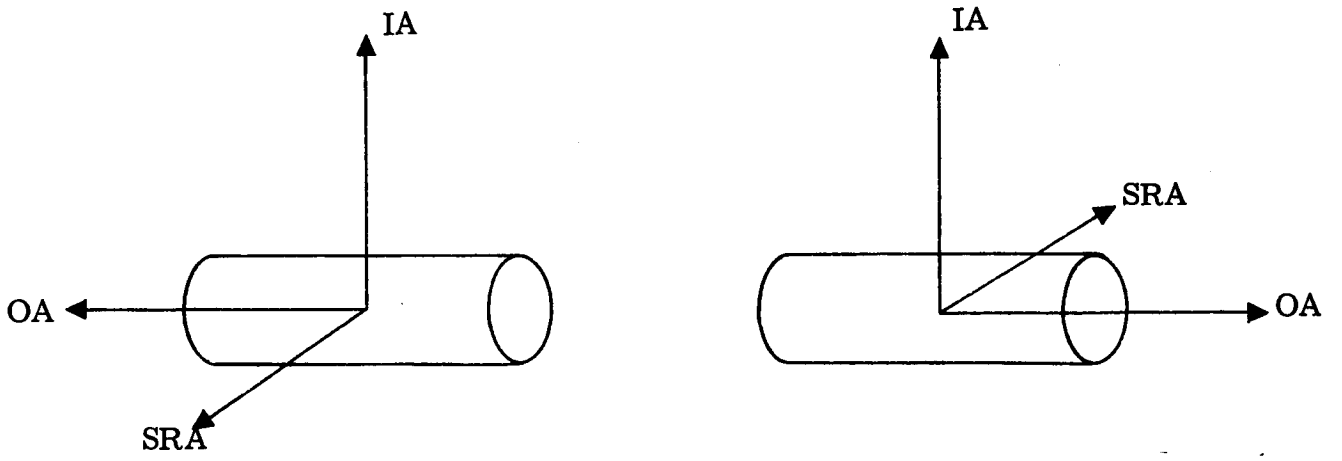

Figure 4.1-2 Orientation of Gyro Pairs

In addition to reducing the motion-induced gyro errors caused by necessary physical parameters, all the errors generated by imperfect construction are averaged. Consequently, RMS errors due to mass unbalance, anisoelasticity, gimbal products of inertia, etc., are reduced by a factor of $1/\sqrt{2}$ when the outputs of two identical gyros are averaged.

The effect of mismatching the two gyros is easily demonstrated. If the difference in effective anisoinertia is designated $\delta\,\Delta I$ and a difference in I_{oo} is $\delta\, I_{oo}$, the uncompensated portion of anisoinertia and output axis acceleration errors for this scheme is represented as a drift rate:

$$\text{drift rate due to mismatch} = 1/2\,(\delta\Delta I\,\omega_i\omega_s + \delta\, I_{oo}\,\dot{\omega}_o) \qquad (4.1\text{-}1)$$

In terms of the uncompensated drift rate caused by these two major error sources, the drift rate due to mismatch is the same fraction as the ratio of mismatch in a particular parameter to the nominal value of that parameter. For example, if $\delta \Delta I/\Delta I$ and $\delta I_{oo}/I_{oo}$ are always less than 1% the compensated drift rate from a pair of gyros (as a result of anisoinertia and output axis acceleration) is always less than 1% of the uncompensated value. Since accurate knowledge of such basic sensor parameters as gyro gain is always important, a mismatch in these quantities is apt to be much smaller than in inertia terms. As in the case of errors due to imperfect gyro construction discussed earlier, RMS errors due to mismatch of parameters do add directly and the total mismatch drift rate behaves as the root sum square of its components.

If the two identical sensors are misaligned, perfect cancellation of errors will not occur. For example, net misalignment angles about the spin and input axes of 10 $\widehat{\text{sec}}$ will generate an error in the averaged gyro outputs of

$$\begin{matrix}\text{misalignment} \\ \text{drift rate}\end{matrix} = 5.0 \times 10^{-5} \frac{I_{oo}}{H} (\dot{\omega}_s - \dot{\omega}_i) \qquad (4.1\text{-}2)$$

It can be seen from Eq. (4.1-2) that misalignment errors will be a small fraction of the corresponding uncompensated drift rates.

Specially Designed Measurement Devices - As an alternative to the use of redundant sets of gyros, several means for measuring angular motion with additional devices or with modifications to gyros have been proposed. In all cases it is anticipated that the measurements made are used to provide either corrective torques on the gimbals or corrections directly to the outputs. Figure 4.1-3 illustrates the application of corrections to a gyro based on measurements of the environment (and in the case of crosscoupling errors, of the gimbal output angle). Part (a) of the figure demonstrates correction of the gyro output. Figure 4.1-3(b) illustrates the application of correction torques in the form of pulses. This makes use of the very accurate pulsing electronics and torquer already available in the instrument. The use of analog corrective

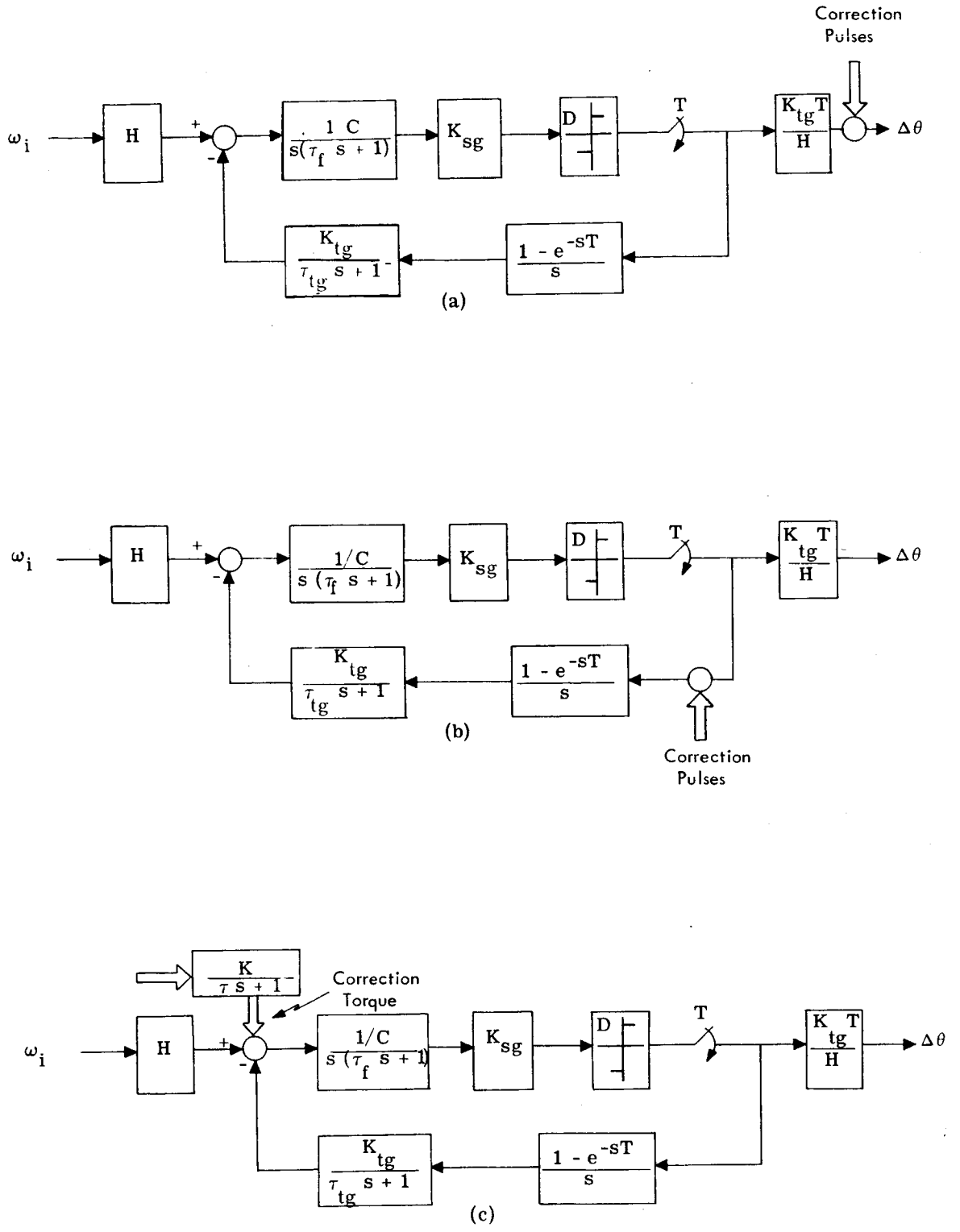

Figure 4.1-3 Gyro Corrections Based on Measurements of the Environment

torquing is represented by Fig. 4. 1-3(c). The possibility of using a separate set of torquer windings for this scheme is indicated by including an additional block for torquer dynamics. Both of the latter approaches offer the advantage of reducing the gimbal output angle (hence crosscoupling errors) as a consequence of applying corrections.

Output axis angular acceleration can be compensated using an instrument, similar in construction to a floated gyro, but having a float that is a homogeneous cylinder (Ref. 15). This instrument has signal and torque generators, and the float is held to small off-null angles by a tight rebalance loop. The theory of operation is that, if this unit is mounted rigidly to a single-degree-of-freedom gyro with output axes parallel, then the signal applied to the torque generator of the compensator float is proportional to the output-axis error torque experienced by the gyro. Thus, the same signal can be applied to the gyro for compensation purposes. This scheme, and others involving angular accelerometers having an output axis moment of inertia different from the gyro being compensated are conceptually identical with the use of matched gyro pairs described above. Analysis of errors in the compensated gyro output is the same as for paired gyros.

Several of the important angular motion induced gyro errors are generated by angular rates about the spin and input axes. In order to compute corrective torques, small additional rate gyros can be installed. The necessary accuracy of these rate gyros can be determined. For example, if two additional rate gyros are used to measure the angular rates ω_i and ω_s experienced by a primary gyro, the residual drift rate due to anisoinertia is given by

$$\text{residual drift rate} = (\epsilon_1+\epsilon_2)\,\omega_{\Delta I}+\left(\frac{I_{ii}-I_{ss}}{H}\right)b_1 b_2 \qquad (4.1\text{-}3)$$

where ϵ_1 and ϵ_2 are scale factor errors (in fractional form) in the two gyros and b_1 and b_2 are corresponding bias errors. The symbol $\omega_{\Delta I}$ represents the

uncompensated anisoinertia error. It can be seen from Eq. (4.1-3) that scale factor errors in the additional rate gyros of 0.5% or less are needed to reduce the anisoinertia error in the compensated gyro output by two orders of magnitude. For the gyro described in Section 2.5, the product of rate gyro bias errors, $b_1\, b_2$ must be less than 10^8 $(\text{deg/hr})^2$ to prevent generation of an additional drift rate of 0.01 deg/hr by this compensation technique. Obviously, bias errors in the additional sensors will not harm the accuracy of compensation in this case.

Crosscoupling errors can be compensated by applying a corrective torque proportional to a measured float angle and the angular rate, ω_s, indicated by an additional rate gyro. In this case, the compensation errors are given by

$$\begin{matrix}\text{crosscoupling} \\ \text{compensation} \\ \text{error}\end{matrix} \cong \left(\epsilon + \frac{\delta\alpha_o}{\alpha_o}\right) \omega_{\alpha_o} \qquad (4.1\text{-}4)$$

where ϵ is the scale factor error in the rate gyro and the symbol ω_{α_o} represents the uncompensated crosscoupling error. The ratio $\delta\alpha_o/\alpha_o$ is effectively a scale factor error in measuring the float angle. From Eq. (4.1-4) it is reasonable to expect that crosscoupling errors can be reduced by several orders of magnitude through this form of compensation.

4.1.3 Summary

Three approaches to the correction of gyro errors have been discussed. One uses indications of the angular motion environment available from the outputs of the basic gyro triad, while another requires three additional rate gyros and three angular accelerometers. Both of these schemes use the angular motions to compute correction torques for application about the output axes of the three essential gyros. A third method uses three additional gyros, identical with the original three, and averages their outputs to remove several

major motion induced errors. Computer requirements are essentially the same for the first two approaches, but the calculation load is much less when paired gyros are used.

The techniques employing additional measurement devices are shown to be capable of reducing major motion-induced gyro errors by several orders of magnitude. Unfortunately, the inclusion of several more angular motion sensors in the strapdown system increases its cost and weight while reducing reliability. The first approach, using the outputs of the basic gyro triad to compute torque corrections, presents a difficult stability analysis problem but adds little to the complexity of the strapdown sensor package. For that reason it is recommended that the stability and accuracy analysis of a gyro triad compensated in this manner be thoroughly investigated through simulation.

4.2 LIMIT CYCLE ERRORS

4.2.1 System Errors Generated by Limit Cycles

The limit cycle characteristics of binary pulse torqued gyros are a source of large system errors if they are allowed to pass unhindered into the direction cosine matrix calculations. For example an n, n mode limit cycle will produce an oscillatory attitude error with a triangular waveform. The first component of the Fourier expansion of this oscillation is a sinusoid with the same period as the limit cycle and an amplitude of $\frac{8}{\pi^2}$ times the peak value of the triangular waveform. The peak angular error is given in terms of the angle increment $\Delta\theta$ and the mode number as

$$\text{peak angular error} = \frac{n\Delta\theta}{2}$$

The first term in the harmonic expansion of the limit cycle angular error can be written as

$$\text{angular error} \cong \frac{4n\Delta\theta}{\pi^2} \sin(\omega_\ell \tau + \rho) \qquad (4.2\text{-}1)$$

However,

$$2n = \frac{2\pi}{T\omega_\ell}$$

and

$$\Delta\theta = \omega_{i_{max}} T$$

Equation (4.2-1) can be expressed in terms of the maximum input angular rate, $\omega_{i_{max}}$, and the limit cycle frequency:

$$\text{angular error} \cong \frac{4}{\pi} \frac{\omega_{i_{max}}}{\omega_\ell} \sin(\omega_\ell \tau + \rho) \qquad (4.2\text{-}2)$$

If two identical gyros experience limit cycles at the same frequency with $\pi/2$ phase difference, the erroneous indication of constant angular rate about the third axis is

$$\text{system drift rate} = 1/2 \left(\frac{4}{\pi} \frac{\omega_{i_{max}}}{\omega_\ell} \right)^2 \omega_\ell$$

$$= \frac{8}{\pi^2} \frac{\left(\omega_{i_{max}}\right)^2}{\omega_\ell} \qquad (4.2\text{-}3)$$

Equation (4.2-3) demonstrates the inverse relationship between potential limit cycle induced system drift rates and the limit cycle frequency. When

$$\omega_\ell = 3.18 \times 10^3 \text{ rad/sec (see Section 2.4.2)}$$

and

$$\omega_{i_{max}} = 1 \text{ rad/sec}$$

the maximum potential system drift rate due to out-of-phase limit cycles in only <u>two</u> of the three gyros is

$$\text{potential system drift rate} = 53 \text{ deg/hr}$$

(Consideration of the next term in the harmonic expansion provides an additional drift rate of only 0.2 deg/hr.) Clearly, errors of this magnitude must not be permitted to occur as a result of rebalance loop limit cycles. Equation (4.2-3) suggests two means to keep potential system errors due to limit cycles small (if they are permitted to enter the direction cosine calculations). If the vehicle is known to be operating in a benign angular motion environment, reduction of $\omega_{i_{max}}$ will reduce these errors. It may be desirable to provide several maximum gyro rebalance torque levels (equivalent to several values of $\omega_{i_{max}}$). In addition, it is desirable to get the highest limit cycle frequency possible through the use of dynamic compensation in the gyro loop (see Section 4.2.3).

A third approach to reducing this error is to cause different limit cycle frequencies to occur in each of the three gyros. When the difference between two limit cycle frequencies is small compared to the cycle frequencies:

$$\frac{\Delta\omega}{\omega_\ell} \ll 1$$

the maximum potential system attitude error is given by

$$\text{peak attitude error} \cong \frac{1}{\Delta\omega}\frac{8}{\pi^2}\frac{\left(\omega_{i_{max}}\right)^2}{\omega_\ell} \qquad (4.2\text{-}4)$$

Notice that the approximate expression in Eq. (4.2-4) is simply Eq. (4.2-3) divided by the difference between limit cycle frequencies. For the conditions described above, it is only necessary to separate the limit cycle frequencies by 2.5 Hz in order to keep the peak system error described in Eq. (4.2-4) below 3.6 $\widehat{\text{sec}}$. Frequency separation is an attractive approach to bounding system attitude errors from gyro limit cycles. Using Eq. (2.4-11), it is determined that any difference in the product $\tau_{tg}\,\tau_f$ of more than 1% between the two gyros will cause a limit cycle frequency difference of more than 2.5 Hz in the case under consideration. (Of course the effect of sampling is ignored in this calculation.)

4.2.2 Limit Cycle Trapping

To the extent that the limit cycle is well defined it is possible to remove this oscillatory error by filtering the gyro output before it enters the transformation matrix computation. In particular, if an n, n mode limit cycle is known to be the only one which occurs in the absence of gyro input, summation of the gyro output over 2n sample periods will remove the limit cycle error. Since indications of angular motion about the gyro input axis appear as modifications to the limit cycle output mode these will not be removed by the summation if they occur at frequencies well below that of the limit cycle.

Any changes in the gyro output mode which are symmetric and occur entirely within a particular set of 2n periods will not appear at the input to the computer. Information can be lost in this way. Any alteration of the gyro output limit cycle mode that has a frequency characteristic higher than that of the limit cycle is partially filtered out by this scheme.

Errors Resulting From Trying to Trap the Wrong Limit Cycle—As stated above, entrapment of erroneous gyro outputs requires a precise knowledge of the limit cycle frequency. If the limit cycle does not occur at the expected frequency serious system errors can result. For example, consider summation over 2n gyro sample periods. Suppose the limit cycle has a mode characterized by n' positive outputs followed by n' negative pulses. The error in computer input resulting from imperfectly trapping the limit cycle appears as follows:

n' even		n' odd	
Input Number	Error	Input Number	Error
1	$\lvert n-n'\rvert\Delta\theta/n$	1	$\lvert n-n'\rvert\Delta\theta/n$
2	$\lvert n-n'\rvert\Delta\theta/n$	2	$\lvert n-n'\rvert\Delta\theta/n$
.	.	.	.
.	.	.	.
.	.	.	.
$n'/2\lvert n-n'\rvert$	$\lvert n-n'\rvert\Delta\theta/n$	$(n'/2\lvert n-n'\rvert)-1$	$\lvert n-n'\rvert\Delta\theta/n$
$(n'/2\lvert n-n'\rvert)+1$	$-\lvert n-n'\rvert\Delta\theta/n$	$n'/2\lvert n-n'\rvert$	0
.	.	$(n'/2\lvert n-n'\rvert)+1$	$-\lvert n-n'\rvert\Delta\theta/n$
.	.	.	.
.	.	.	.
$n'/\lvert n-n'\rvert$	$-\lvert n-n'\rvert\Delta\theta/n$	$n'/\lvert n-n'\rvert$	$-\lvert n-n'\rvert\Delta\theta/n$

Correct and incorrect limit cycle trapping are illustrated in Fig. 4.2-1 for the case where no input motion is taking place.

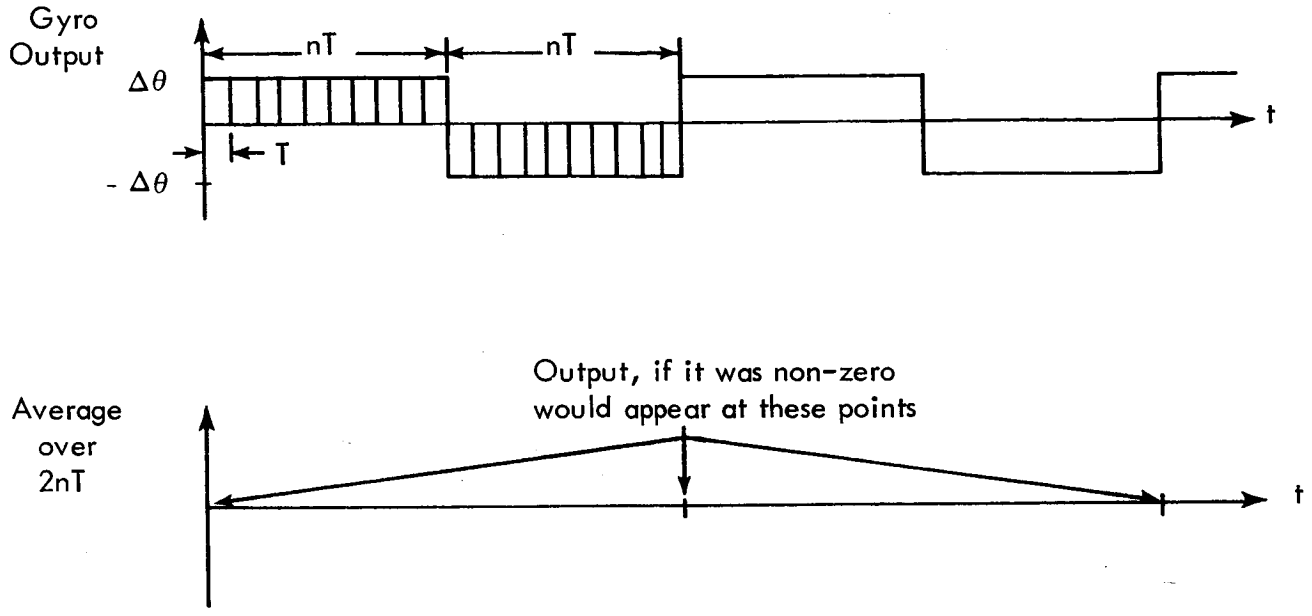

(a) correct limit cycle trapping

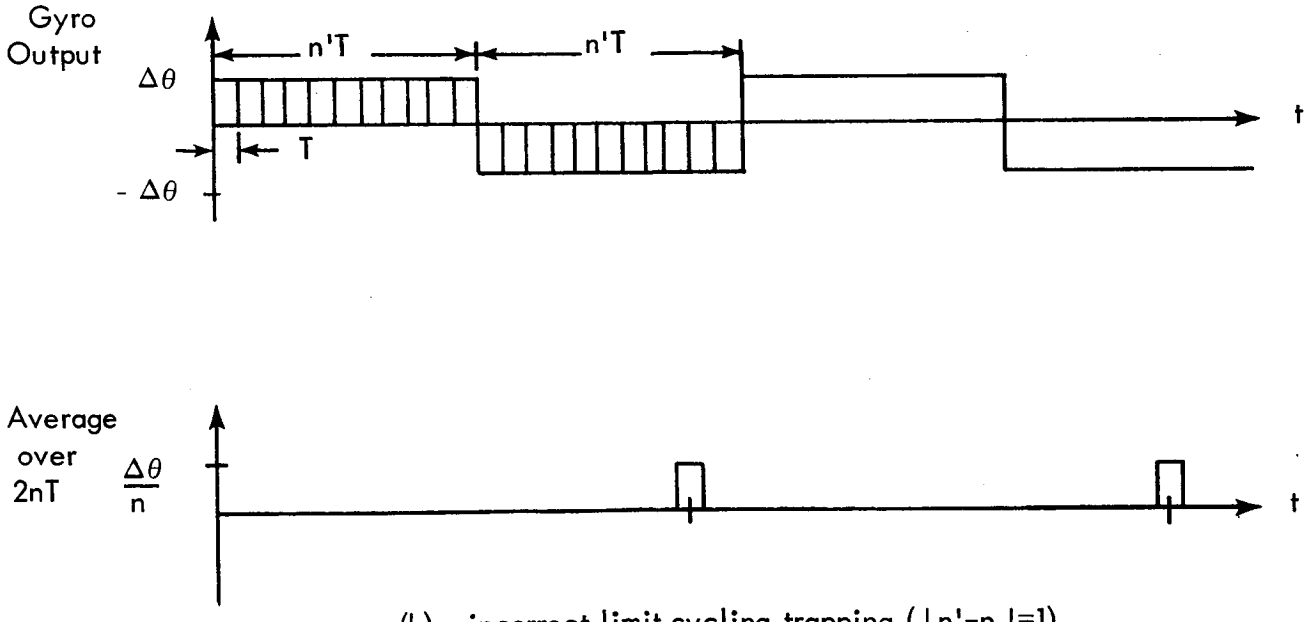

(b) incorrect limit cycling trapping ($|n'-n|=1$)

Figure 4.2-1 Illustration of Incorrect Limit Cycle Trapping

The erroneous angular oscillations generated have a frequency of $\omega_\ell \omega_\ell' T/\pi|n-n'|$. When n' is even and $|n-n'| = 1$, the first component of the Fourier series for the triangular attitude error oscillation is $2n'\Delta\theta/n\pi^2$. For all but very small values of n' the amplitude is essentially the same when n' is odd (i.e., $2(n' - 1)\Delta\theta/n\pi^2$). When n' is even, a potential constant system attitude drift rate due to similar incorrect entrapment about two orthogonal vehicle axes is given by

$$\text{system drift rate} = 1/2 \left(\frac{2}{\pi^2} \frac{n'}{n} \Delta\theta\right)^2 \frac{\omega_\ell \omega_\ell' T}{\pi} |n-n'|$$

$$= \frac{2}{\pi^5} \left(\frac{n'}{n}\right)^2 \omega_\ell \omega_\ell' \left(\omega_{i_{max}}\right)^2 T^3 |n-n'| \qquad (4.2\text{-}5)$$

Assuming

$$\frac{n'}{n} \cong 1, \quad |n-n'| = 1$$

and

$$\omega_\ell \cong \omega_\ell' = 3.18 \times 10^3 \text{ rad/sec}$$

Equation (4.2-5) provides the relation illustrated in Fig. 4.2-2 between system drift rate due to incorrect limit cycle trapping and the sample period T.

4.2.3 Dynamic Compensation of the Gyro Loop

From the point of reducing system errors caused by gyro limit cycles, high values of ω_ℓ are desireable. In addition, small limit cycle periods will reduce potential acceleration resolution errors at critical moments such as booster burnout. Also, high limit cycle frequencies diminish float angle excursions, thereby reducing uncompensated crosscoupling errors. Dynamic compensation within the rebalance loop is useful in raising

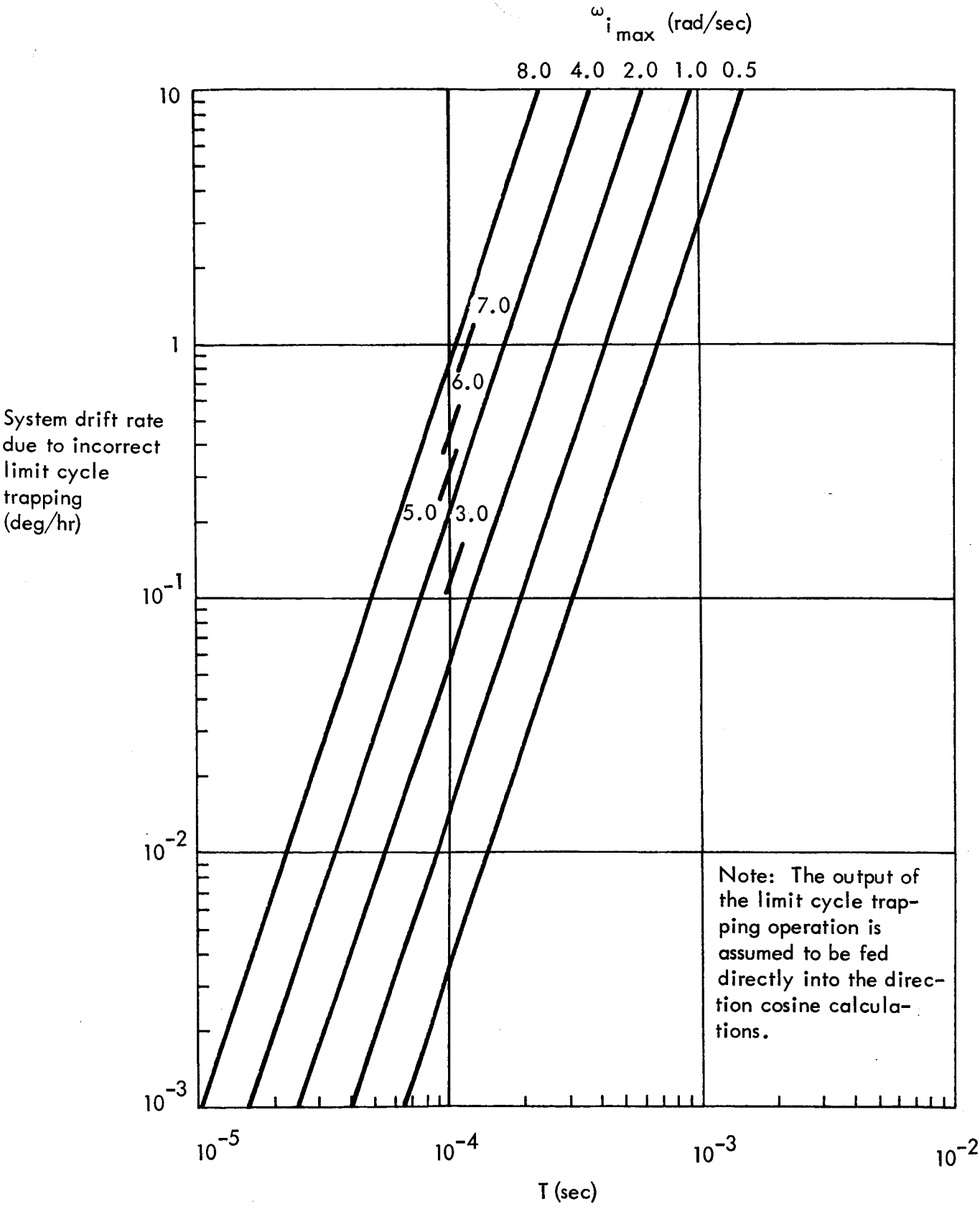

Figure 4.2-2. Maximum Potential System Drift Rate From Incorrect Limit Cycle Trapping ($|n'-n| = 1$)

the moding frequency of pulse torqued gyros. However, with the exception just noted, it does not help remove the major motion-induced gyro errors. Table 2.5-2 establishes the fact that very large system drift rates are generated by angular motions whose effects are rectified by gyro physical parameters (such as anisoinertia) and appear as constant error torques on the gimbal output axis. No compensation of the gyro loop can prevent the establishment of this torque and no practical gyro will prevent its appearance as a constant angular rate error at the gyro output unless a counter-torque is applied.

Compensation within the rebalance loop can help reduce gyro output errors by changing the transmission characteristics of the gyro in order to attenuate the effects of error torques on the basis of their frequency. Unfortunately, many of the serious error torques occur in the same range of frequencies as the true input angular rate the gyro must measure. Therefore reduction of errors at the gyro output by frequency filtering implies the creation of new errors because some of the true input motion is thrown away. If, in any band of frequencies, the error torques are considerably larger than those generated by input motions (for example, if the gyro rotor is not properly balanced), loop compensation to reduce transmission at those frequencies might be useful. In addition, proper compensation of the electronic rebalance loop around a single-degree-of-freedom gyro can increase its bandwidth and prevent high frequency vehicle coning motion from going undetected.

Location of Compensation Within the Rebalance Loop - Many potential locations exist for dynamic compensation within a gyro rebalance loop. Figure 4.2-3 illustrates four of them. In general, any compensation occuring between the sampling operation and the zero order hold shown is digital in nature, while the remainder are analog. Figures 4.2-3(a) and 4.2-3(b) illustrate digital compensation in the feedback and forward signal paths respectively. Both approaches can be used to change the transmission characteristics of the gyro and if linear compensation is used a large body

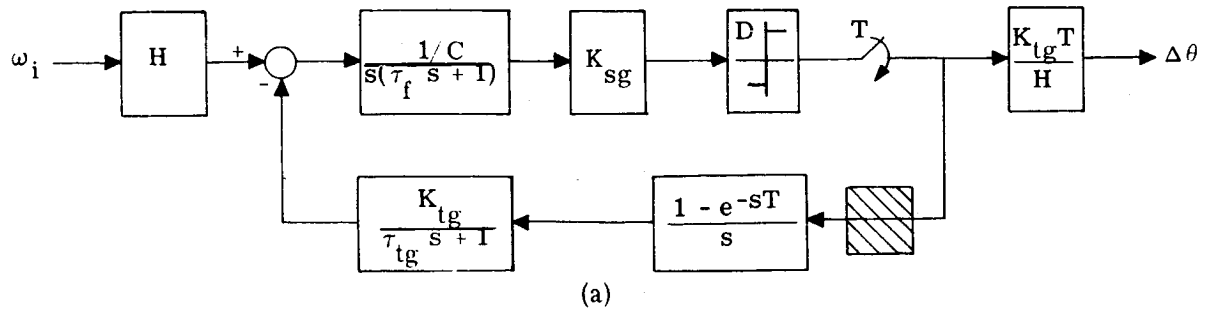

(a)

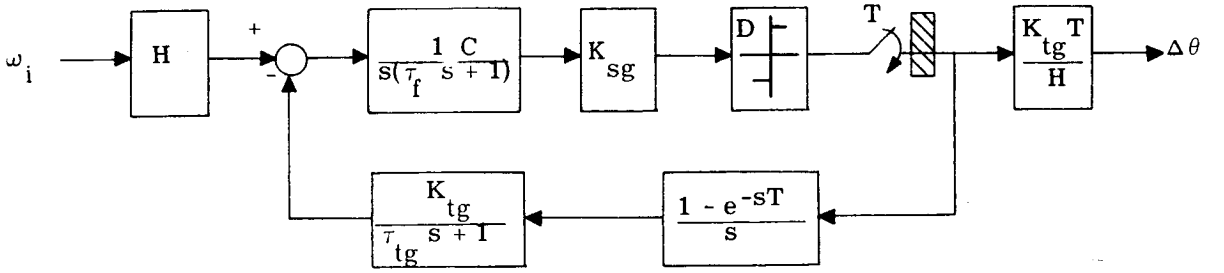

(b)

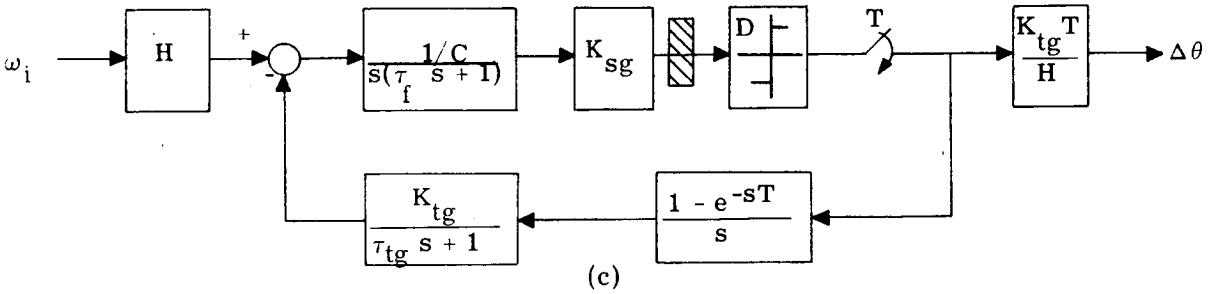

(c)

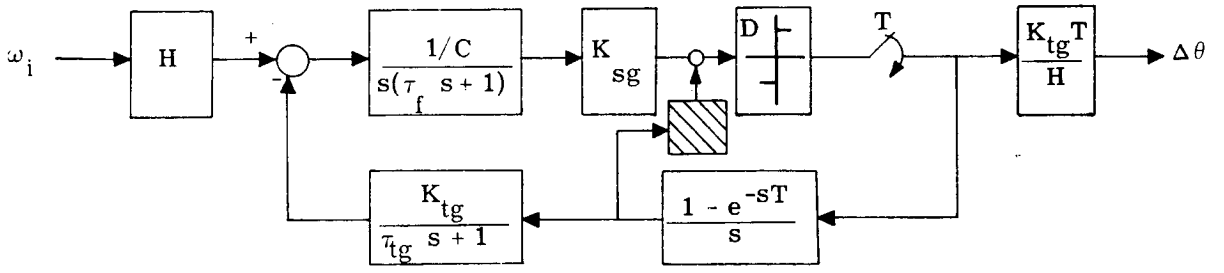

(d)

Figure 4.2-3 Dynamic Compensation of the Gyro Loop (a and b show digital compensation, c and d show analog compensation)

of knowledge exists to aid the designer (see Ref. 17). The feedback path compensation shown can also be analog in nature. In that case it would be located to the left of the zero order hold in the diagram. Both of these forms of loop compensation are used to change the limit cycle characteristics of pulse rebalanced gyros. (See Appendix E for a discussion of limit cycle compensation.)

The third loop in the figure illustrates a possible location for compensation to remove an error that occurs over a narrow frequency band. It is essentially a notch filter placed to reduce the effective float transmission characteristic at that frequency. Finally, an alternative signal path for compensation is illustrated. This approach is suggested (Ref. 18) as a means for reducing limit cycle mode length in binary torqued gyros.

4.2.4 Application of Dither Signals At the Nonlinearity Input

One suggested approach to controlling limit cycle frequency and reducing system errors caused by nonlinear torquing electronics is to introduce a deliberate periodic signal at the input to the nonlinear detection circuit (see Ref. 21). The periodic signal, d(t), frequently called dither, can be a sinusoid, triangular wave, sawtooth, etc. The gyro is still torqued according to the nonlinearity output which is sampled every T seconds. If the amplitude and frequency of the dither signal are well chosen, averaging the nonlinearity output over one dither cycle will produce an essentially linear indication of float angle.

Figure 4.2-4 illustrates use of a triangular dither waveform. If the float angle varies slowly relative to the dither frequency, the average binary nonlinearity output (over one dither period) depends on the float angle as shown in Fig. 4.2-4(c). A similar relation results for a ternary nonlinearity in a well scaled rebalance loop, that is, one with sufficient torquing level. In that case the linear slope changes at the input values $\pm (A_d - \delta)$.

The introduction of a periodic signal at the input to the nonlinear detection logic of a pulse torqued gyro establishes a controllable period for averaging the output pulses. As in the case of limit cycle trapping, signals at frequencies below that of the dither will be attenuated. On the other hand the

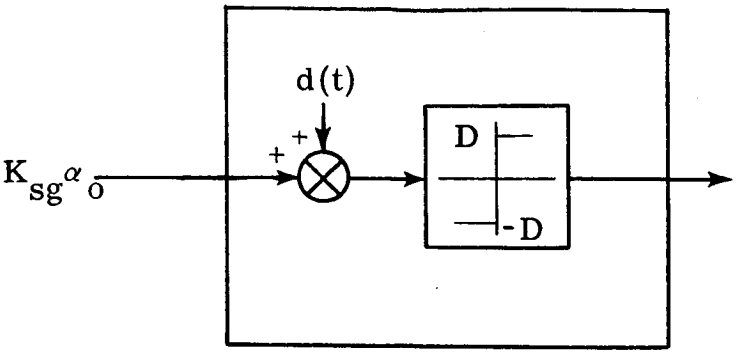

(a) introduction of dither signal

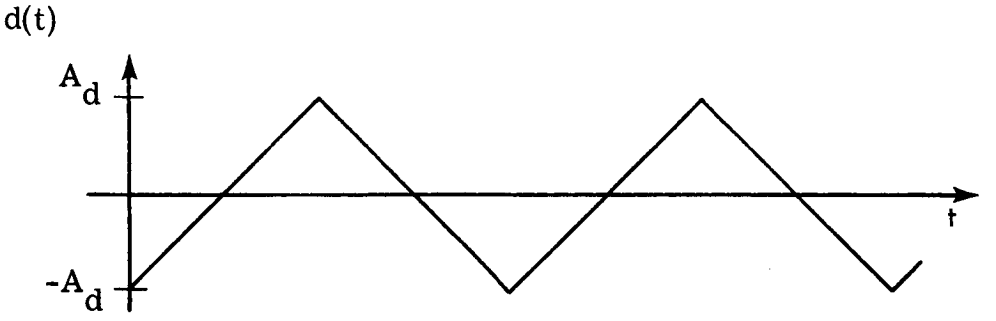

(b) triangular dither waveform

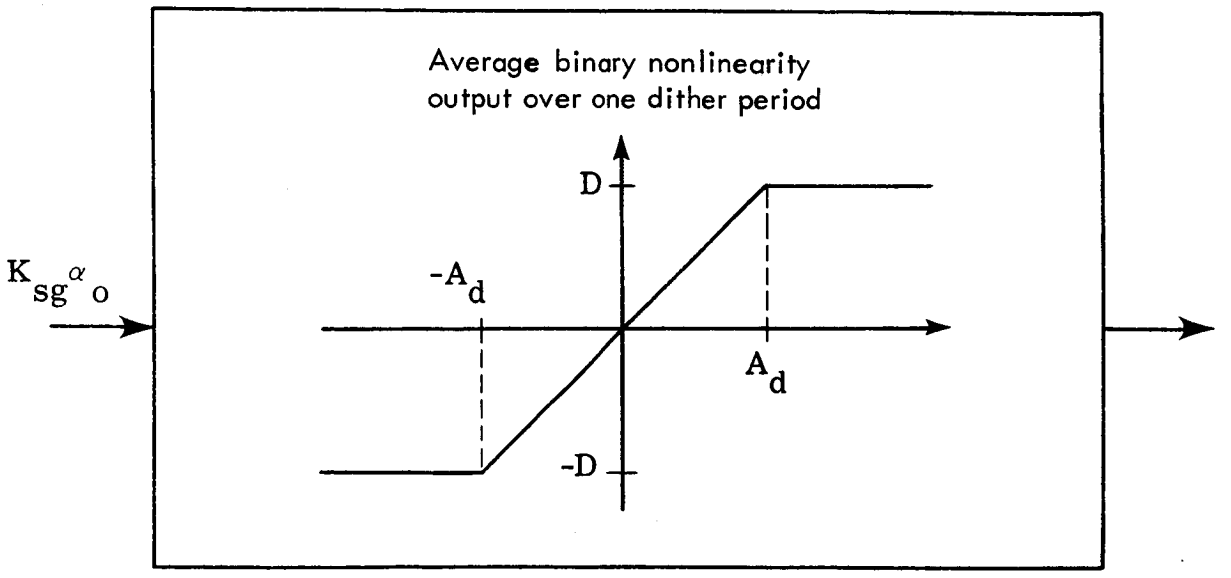

(c) input output relation for "slow" signals (equivalent nonlinearity)

Figure 4.2-4 Compensatory Use of a Dither Signal at the Nonlinearity Input

dither period must be kept well above the sampling period or the linearization illustrated in Fig. 4.2-4 (c) will be distorted by large quantization errors. Consequently, the gyro exhibits a forced oscillation at the dither frequency. Although errors due to this oscillation do not appear at the input to the direction cosine calculations, sizeable float angles can be created and associated cross-coupling errors can be large. Use of dither is regarded as another approach to compensation of the rebalance loop. The resulting linearized loop model can be treated by linear techniques for all float angles less than A_d/K_{sg} rad.

5. CHOOSING GYRO PARAMETERS

Major strapdown system errors are generated by mechanisms which depend on basic single-degree-of-freedom gyro parameters. This fact suggests that gyro-induced attitude errors can be reduced by proper design of the angular motion sensors. In this chapter we investigate the accuracy improvements that can be achieved through gyro optimization.

5.1 GYRO ERRORS DUE TO RANDOM MOTION

In order to select the optimum set of gyro parameters for a practical mission it is necessary to compute gyro and system errors generated by random vehicle motion. Presently available descriptions of random motion are limited and the analysis is therefore restricted by several simplifications. In particular, sinusoidal angular rates about the three orthogonal inertial sensor package axes are assumed to have the same phase. This permits specification of co-spectral density functions between pairs of axes in terms of a single spectral density function and proportionality constants. In addition, the coherence function* between angular rates about different axes is unity in this case. Figures 3.4-1 and 3.4-2 indicate that such in-phase angular rates provide the chief source of constant system drift rate, particularly when the gyro bandwidth exceeds the highest motion frequency. Gyro loop dynamics are described by a linear, second order transfer function.

*See Ref. 13, p. 33.

Constant Gyro Drift Rates – If the angular rate vector, ω, in Fig. 5.1-1 maintains a fixed orientation in the sensor package, the major constant gyro errors can be expressed in terms of the spectral density function $\Phi_{\omega\omega}(\nu)$, direction cosines describing the projections of ω on the three principal axes and the gyro transfer function:

$$\begin{matrix}\text{constant gyro} \\ \text{drift rate}\end{matrix} = K_1 K_2 \int_0^\infty H(\nu)\, \Phi_{\omega\omega}(\nu)\, d\nu \qquad (5.1\text{-}1)$$

where K_1 and K_2 are constants which represent the orientation of the ω vector and appropriate gyro physical parameters. The function $H(\nu)$ is included to represent gyro transmission characteristics when they appear. For example, if spin-input crosscoupling errors are considered K_2 is the steady state gyro float angle sensitivity (rad/(rad/sec)) and $H(\nu)$ is given by

$$H(\nu) = \text{Real}\left\{ G(s)\Big|_{s=j\nu} \right\} \qquad (5.1\text{-}2)$$

where G(s) is the Laplace Transform gyro transfer function. K_1 is the product of direction cosines between the ω vector and the spin and input axes of the gyro under consideration and a minus sign precedes the expression.

Orientation of the Angular Vibration Vector – It is not realistic to expect the ω vector to maintain a fixed attitude within the vehicle. Instead, a simplified description of varying orientation is used: the random angular vibration vector is presumed to maintain a fixed direction in vehicle coordinates for intervals of equal length T' and to assume a new attitude at the end of each interval. The orientations are independent from one period to any other but may obey some probability distribution to account for different amplitudes in the vibration spectra about the vehicle axes. This is a good description of important random angular motions such as structural vibration and lightly damped vehicle dynamics.

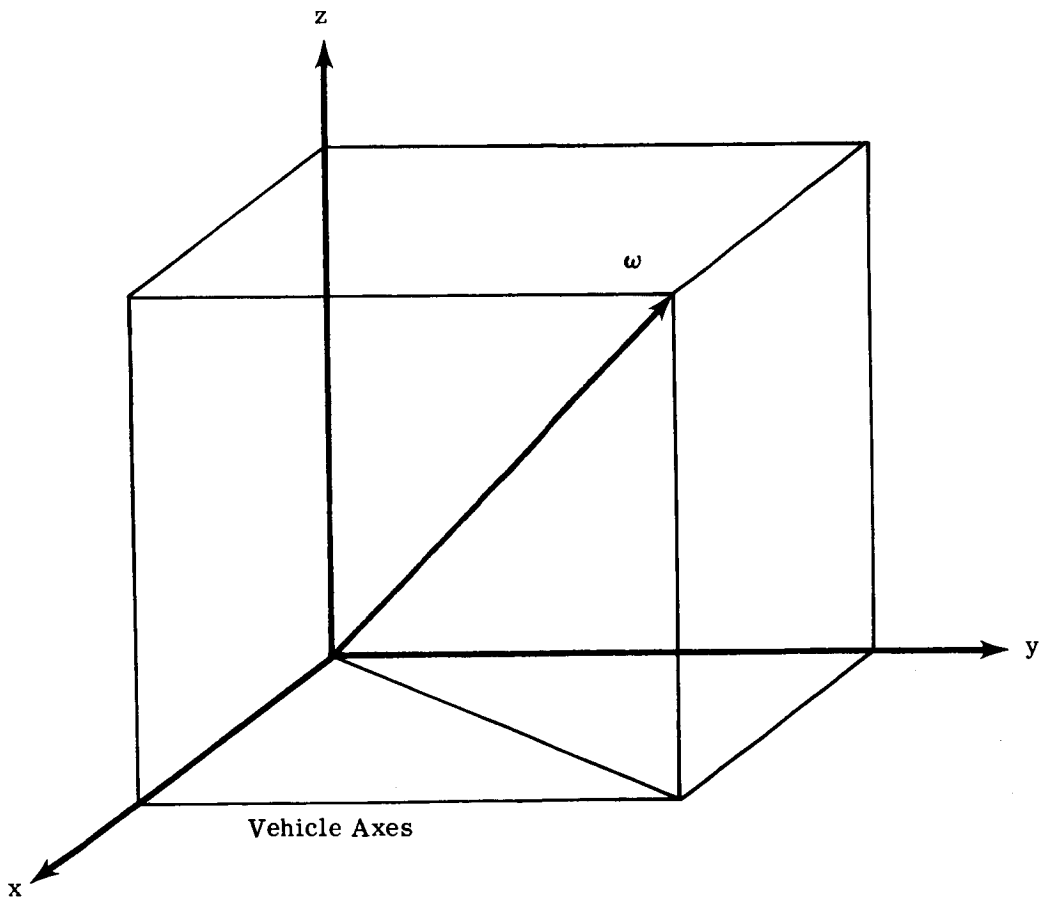

Figure 5.1-1 In Phase Angular Oscillations

Using Eq. (5.1-1), the system attitude error due to a constant gyro error grows by the amount

$$\delta(i) = K_1(i)\, K_2\, T' \int_0^\infty H(\nu)\, \Phi_{\omega\omega}(\nu)\, d\nu \qquad (5.1\text{-}3)$$

during the i^{th} interval of length T'. Since the orientation of ω is independent from one interval to another the coefficient $K_1(i)$ is also independent. Assuming symmetric distributions for the orientation of ω,

$$\overline{\delta(i)} = 0 \quad \text{for all } i$$

$$\overline{\delta(i)\,\delta(j)} = 0 \quad \text{for } i \neq j \qquad (5.1\text{-}4)$$

The mean square total system attitude error at the end of N intervals is given by

$$\overline{[\varphi(N)]^2} = \sum_{i=1}^{N} \overline{[\delta(i)]^2} \qquad (5.1\text{-}5)$$

If T' is constant and if $\Phi_{\omega\omega}(\nu)$ and the probability distribution for the orientation of ω are stationary,

$$\overline{[\varphi(N)]^2} = N\,\overline{\delta^2}$$

$$= N\,\overline{K_1^2}\,K_2^2 \left[\int_0^\infty H(\nu)\, \Phi_{\omega\omega}(\nu)\, d\nu\right]^2 \qquad (5.1\text{-}6)$$

Equation (5.1-6) uses an integral expression to provide the average drift rate over an interval T′. However, the integral is only correct when considering averages over an infinite time. Appendix G illustrates conditions for which the integral is approximately correct for finite-time averages. We will assume those conditions are satisfied in the examples which follow.

The constant system drift rate resulting from output axis angular acceleration errors can also be viewed as an integral over the random motion spectrum according to

$$\begin{matrix}\text{constant system} \\ \text{drift rate} \\ \text{per gyro}\end{matrix} = K_3^2 \frac{I_{oo}}{H} \int_0^\infty H(\nu)\, \Phi_{\omega\omega}(\nu)\, d\nu \qquad (5.1\text{-}7)$$

where K_3 is the direction cosine between the ω vector and the output axis of the gyro whose error is being considered and H is defined as

$$H(\nu) = \left[G(s) \Big|_{s=j\nu} \right]^2$$

Since

$$\overline{K_3^2} \neq 0$$

the mean square system attitude error resulting in this case is not dependent on the interval T′:

$$\overline{\left[\varphi(N)\right]^2} = N^2 (T')^2 \overline{K_3^2} \left(\frac{I_{oo}}{H} \right)^2 \left[\int_0^\infty H(\nu)\, \Phi_{\omega\omega}(\nu)\, d\nu \right]^2 \qquad (5.1\text{-}8)$$

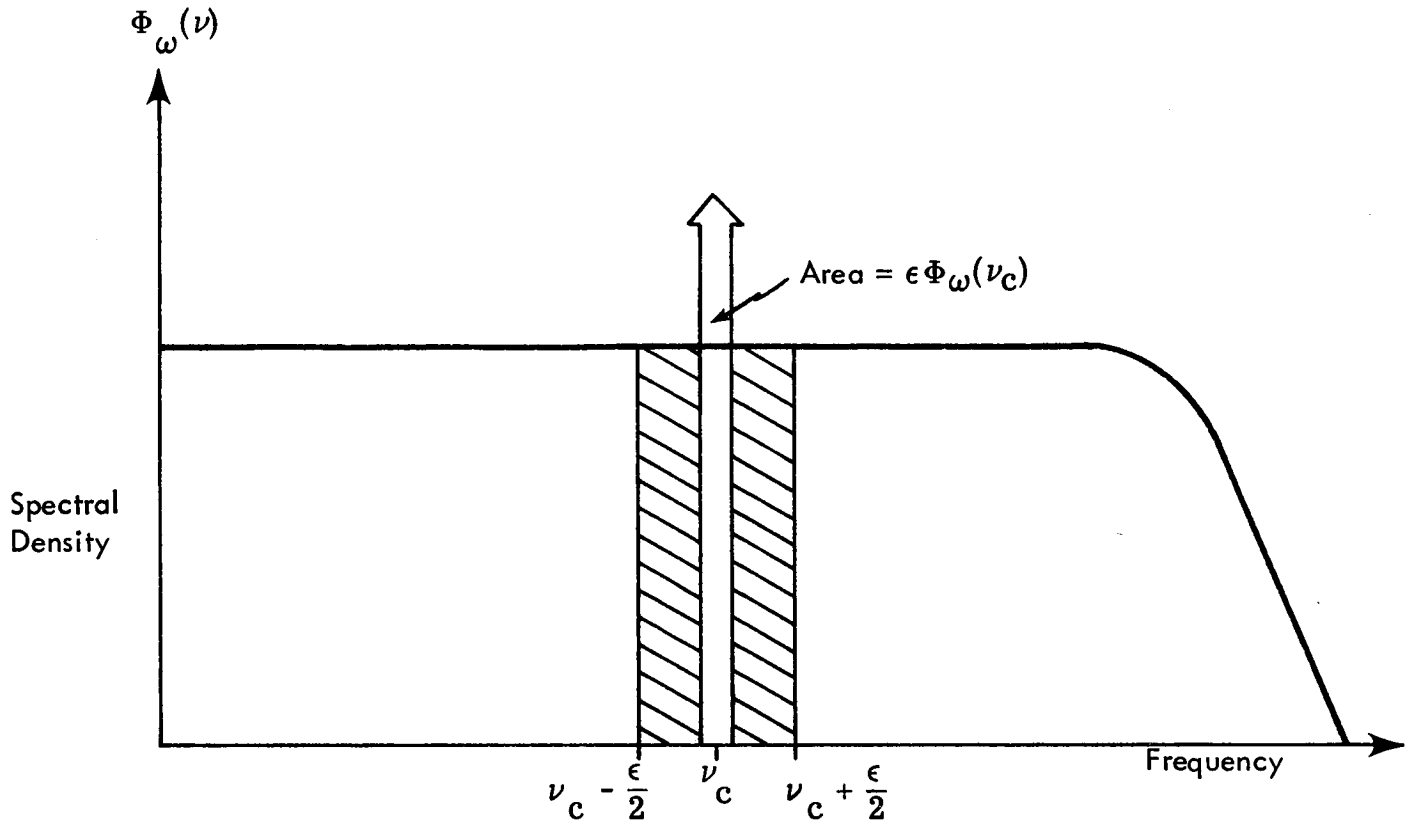

$$\omega = \sqrt{2\epsilon\,\Phi(\nu_c)}\ \sin \nu_c t$$

Figure 5.1-2. Frequency Spectrum Reduction

Constant System Drift Rates From Correlated Errors in Pairs of Gyros – In addition to constant system drift rates which result from constant angular rate errors in individual gyros and from output axis pseudo-coning effects, growing attitude errors can also be generated by properly correlated oscillatory errors from pairs of gyros. Calculation of this kind of system drift rate cannot be accomplished without statistical descriptions of the random angular motion which are considerably more complex than the spectral density function. As an approximate approach to the problem, $\Phi_{\omega\omega}(\nu)$ was divided into segments and each section was approximated by a pure sinusoid at the center frequency having the same power as the segment it represents (see Fig. 5.1-2). The sinusoids obtained were used to compute time-varying gyro errors according to Eq. (2.2-1). Properly correlated errors from pairs of gyros were then used to compute the constant system drift rate resulting from this form of pseudo-coning. In the examples which follow, this contribution to system attitude errors was found to be insignificant.

5.2 OPTIMIZATION OF GYRO PARAMETERS

Designable Parameters – In any attempt to specify a gyro which minimizes the motion induced errors described in Chapter 2, the sources of inaccuracy can be divided into two broad categories: errors whose generation involves parameters basic to the sensor operation and errors arising from imperfect construction and other considerations which the designer always tries to minimize. Examples of the latter category include anisoelasticity and torquer scale factor errors. A list of the first group, referred to hereafter as "designable parameters," is provided by Fig. 5.2-1. Subsequent discussion will concentrate on the designable parameters because when dealing with all other error sources, the design goal is obviously to minimize the factor under consideration. In many cases the designable parameters can be lumped together and the optimum design problem involves specifying the best values for groups

of parameters. Figure 5.2-2 illustrates parameter groupings possible for a simple model of a ternary pulse rebalanced gyro.

Limiting Constraints – Several gyro parameters or groups of parameters are confined within limits imposed by the environment or by hardware considerations. For example, the parameter group $K_{tg}D/H$ (D' in Fig. 5.2-2(b)) must exceed the maximum anticipated input angular rate. If this condition is violated, the gimbal angle cannot be held near null and, in practical gyros, the gimbal will rotate until it is restrained by mechanical stops, causing the history of input angular motion stored in the float to be rendered incorrect.

When a maximum gyro output angle increment, $\Delta\theta_{max}$, is specified in order to keep quantization and commutativity errors in the direction cosine matrix calculations within certain bounds, the gyro sample period T must obey the relation: $K_{tg}DT/H \leq \Delta\theta_{max}$. If the gimbal is not torqued for the entire period, the pulse length τ_p must be substituted for T in this relation. In other words, once the torque generator output has been scaled to imply an input angular rate, the value of an output pulse is directly related to the torque pulse period. Also, the inequality discussed earlier becomes $(\tau_p/T)\, K_{tg}D/H \geq \omega_{i_{max}}$ if torquing does not occur over the entire period. These expressions may be further modified if the torquer lag precludes application of essentially rectangular torque pulses.

A theoretical restriction is imposed on the rotor moments of inertia I_{ii_r} and I_{ss_r} if, as is common in single-degree-of-freedom gyros, the rotor shape is a wheel. This restriction is that $I_{ii_r} \geq I_{ss_r}/2$. Furthermore, since $I_{oo_r} = I_{ii_r}$ the important parameter group I_{oo}/H is bounded according to $I_{oo}/H > \frac{1}{2\Omega}$.

In the optimization examples which follow, the above constraints provide limits on the range over which parameters can be varied, reducing the size of the parameter space which must be searched to find the optimum.

SINGLE DEGREE OF FREEDOM FLOATED RATE GYRO

- Rotor Spin Angular Momentum, H
- Gimbal Plus Rotor Output Axis Moment of Inertia, I_{oo}
- Fluid Damping Coefficient, C
- Rotor Spin Axis Moment of Inertia, I_{ss_r}
- Gimbal Plus Rotor Anisoinertia, $I_{ss}-I_{ii}$
- Torque Generator Time Constant, τ_{tg}
- Signal Generator Sensitivity, K_{sg}
- Torque Generator Sensitivity, K_{tg}
- Wheel Speed Regulation Loop Frequency Response
- Pulse Torquing Period, T
- Torque Level, D
- Gimbal Angle Threshold, δ

} pulse torqued gyros

Figure 5.2-1 Designable Parameters.

Simplifications Used in the Examples – The examples which follow are concerned with binary pulse torqued gyros. The gyro transmission characteristics are those of a linearized second order system, and depend on τ_f and τ_{tg} according to the equations provided in Section 2.4.3. One of the basic results of that section is that the transmission characteristics of the linearized gyro loop are independent of loop gains K_{sg}, K_{tg} and D. Also, it is assumed in the examples that gyro errors due to limit cycles are not allowed to reach the direction cosine calculations. Consequently, these three parameters do not appear in the examples. Following Section 2.4.3, the gyro sample period, T, is not considered significant in determining the limit cycle (and therefore the transmission characteristics.). In addition, no maximum size for the gyro output increment, $\Delta\theta$, is established. The sample period does not enter the examples as a parameter to be optimized. Finally, since only a binary pulse torqued gyro is considered the nonlinearity threshold, δ, does not enter the design problems. The remainder of the designable parameters listed in Fig. 5.2-1, a total of six, remain available for manipulation in the examples. Of these, the terms $I_{ss} - I_{ii}$ and I_{ss_r} are grouped to describe the effective anisoinertia. The time constants τ_{tg} and $\tau_f = I_{oo}/C$ describe linearized gyro dynamics, particularly the gyro bandwidth. When the effect of gyro loop damping ratio is ignored the independent groups of designable parameters are reduced to three: gyro bandwidth (depending on τ_{tg}, C and I_{oo}), the ratio I_{oo}/H and the ratio of an effective anisoinertia to I_{oo}. When the major contribution of anisoinertia errors is assumed to take place in a frequency range where the effective anisoinertia is constant, this term is assumed to be removed by design and the optimization takes place in the two parameter space of the gyro bandwidth and I_{oo}/H.

The characteristic time T′ describing the correlation of the ω vector orientation in vehicle axes also enters in the gyro optimization. When expressed as a function of time, the mean square system attitude error, $\bar{J}(t)$, behaves as

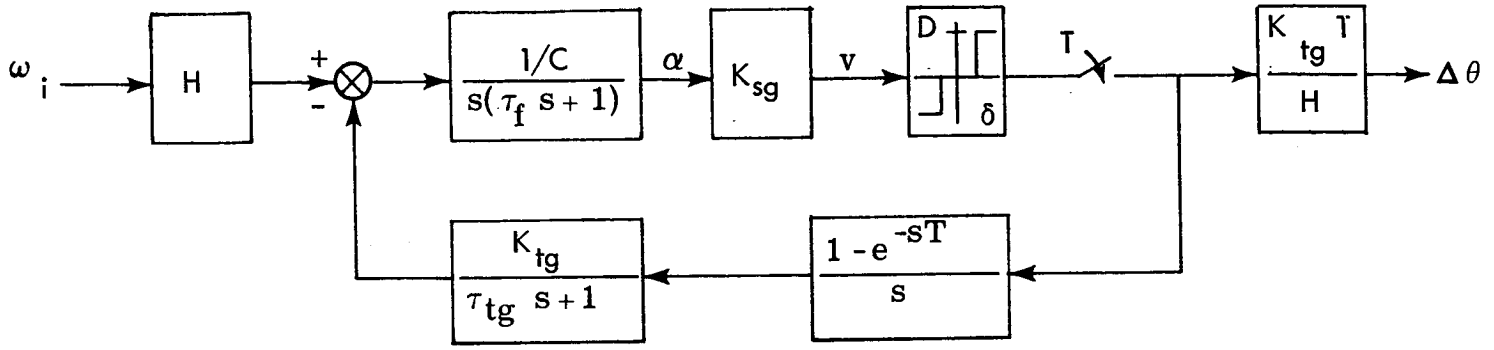

(a) Simple representation of ternary pulse rebalanced gyro loop

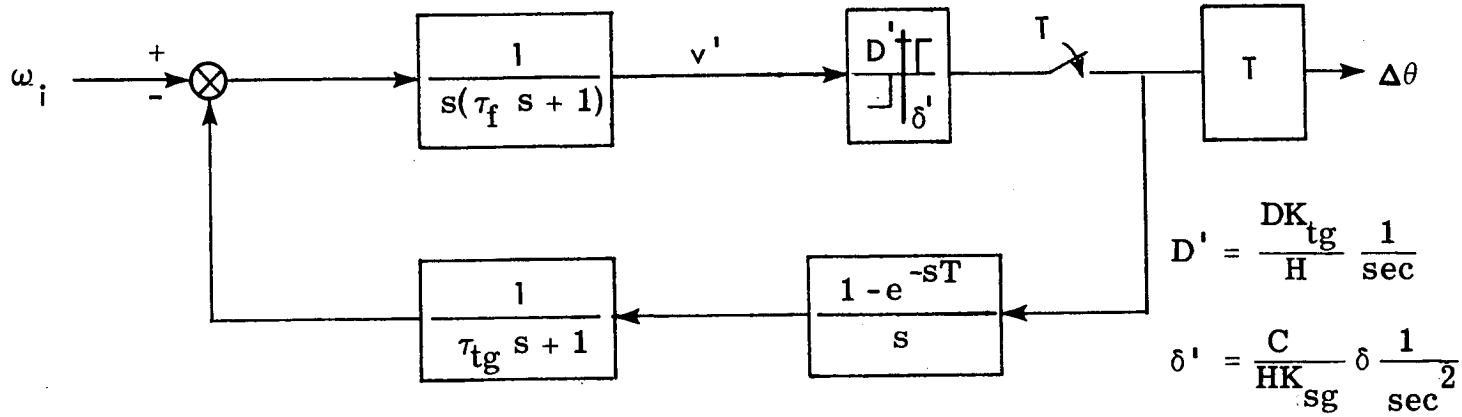

(b) Illustration of parameter grouping possible

$$D' = \frac{DK_{tg}}{H}\,\frac{1}{\text{sec}}$$

$$\delta' = \frac{C}{HK_{sg}}\,\delta\,\frac{1}{\text{sec}^2}$$

$$v' = \frac{C}{HK_{sg}}\,v\,\frac{1}{\text{sec}^2}$$

Figure 5.2-2 Parameter Grouping in a Ternary Torqued Pulse Rebalanced Gyro

$$\bar{J}(t) = AT't + Bt^2 \qquad (5.2\text{-}1)$$

where the first term comes from gyro errors represented in Eq. (5.1-6) and the second from errors expressed in Eq. (5.1-8).

Optimization Procedure – The optimization procedure used in the examples can be summarized as follows:

1. A starting set of gyro parameters is specified. To the extent that the effect of the individual parameters is understood, a set of values which may be close to the optimum is chosen.

2. The major system error contributors are determined for the initial gyro parameters. In the given environment some gyro error terms may not be significant and their elimination simplifies the optimization problem.

3. The system attitude error is expressed as a function of the major error sources and in terms of the designable gyro parameters. The motion environment is reduced to the form of numerical coefficients at this point but gyro parameters appear explicitly in the expression.

4. The figure-of-merit is minimized with respect to all the gyro parameters appearing in the equation developed in step 3. Since all error sources do not contribute to system error growth in the same manner this usually requires specification of an "evaluation time", t, and minimization of the system error at that time.

5. At the conclusion of minimization a check is made to see if the same error terms dominate when the gyro has the optimum set of parameters. If not, steps two through five are repeated.

5.3 EXAMPLE I

The vehicle angular motion experienced by the sensor package in this problem consists of a constant angular rate of 0.1 rad/sec about one vehicle axis and a random angular rate motion about each axis described by a constant spectral density $\Phi = 10^{-3}$ $(rad/sec)^2/Hz$ from zero to 1000 Hz. The random motion correlation period, T', is 0.5 sec. This environment is presumed to be representative of that experienced in a lunar module during powered descent.

Step 1 – The initial set of gyro parameters is that provided in the example of Section 2.5. In addition, the float damping coefficient and torque generator time constant are 8×10^5 dyne-cm-sec and 50 μsec respectively. Linearization of a binary pulse torqued gyro with these characteristics yields a second order gyro transfer function with natural frequency of 972 Hz and a damping ratio of 0.26. However, in order to simplify the problem for hand calculations the gyro is assumed to have a unity transfer function over the entire random angular motion bandwidth. As a result of this assumption, there are no potential system errors due to undetected vehicle coning motion unless the gyro parameters change. This bandwidth-dependent error must be considered when different gyro characteristics result from optimization.

Step 2 – The dominant system error sources generated in the gyro whose characteristics are given above all result from random motion. They are the constant drift rates due to anisoinertia errors at high motion frequencies, spin-input crosscoupling and pseudo-coning from output axis angular acceleration errors. System errors arising from the constant angular rate postulated were negligible, as were system pseudo-coning errors generated by oscillatory errors in pairs of gyros.

Step 3 – The expression for the system attitude error growth, as reflected in the figure-of-merit discussed in Chapter 3, is:

$$\bar{J}(t) = 3\left[\frac{I_{oo}\,\Phi\,\omega_n}{2\pi\,H}\right]^2 t^2 + 3T'\left\{\left[\frac{H\,\Phi}{2\pi\,I_{oo}\,\omega_n} + \frac{(I_{ii} - I_{ss_g})\,\Phi\,\omega_n}{2\pi\,H}\right]^2\right\} t \qquad (5.3\text{-}1)$$

For simplicity the gyro bandwidth ω_{BW} is equated with natural frequency ω_n. The first term in Eq. (5.3-1) describes the contribution of output axis angular acceleration gyro errors through pseudo-coning. The second term results from constant gyro errors due to spin-input crosscoupling and high frequency (oscillations above the rotor speed regulation loop bandwidth) anisoinertia terms. The figure-of-merit, $\bar{J}(t)$, is in $(\text{rad})^2$ and T' and t are to be specified in seconds.

It is desired to minimize $\bar{J}(t)$ at some specific time, t'. By making the following definitions:

$$a \triangleq \frac{t'}{T'}$$

$$b \triangleq \frac{I_{ii} - I_{ss_g}}{I_{oo}}$$

$$c \triangleq \frac{I_{oo}}{H}$$

$$R \triangleq \frac{3\,\Phi^2\,(T')^2}{4\pi^2}$$

Equation (5.3-1) can be written in a form more suitable for analytic optimization:

$$\frac{\bar{J}(t')}{aR} = ac^2\,\omega_n^2 + \left[\frac{1}{c\,\omega_n} + bc\,\omega_n\right]^2 \qquad (5.3\text{-}2)$$

If any attempt has been made to reduce anisoinertia errors by design of gimbal and rotor moments of inertia, $b \ll 1$. This fact is also reflected in Eq. (5.3-2) by the observation that $\bar{J}(t')/aR$ is minimized with respect to b when $b = 0$ regardless of the other parameters. In addition, it is reasonable to assume that $a \gg 1$. The use of these two inequalities permits Eq. (5.3-2) to be reduced to

$$\frac{\bar{J}(t')}{aR} = ac^2 \omega_n^2 + \frac{1}{c^2 \omega_n^2} + 2b \qquad (5.3\text{-}3)$$

This is the equation that is used to determine the optimum set of gyro parameters as reflected in the quantities b, c and ω_n.

Step 4 – It can be seen from Eq. (5.3-3) that the optimum value of the parameter group b is zero. Designing the effective anisoinertia for high frequency oscillations to be zero minimizes system errors from this cause independently. Setting the partial derivatives of $\bar{J}(t')/aR$ with respect to c and ω_n equal to zero provides two identical equations for the optimum groups of gyro parameters:

$$ac^4 \omega_n^4 = 1 \qquad (5.3\text{-}4)$$

Evaluation of second partial derivatives reveals that Eq. (5.3-4) specifies a minimum. If ω_n is selected to permit accurate measurement of all anticipated angular rates by the gyros, Eq. (5.3-4) provides the optimum value of the parameter group c for each choice of evaluation time t' and correlation period T'. Using Eq. (2.4-23) and assuming that $\tau_f \gg \tau_{tg}$, Eq. (5.3-4) provides a relation for I_{oo}, C and H in terms of τ_{tg} and t'/T':

$$\frac{I_{oo} C}{H^2} = \frac{2 \tau_{tg}}{\sqrt{a}} \qquad (5.3\text{-}5)$$

The minimum value of $\bar{J}(t')/aR$ is given by

$$\left[\bar{J}(t')/aR\right]_{min} = 2(\sqrt{a} + b) \qquad (5.3\text{-}6)$$

Choosing $t' = 1$ min and $\omega_n = 1000$ Hz, $a = 120$ and the optimum value of the parameter group c is 4.82×10^{-5} sec (the starting value of c was 1.25×10^{-3} sec). This requires $\Omega > 1650$ Hz. The minimum system error is:

$$[\bar{J}(t')]_{min} \tilde{=} (0.406 \text{ deg})^2$$

This figure compares with a value for $\bar{J}(t')$ of $(7.21 \text{ deg})^2$ when the original gyro parameters are substituted into Eq. (5.3-3).

Step 5 – Computation of all the gyro-induced system errors reveals that the dominant error sources have not changed as a consequence of gyro parameter optimization.

Effect of Compensating Output Axis Acceleration Errors – The fact the optimum value of $c = I_{oo}/H$ is much less than that obtained with the initial set of gyro parameters reflects tha fact that in this example output axis angular acceleration errors are the major contributors to system attitude errors. If we assume that these gyro errors are reduced to 10% of their former value by some kind of compensation, Eq. (5.3-3) becomes

$$\frac{\bar{J}(t')}{aR} = 0.01\, ac^2 \omega_n^2 + \frac{1}{c^2 \omega_n^2} + 2b \qquad (5.3\text{-}7)$$

The optimum set of parameters obey

$$b = 0$$

$$ac^4 \omega_n^4 = 100 \qquad (5.3\text{-}8)$$

and

$$\left[\frac{\bar{J}(t')}{aR}\right]_{min} = \frac{2\sqrt{a}}{10} \qquad (5.3\text{-}9)$$

If ω_n = 1000 Hz, the optimum value of c is 1.52×10^{-4} ($\Omega > 525$ Hz) and

$$[\bar{J}(t')]_{min} = (0.129 \text{ deg})^2$$

5.4 EXAMPLE II

The second design example presumes an angular motion environment representative of that which may be experienced by a strapdown inertial navigator in a large transport airplane. Random angular motion about each axis is described by a flat spectral density of 10^{-4} $(\text{rad/sec})^2/\text{rad/sec}$ (notice the units are different from those in the first problem) out to $\nu_r = 2\pi$ rad/sec and zero elsewhere. In addition a sinusoidal angular motion exists about two axes (x and z). This has an amplitude of 0.1 rad/sec with frequency of $2\pi/10$ rad/sec (0.1 Hz). The motions have the same phase and represent the dutch roll oscillation mode of the aircraft.*

Step 1 – The starting gyro parameters and sensor orientations are identical with those chosen for the first example.

Step 2 – The significant system attitude error contributions from the sinusoidal motion result from pseudo-coning due to output axis acceleration errors in the x and y gyros and the constant errors generated in the z gyro by spin-input crosscoupling and anisoinertia effects.

*The phase difference between x and z axis oscillations due to the dutch roll mode may range from 125 degrees up to 180 degrees for different aircraft. The 180 degree value is chosen here for simplicity.

Step 3 – Because the dutch roll oscillation axis is fixed in the vehicle, it generates errors which cause J to grow as a parabola. The anisoinertia in this case is $I_{ii} - I_{ss}$ since the oscillation is well within anticipated wheel speed regulation loop bandwidths. In terms of the oscillation amplitude, B = 0.1 rad/sec, and $\Delta I = I_{ii} - I_{ss}$, the contribution of the dutch roll motions to J(t) (or $\bar{J}(t)$) is given by:

$$J_{d.r.}(t) = B^4 t^2 \left[\frac{c^2}{2} + c^2 \left(\left(\frac{\Delta I}{2 I_{oo}} \right)^2 + \frac{\Delta I}{2 I_{oo}} \right) + \frac{1}{2 \omega_n^2} + \frac{1}{4 c^2 \omega_n^2} + \frac{\Delta I}{2 I_{oo} \omega_n^2} \right] \qquad (5.4\text{-}1)$$

Under the assumption that $\Delta I / I_{oo} << 1$ (again minimizing J with respect to the anisoinertia term simply involves setting ΔI to zero):

$$J_{d.r.}(t) \cong \frac{B^4 t^2}{2} \left[c^2 + \frac{1}{2 c^2 \omega_n^4} + \frac{1}{\omega_n^2} \right] \qquad (5.4\text{-}2)$$

In Eq. (5.4-2) J is in $(\text{rad})^2$ and t is in seconds.

The significant contributors to system error as a result of the random angular motion are pseudo-coning due to output axis acceleration errors, and constant gyro errors caused by spin-input crosscoupling and anisoinertia. A restriction is arbitrarily imposed to the effect that all random motion is sensed by the gyro, that is $\omega_n > \nu_r$. In terms of the random motion spectral density Φ and bandwidth ν_r the contribution to $\bar{J}(t)$ is given by

$$\bar{J}_{r.}(t) = 3 \Phi^2 (\nu_r)^2 c^2 t^2 + 3 T \Phi^2 (\nu_r)^2 \left(\frac{1}{c^2 \omega_n^4} + \frac{2 \Delta I}{I_{oo} \omega_n^2} + \left(\frac{\Delta I}{I_{oo}} \right)^2 c^2 \right) t \qquad (5.4\text{-}3)$$

Defining

$$d \triangleq \frac{\Delta I}{I_{oo}}$$

and noticing that for this problem

$$B^4 >> 3\,\Phi^2\,\nu_r^2$$

the expression for $\bar{J}(t')$ is

$$\frac{\bar{J}(t')}{a(T')^2} = \left(\frac{a\,B^4}{2} + 3\,\Phi^2\,\nu_r^2\,d^2\right)c^2 + \left(\frac{a\,B^4}{4} + 3\,\Phi^2\,\nu_r^2\right)\frac{1}{c^2\,\omega_n^4} + \left(\frac{a\,B^4}{2} + 6\,\Phi^2\,\nu_r^2\,d\right)\frac{1}{\omega_n^2} \qquad (5.4\text{-}4)$$

$$\triangleq k_1\,c^2 + k_2\left(\frac{1}{c^2\,\omega_n^4}\right) + k_3\,\frac{1}{\omega_n^2}$$

Minimization of $\bar{J}(t')/a(T')^2$ with respect to ω_n leads to the requirement $\omega_n = \infty$ in order to remove crosscoupling errors. Of course, an infinite gyro bandwidth is not feasible but one can be easily chosen to satisfy the requirement $\omega_n > \nu_r$. Optimization of $\bar{J}(t')/a(T')^2$ with respect to d requires that ΔI be zero. The minimum system error occurs when

$$c^4 = \frac{k_2}{k_1\,\omega_n^4} \qquad (5.4\text{-}5)$$

and

$$\bar{J}(t')_{\min} = \frac{a(T')^2}{\omega_n^2}\,(2\sqrt{k_1\,k_2} + k_3) \qquad (5.4\text{-}6)$$

Step 4 – If t′ is chosen as 2 hours and T′ as one minute, a = 120. For the same value of ω_n as the starting gyro (972 Hz), the optimum value of c is 1.38×10^{-4} sec and

$$[\bar{J}(t')]_{min} = (0.68 \text{ deg})^2$$

Using the original set of gyro parameters $\bar{J}(t')$ is $(3.67 \text{ deg})^2$.

Step 5 – The major contributors to system error are the same for the optimum gyro.

Again output axis errors, in the form of pseudo-coning, are the largest contributors to $\bar{J}_{min}(t')$. Reduction through compensation of these errors by a factor of ten changes the coefficients k_1, k_2 and k_3. The equation (Eq. (5.4-5)) for the optimum value of c remains unchanged but the optimum value value of c becomes 4.36×10^{-4} sec and

$$[\bar{J}(t')]_{min} = (0.22 \text{ deg})^2$$

The optimum set of gyro parameter groups for the output axis motion compensated gyros are:

$$\omega_n \left(\tau_{tg}, \frac{I_{oo}}{C} \right) = 972 \text{ Hz}$$

(arbitrarily chosen to satisfy $1.0 \text{ Hz} \leq \omega_n \leq \infty$ and the fact that errors decrease with large values of ω_n)

$$\frac{I_{oo}}{H} = 4.36 \times 10^{-4} \text{ sec}$$

$$I_{ii} = I_{ss}$$

$$I_{ss_r} \text{ is arbitrary}$$

5.5 SUMMARY

The examples presented in this chapter serve to illustrate an approach to the determination of the optimum set of gyro designable parameters. Many of the calculations performed were of a coarse nature but the use of digital computers permits detailed analysis of any degree desired. The equation for the growth of system attitude errors in the example is a function of three groups of designable parameters. These three groups in turn depend on a total of six parameters (wheel speed regulation loop bandwidth does not appear because it was assumed high or low depending on the motion spectrum). The most common groupings were I_{oo}/H, $(I_{ii} - I_{ss_g})/I_{oo}$, $(I_{ii} - I_{ss})/I_{oo}$ and ω_n. The natural frequency, ω_n, in turn is a function of $\tau_f = I_{oo}/C$ and τ_{tg}.

Significant decreases in system RMS attitude error at the evaluation time, t', resulted when optimum gyro parameters were substituted for those originally assumed. However, error growth when the optimum set of gyros is used may still be prohibitive and compensation is necessary to further reduce strapdown system drift rate. In the examples, compensating the optimum gyro to reduce its chief error source does not produce a "one-to-one" reduction in system error. The intent of this chapter is to demonstrate a useful approach to the synthesis of an optimum (but mission dependent) set of gyro parameters and to indicate the system error reduction that can be achieved by parameter manipulation. No comment is made on the difficulty involved in building a gyro containing the optimum parameter groups specified in the examples.

PRECEDING PAGE BLANK NOT FILMED.

6. CONCLUSION

6.1 CONCLUSIONS

During the course of Phase I research, several useful tools for the analytic design of single-degree-of-freedom strapdown floated integrating gyros have been developed. These include a quantitative figure-of-merit on which optimum gyro design can be based, and a quasi-linear description of the transmission characteristics of binary-torqued rebalance loops, as well as necessary gyro error models, compensation methods, and environment descriptions. The design procedure developed is well suited for implementation on a digital computer, although the text design examples were highly simplified to allow a pencil-and-paper solution.

Several comclusions can be drawn from the examples presented, although these are necessarily preliminary in nature, depending upon the approximations made. Foremost among these is the conclusion that gyro parameter manipulation cannot always provide sufficient reduction in gyro errors: the system drift rates calculated for the optimized gyros in Chapter 5 remained unsatisfactory for many applications. Consequently, it seems that error reduction in single-degree-of-freedom strapdown gyros must be aided by some means in addition to manipulation of the basic sensor parameters; external compensation appears necessary.

Given the need for compensation, the gyro errors can be divided according to the means employed to reduce them. Certain parameters are specified in order to minimize the errors generated by their existence while the errors caused by other parameters are reduced through compensation.

Compensation, of course, implies calibration. The rotor speed loop, for example, must be damped to minimize anisoinertia errors. In addition, the rotor speed loop frequency response must be measured to enable compensation of residual dynamic errors.

Another interesting conclusion is that the rebalance loop bandwidth may be heavily dependent on torquer dynamic characteristics. In particular, the quasi-linear binary-torqued gyro model showed the loop bandwidth to be inversely proportional to the square-root of the torquer time constant. This indicates that the torquer dynamic characteristics should be carefully specified in optimum gyro design. Furthermore, the torque generator design should include the consideration of accommodating additional torquing signals for purposes of gyro error compensation. As a consequence of required gyro torquing accuracy, the necessary stability of rebalance loop electronics is to be emphasized.

Compensation within the gyro rebalance loop appears to have limited value. While it can produce improvements in gyro transmission characteristics and reduce limit cycles when they exist, its value in removing motion induced gyro errors on the basis of frequency discrimination is limited. For example, since the DC sensitivity of the gyro is fixed, the major system errors arising from constant error torques in individual gyros are not affected by the choice of compensation and switching logic. One main contribution of loop compensation to error reduction results from increasing gyro bandwidth.

Finally, it can be concluded that the importance of motion-induced errors precludes use of the static testing procedures common for platform gyros. In order to determine the quality of performance, strapdown gyros must be subjected to dynamic testing. In addition, a large list of items to be determined by gyro testing is suggested by the work to date. If certain gyro error sources are to be removed through the calculation of compensating torques or output signals, gyro tests should be performed with the additional

compensation equipment and, under some conditions, whole strapdown sensor packages may require testing as a unit.

6.2 CONTINUATION OF EFFORT

The results of the work reported herein suggest several areas of continuing investigation. First, as a means of consolidating the conclusions just stated and to establish the validity of several approximations used, a digital simulation will be made of the dynamics of single-degree-of-freedom strapdown gyros. Included in the simulation will be the equations relating system level performance to gyro errors. The computer program will be in a flexible, modular form to permit its use for studying other single-degree-of-freedom sensors.

A catalog will be made of existing and proposed devices for measuring the vehicle motion environment and computing motion-induced gyro errors. An effort will be made to determine the size and types of errors in these instruments as a means of estimating how accurately gyro errors can be compensated. All proposed techniques will be evaluated using the digital simulation program.

Based on insight gained in the work of Phase I, laboratory experiments will be designed to test proposed devices and calculations for the reduction of gyro-induced system errors. Laboratory tests will also be specified to determine the validity of mathematical descriptions for gyro error generation that have been used in the effort reported above.

An investigation will be conducted into the feasibility of a digital computer gyro design program which will be capable of specifying the optimum set of gyro parameters and compensation devices for any given vehicle environment (mission). Alternately, the program may be able to choose the best

strapdown sensors from a catalog of available instruments. The basic inputs are conceived to be vehicle environment, design goals and the accuracies, weights, and power consumption tradeoffs that represent the state-of-the-art at a particular time.

Finally, the experience gained in analyzing the single-degree-of-freedom gyro will be applied to the single-degree-of-freedom pendulous accelerometer. An attempt will be made to provide a unified approach to the selection of gyros and accelerometers to meet specifications for a particular strapdown system mission.

REFERENCES

1. Weinstock, H., Effect of Angular Vibration on Gyroscope Performance, M. I. T. Department of Aeronautics and Astronautics, Notes from Summer 1963 Program 16. 39S.

2. Weinstock, H., Effects of Linear Vibration on Gyroscope Instruments, M. I. T. Department of Aeronautics and Astronautics, Notes from Summer 1963 Program 16. 39S.

3. Gelb, A., and Vander Velde, W. E., Multiple-Input Describing Functions and Nonlinear System Design, McGraw-Hill Book Co., Inc., June 1968.

4. Truxal, J. G., Automatic Feedback Control System Synthesis, McGraw-Hill Book Co., Inc., 1955.

5. Del Toro, V., and Parker, S. R., Principles of Control Systems Engineering, McGraw-Hill Book Co., Inc., 1960.

6. Gelb, A. and Vander Velde, W. E., On Limit Cycling Control Systems, IEEE Trans. on Automatic Control, Vol. AC-8, No. 2, April 1963.

7. Broxmeyer, C., Inertial Navigation Systems, McGraw-Hill Book Co., Inc., 1964.

8. Aseltine, J. A., Transform Method in Linear System Analysis, McGraw-Hill Book Co., Inc., 1958.

9. United Aircraft Corporate Systems Center, Report SCR 328-I, Vol. I, A Study of the Critical Computational Problems Associated with Strapdown Inertial Navigation Systems, February 1967.

10. Jolley, L. B. W., Summation of Series, Second Edition, Dover Publications, Inc., 1961.

11. Macomber, G. R., and Fernandez, M., Inertial Guidance Engineering, Prentice-Hall, Inc., 1962.

REFERENCES (Cont.)

12. Rice, S.O., Mathematical Analysis of Random Noise, Selected Papers on Noise and Stochastic Processes, Wax, N., ed., Dover Publications, Inc., New York, 1954.

13. Bendat, Julius S., and Piersol, Allan G., Measurement and Analysis of Random Data, John Wiley & Sons, Inc., New York, 1966.

14. Sher, L., Errors of the Single-Degree-of-Freedom Strapdown Gyroscope, Internal Document GSI-67-01, NASA Electronics Research Center, October 1967.

15. Broxmeyer, C., and Wishner, H., Vehicle-Fixed Component Inertial Guidance System Study, NAVWEPS Report 8668, December 1964.

16. Sitomer, James L., The 18 PRIG and 16 PM PIPA High Performance Strapped-Down Sensors, M.I.T. Instrumentation Laboratory Report E-1941, (Confidential), April 1966.

17. Kuo, B.C., Analysis and Synthesis of Sampled-Data Control Systems, Prentice-Hall, Inc., 1963.

18. Schwartz, Bernard, Strapdown Inertial Navigation Systems, Sperry Engineering Review, Vo. 20, No. 1, 1967.

19. Gelb, Arthur, and Sutherland, Arthur A., Jr., Design of Strapdown Gyroscopes for a Dynamic Environment, Semi-Annual Report, The Analytic Sciences Corporation, TR-101-1, 7 July 1967.

20. Wiener, T.F., Theoretical Analysis of Gimballess Inertial Reference Equipment Using Delta-Modulated Instruments, Sc.D. Thesis, M.I.T. Department of Aeronautics and Astronautics, March 1962.

21. Scoville, A.E., and Yamron, J., The Mechanization of a Strapdown Inertial System Based on Time-Modulated Torquing, AIAA/JACC Guidance and Control Conference, August 1966.

APPENDIX A

DERIVATION OF ANGULAR MOTION INDUCED ERROR TORQUES FOR THE SDF GYRO

The single-degree-of-freedom gyro float torques caused by case angular motion are derived herein. We begin by writing the torque on the float assembly (i.e., gimbal plus rotor), in the form

$$\underline{M}_f = \left(\frac{d\underline{H}_f}{dt} \right)_I \qquad \text{(A-1)}$$

which is the rate of change in angular momentum of the float relative to inertial space. Rewriting this equation relative to the gimbal frame using the law of Coriolis yields

$$\underline{M}_f = \left(\frac{d\underline{H}_f}{dt} \right)_G + \underline{\omega}_{IG} \times \underline{H}_f \qquad \text{(A-2)}$$

where $\underline{\omega}_{IG}$ is the angular velocity of the gimbal with respect to inertial space. At this point we adopt the notation of subscripted square brackets to denote the frame in which vectors are expressed. Thus, writing components of all vectors of Eq. (A-2) in the gimbal (G) frame yields

$$[\underline{M}_f]_G = \left[\left(\frac{d\underline{H}_f}{dt} \right)_G \right]_G + [\underline{\omega}_{IG}]_G \times [\underline{H}_f]_G \qquad \text{(A-3)}$$

Continuing, note that the angular velocity of the gimbal with respect to inertial space can be written as the vector sum of the angular velocity of the case with respect to inertial space and the angular velocity of the gimbal with respect to the case, viz:

$$[\underline{\omega}_{IG}]_G = [\underline{\omega}_{IC}]_G + [\underline{\omega}_{CG}]_G \qquad \text{(A-4)}$$

Figure A-1 illustrates the geometry of rotor, gimbal and case, including possible misalignment of the rotor relative to the gimbal ($\underline{\beta}$) and the gimbal relative to the case ($\underline{\alpha}$). With the exception of α_o, all other components of $\underline{\alpha}$ and $\underline{\beta}$ are assumed constant. Let the quantities $\hat{o}$, $\hat{s}$, $\hat{i}$ denote unit vectors along the o, s, i axes, respectively, with the obvious extensions to the primed coordinate systems. The required terms in Eq. (A-4) can now be written as:

$$[\underline{\omega}_{CG}]_G = \dot{\alpha}_o \hat{o}' \tag{A-5}$$

and

$$[\underline{\omega}_{IC}]_G = [\underline{\omega}_{IC}]_C - \underline{\alpha} \times [\underline{\omega}_{IC}]_C \tag{A-6}$$

where terms on the right hand side of Eq. (A-6) are all expressed using G-frame unit vectors. If we define

$$[\underline{\omega}_{IC}]_C = \omega_o \hat{o} + \omega_s \hat{s} + \omega_i \hat{i} \tag{A-7}$$

then it follows that

$$\begin{aligned}
[\underline{\omega}_{IC}]_G &= \omega_o \hat{o}' + \omega_s \hat{s}' + \omega_i \hat{i}' \\
&\quad - \begin{vmatrix} \hat{o}' & \hat{s}' & \hat{i}' \\ \alpha_o & \alpha_s & \alpha_i \\ \omega_o & \omega_s & \omega_i \end{vmatrix} \\
&= (\omega_o - \alpha_s \omega_i + \alpha_i \omega_s)\hat{o}' \\
&\quad + (\omega_s + \alpha_o \omega_i - \alpha_i \omega_o)\hat{s}' \\
&\quad + (\omega_i - \alpha_o \omega_s + \alpha_s \omega_o)\hat{i}'
\end{aligned} \tag{A-8}$$

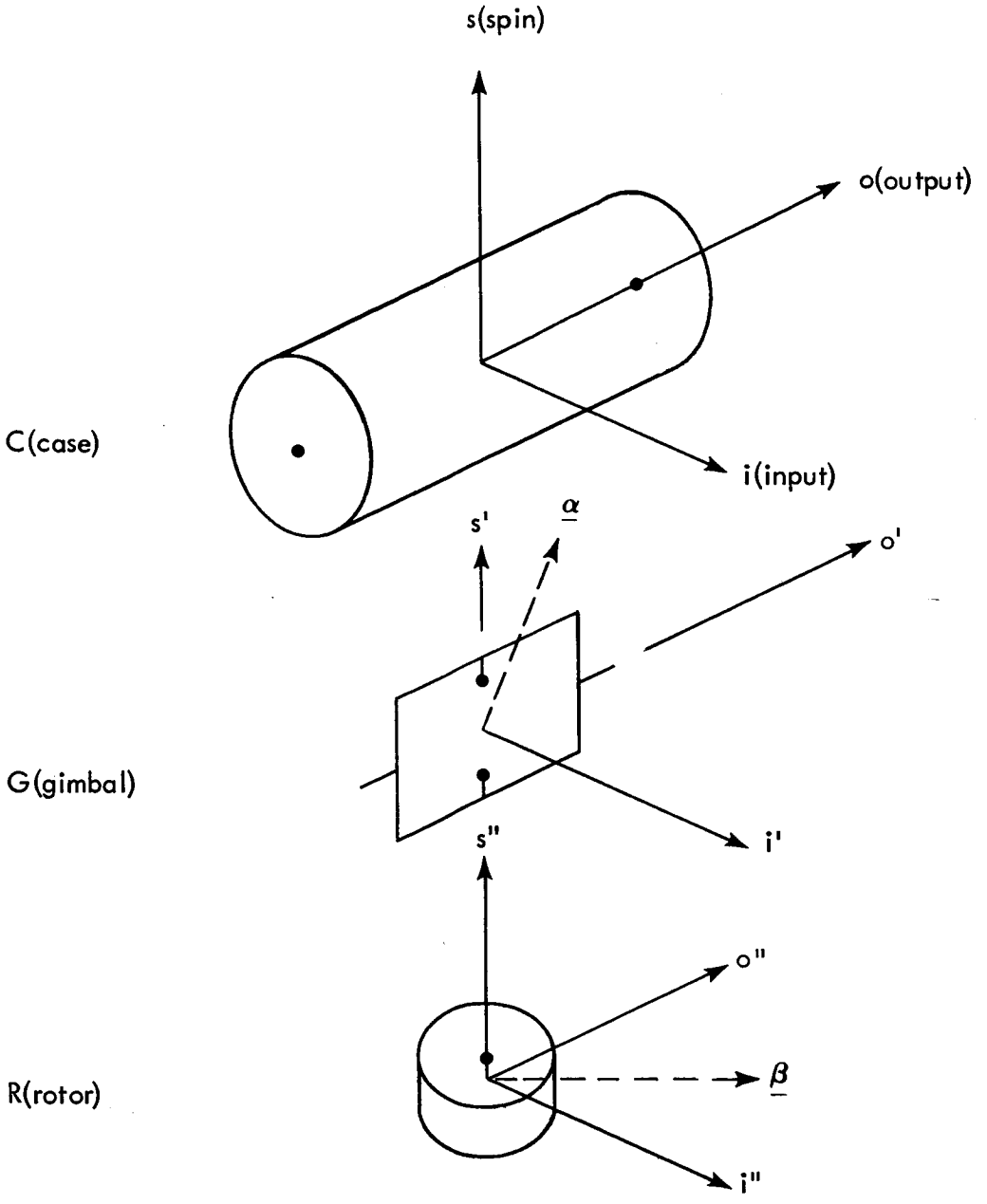

Figure A-1. Exploded View of Single-Degree-of-Freedom Gyro Showing Small Misalignment Angles $\underline{\alpha}$, $\underline{\beta}$.

The angular momentum of the float assembly can be written as the vector dot product of the float moment of inertia tensor (second-order tensor or dyad) and the angular velocity of the gimbal with respect to inertial space. The float angular momentum ($\underline{H}_f$) can be written as the vector sum of the gimbal angular momentum ($\underline{H}_g$) and the rotor angular momentum ($\underline{H}_r$), viz:

$$[\underline{H}_f]_G = [\underline{H}_g]_G + [\underline{H}_r]_G \tag{A-9}$$

Operations with the moment of inertia tensor yield

$$[\underline{H}_g]_G = (\underline{I}_{o_g} \cdot [\underline{\omega}_{IG}]_G)\hat{o}' + (\underline{I}_{s_g} \cdot [\underline{\omega}_{IG}]_G)\hat{s}' + (\underline{I}_{i_g} \cdot [\underline{\omega}_{IG}]_G)\hat{i}' \tag{A-10}$$

where

$$\begin{aligned}
\underline{I}_{o_g} &\triangleq I_{oo_g}\,\hat{o}' + I_{os_g}\,\hat{s}' + I_{oi_g}\,\hat{i}' \\
\underline{I}_{s_g} &\triangleq I_{os_g}\,\hat{o}' + I_{ss_g}\,\hat{s}' + I_{si_g}\,\hat{i}' \\
\underline{I}_{i_g} &\triangleq I_{oi_g}\,\hat{o}' + I_{si_g}\,\hat{s}' + I_{ii_g}\,\hat{i}'
\end{aligned} \tag{A-11}$$

I_{oo_g}, etc., are the gimbal moments of inertia and I_{os_g}, etc., are the gimbal products of inertia. For the rotor we write (where R is the rotor frame)

$$[\underline{H}_r]_G = [\underline{H}_r]_R + \underline{\beta} \times [\underline{H}_r]_R \tag{A-12}$$

where, as before, terms on the right hand side of this equation are all expressed using G-frame unit vectors. Also,

$$[\underline{H}_r]_R = (\underline{I}_{o_r} \cdot [\underline{\omega}_{IR}]_R)\,\hat{o}'' + (\underline{I}_{s_r} \cdot [\underline{\omega}_{IR}]_R)\hat{s}''$$
$$+ (\underline{I}_{i_r} \cdot [\omega_{IR}]_R)\,\hat{i}'' \qquad \text{(A-13)}$$

where, in principal axes, we get:

$$\underline{I}_{o_r} = I_{oo_r}\,\hat{o}''$$
$$\underline{I}_{s_r} = I_{ss_r}\,\hat{s}''' \qquad \text{(A-14)}$$
$$\underline{I}_{i_r} = I_{ii_r}\,\hat{i}''$$

and

$$[\underline{\omega}_{IR}]_R = [\underline{\omega}_{GR}]_R + [\underline{\omega}_{IG}]_R$$
$$= \Omega_s \hat{s}'' + [\underline{\omega}_{IG}]_G - \underline{\beta} \times [\underline{\omega}_{IG}]_G \qquad \text{(A-15)}$$

Ω_s is the rotor speed relative to the gimbal.

At this point it is possible to compute all of the basic expressions of interest. The results are given below, with all calculations valid to first-order in small angles. Terms comprised of products of inertia multiplied by small angles have been dropped.

$$[\underline{\omega}_{IG}]_G = (\dot{\alpha}_o + \omega_o - \alpha_s\omega_i + \alpha_i\omega_s)\hat{o}' + (\omega_s + \alpha_o\omega_i - \alpha_i\omega_o)\hat{s}'$$
$$+ (\omega_i - \alpha_o\omega_s + \alpha_s\omega_o)\hat{i}' \qquad \text{(A-16)}$$

$$
\begin{aligned}
[\underline{H}_f]_G = [& I_{oo}(\dot{\alpha}_o + \omega_o - \alpha_s\omega_i + \alpha_i\omega_s) + I_{os_g}(\omega_s + \alpha_o\omega_i) + I_{oi_g}\omega_i \\
& + I_{oo_r}\beta_i(\omega_s + \alpha_o\omega_i) - I_{ss_r}\beta_i(\Omega_s + \omega_s + \alpha_o\omega_i)]\,\hat{o}' \\
& + [I_{ss}(\omega_s + \alpha_o\omega_i - \alpha_i\omega_o) + I_{os_g}(\dot{\alpha}_o + \omega_o) + I_{si_g}\omega_i \\
& + I_{ss_r}(\Omega_s + \beta_o\omega_i - \beta_i(\omega_o + \dot{\alpha}_o)) + I_{oo_r}\beta_i(\dot{\alpha}_o + \omega_o) - I_{ii_r}\beta_c\omega_i]\,\hat{s}' \\
& + [I_{ii}(\omega_i - \alpha_o\omega_s + \alpha_s\omega_o) + I_{oi_g}(\dot{\alpha}_o + \omega_o) + I_{si_g}\omega_s \\
& - I_{ii_r}\beta_o\omega_s + I_{ss_r}\beta_o(\Omega_s + \omega_s)]\,\hat{i}' \qquad \text{(A-17)}
\end{aligned}
$$

where

$$
\begin{aligned}
I_{oo} &= I_{oo_g} + I_{oo_r} \\
I_{ss} &= I_{ss_g} + I_{ss_r} \qquad \text{(A-18)} \\
I_{ii} &= I_{ii_g} + I_{ii_r}
\end{aligned}
$$

Recalling Eq. (A-3) and the fact that only output axis torques are of interest, we get

$$
\begin{aligned}
[\underline{M}_f]_{o'} = & I_{oo}(\ddot{\alpha}_o + \dot{\omega}_o) + (I_{ii} - I_{ss})\omega_s\omega_i - H\omega_i \\
& + I_{os_g}[\dot{\omega}_s - \omega_o\omega_i] \\
& + I_{oi_g}[\dot{\omega}_i + \omega_o\omega_s] + I_{si_g}[\omega_s^2 - \omega_i^2] \\
& + \alpha_o[(I_{ss} - I_{ii})(\omega_s^2 - \omega_i^2) + H\omega_s] \\
& + \alpha_s[-(I_{ss} - I_{ii})\omega_o\omega_s - H\omega_o - I_{oo}\dot{\omega}_i] \\
& + \alpha_i[(I_{ss} - I_{ii})\omega_o\omega_i + I_{oo}\dot{\omega}_s] \\
& + \beta_o[(I_{ss_r} - I_{ii_r})(\omega_s^2 - \omega_i^2) + H\omega_s] \\
& + \beta_i[(I_{ss_r} - I_{oo_r})(-\dot{\omega}_s + \omega_o\omega_i) - I_{ss_r}\dot{\Omega}_s] \qquad \text{(A-19)}
\end{aligned}
$$

where we have used the definition

$$H = I_{ss_r} \Omega_s$$

The term $-H\omega_i$ represents the "ideal" gyro float torque. All of the remaining terms in Eq. (A-17) are error torques.

APPENDIX B

DESCRIBING FUNCTION CALCULATIONS

Describing Function

The describing function for a nonlinearity may be defined as follows:

$$N_A(A) = \frac{\text{phasor representation of output component at frequency } \omega}{\text{phasor representation of input component at frequency } \omega}$$

$$= \frac{A_1(A)}{A} e^{j\varphi_1(A)} \qquad \text{(B-1)}$$

where $A_1(A)$ and $\varphi_1(A)$ represent the amplitude and phase of the first-harmonic in the output of the nonlinearity when its input is

$$x = A \sin \omega t$$
$$= A \sin \psi \qquad \text{(B-2)}$$

Denoting the output of the nonlinearity by $y(x)$, Fourier series manipulations result in the following form for $N_A(A)$

$$N_A(A) = \frac{j}{\pi A} \int_0^{2\pi} y(A \sin \psi)\, e^{-j\psi} d\psi \qquad \text{(B-3)}$$

If the nonlinearity is odd and memoryless, this can be simplified to

$$N_A(A) = \frac{4}{\pi A} \int_0^{\pi/2} y(A \sin \psi) \sin \psi \, d\psi \qquad \text{(B-4)}$$

Example 1 – Figure B-1(a) illustrates a sinusoidal input and the corresponding output for a binary (two-level) nonlinearity. From Eq. (B-4), the describing function is computed as

$$N_A(A) = \frac{4}{\pi A} \int_0^{\pi/2} D \sin \psi \, d\psi$$

$$= \frac{4D}{\pi A} \qquad \text{(B-5)}$$

Example 2 – Figure B-1(b) illustrates a sinusoidal input and the corresponding output for a ternary (three-level) nonlinearity. From Eq. (B-4), the describing function is computed as

$$N_A(A) = \frac{4}{\pi A} \int_{\psi_1}^{\pi/2} D \sin \psi \, d\psi$$

$$= \frac{4D}{\pi A} \cos \psi_1$$

$$= \frac{4D}{\pi A} \sqrt{1 - \left(\frac{\delta}{A}\right)^2} \qquad \text{(B-6)}$$

Dual Input Describing Function

For our present purposes we define the dc gain of a nonlinearity to be the ratio of dc output to dc input, over one limit cycle period. Thus, for $x = B + A \sin \psi$, we get

$$N_B(A, B) = \frac{1}{2\pi B} \int_0^{2\pi} y(B + A \sin \psi) \, d\psi \qquad \text{(B-7)}$$

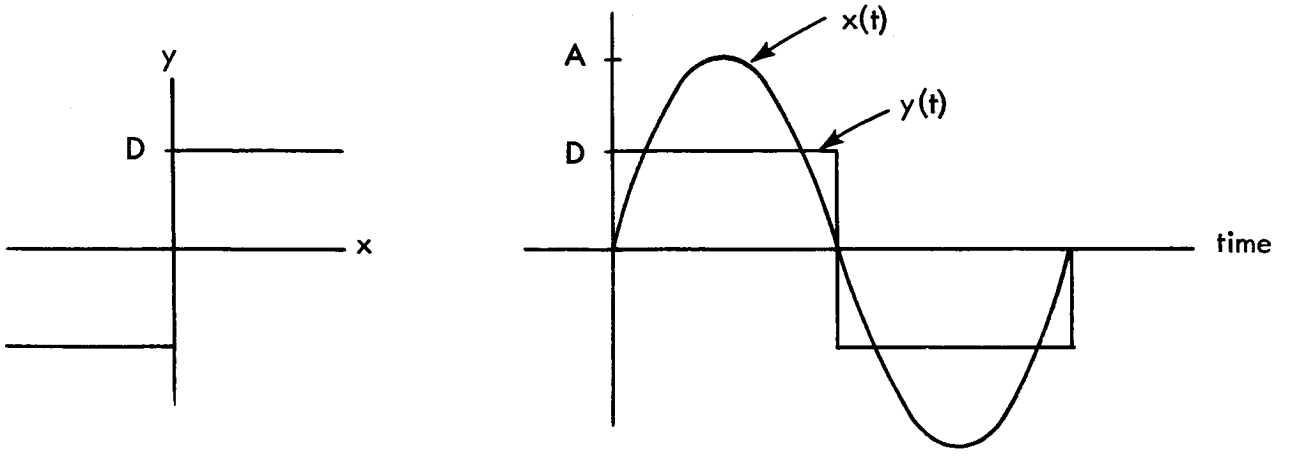

(a) Binary (Two-Level) Nonlinearity

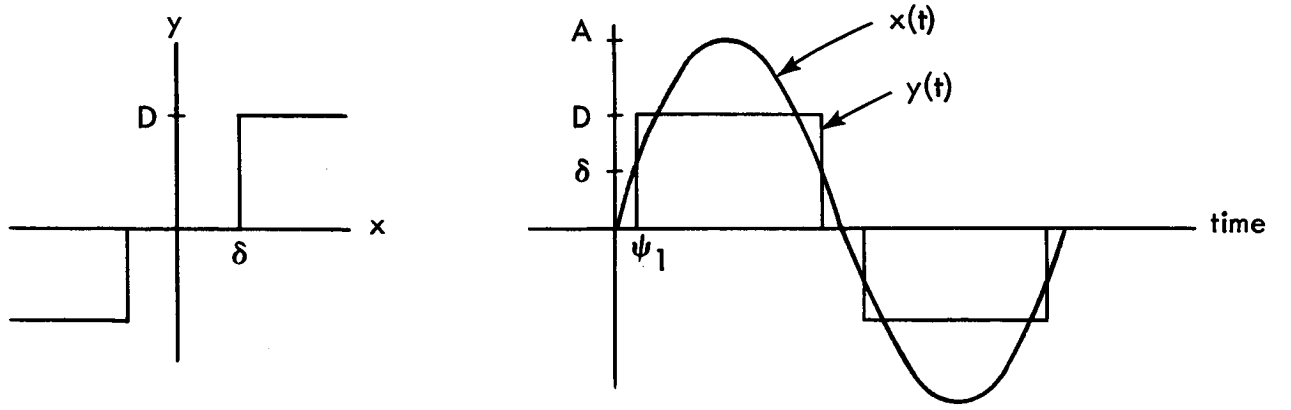

(b) Ternary (Three-Level) Nonlinearity, $\psi_1 = \sin^{-1}(\delta/A)$

Figure B-1. Nonlinearity Input and Output Waveforms.

Example 3 – The model input and corresponding output waveforms for a binary nonlinearity are shown in Fig. B-2a. Equation (B-7) yields

$$N_B(A, B) = \frac{1}{2\pi B}\left[\int_0^{\pi+\psi_2} D\, d\psi + \int_{\pi+\psi_2}^{2\pi-\psi_2} (-D)\, d\psi + \int_{2\pi-\psi_2}^{2\pi} (D)\, d\psi\right]$$

$$= \frac{2D}{\pi B}\,\psi_2$$

$$= \frac{2D}{\pi B}\,\sin^{-1}\left(\frac{B}{A}\right) \qquad \text{(B-8)}$$

Example 4 – A two-segment piecewise-linear asymmetric nonlinearity is illustrated in Fig. B-2b. Equation (B-7) yields, for the equivalent dc gain,

$$N_B(A, B) = \frac{1}{2\pi B}\left[\int_0^{\pi+\psi_2} m_1(B+A\sin\psi)\, d\psi + \int_{\pi+\psi_2}^{2\pi-\psi_2} m_2(B+A\sin\psi)\, d\psi + \int_{2\pi-\psi_2}^{2\pi} m_1(B+A\sin\psi)\, d\psi\right]$$

$$= \frac{m_1+m_2}{2} + \frac{m_1-m_2}{\pi}\left[\psi_2 + \frac{A}{B}\cos\psi_2\right]$$

$$= \frac{m_1+m_2}{2} + \frac{m_1-m_2}{\pi}\left[\sin^{-1}\left(\frac{B}{A}\right) + \frac{A}{B}\sqrt{1-\left(\frac{B}{A}\right)^2}\right] \qquad \text{(B-9)}$$

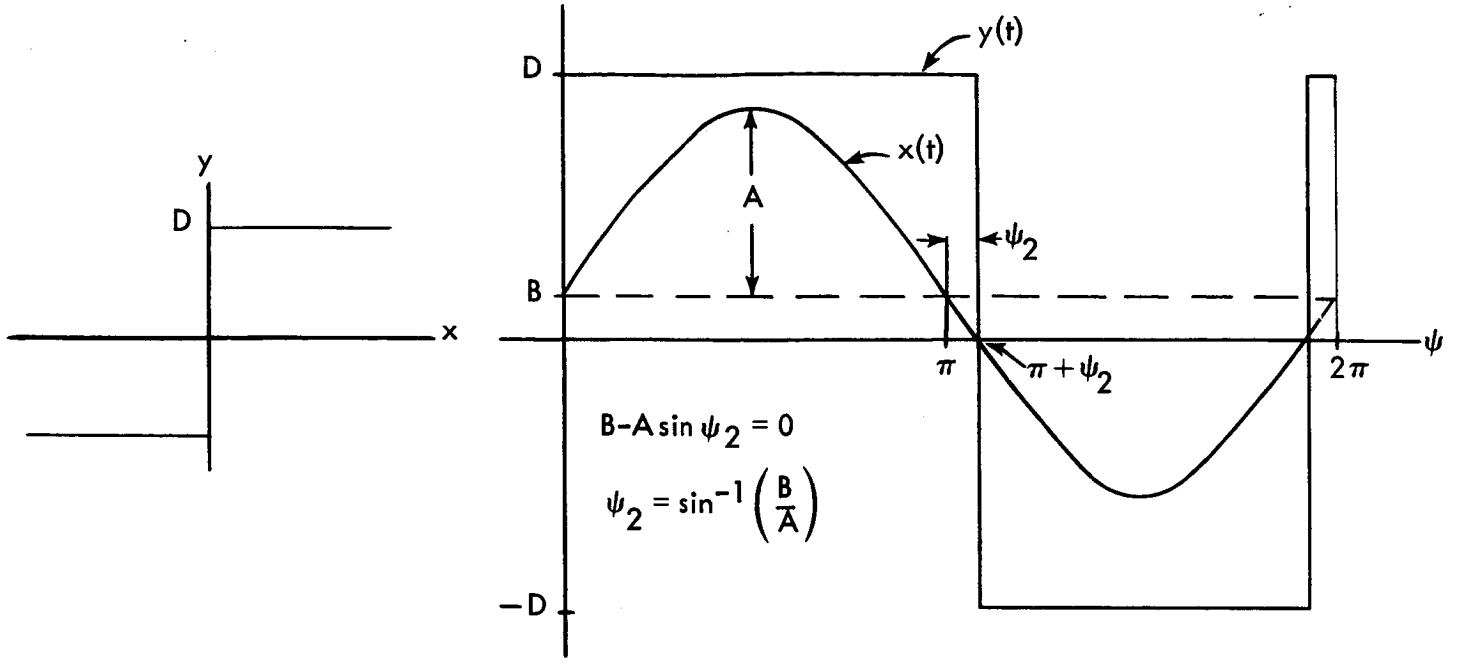

(a) Binary Nonlinearity

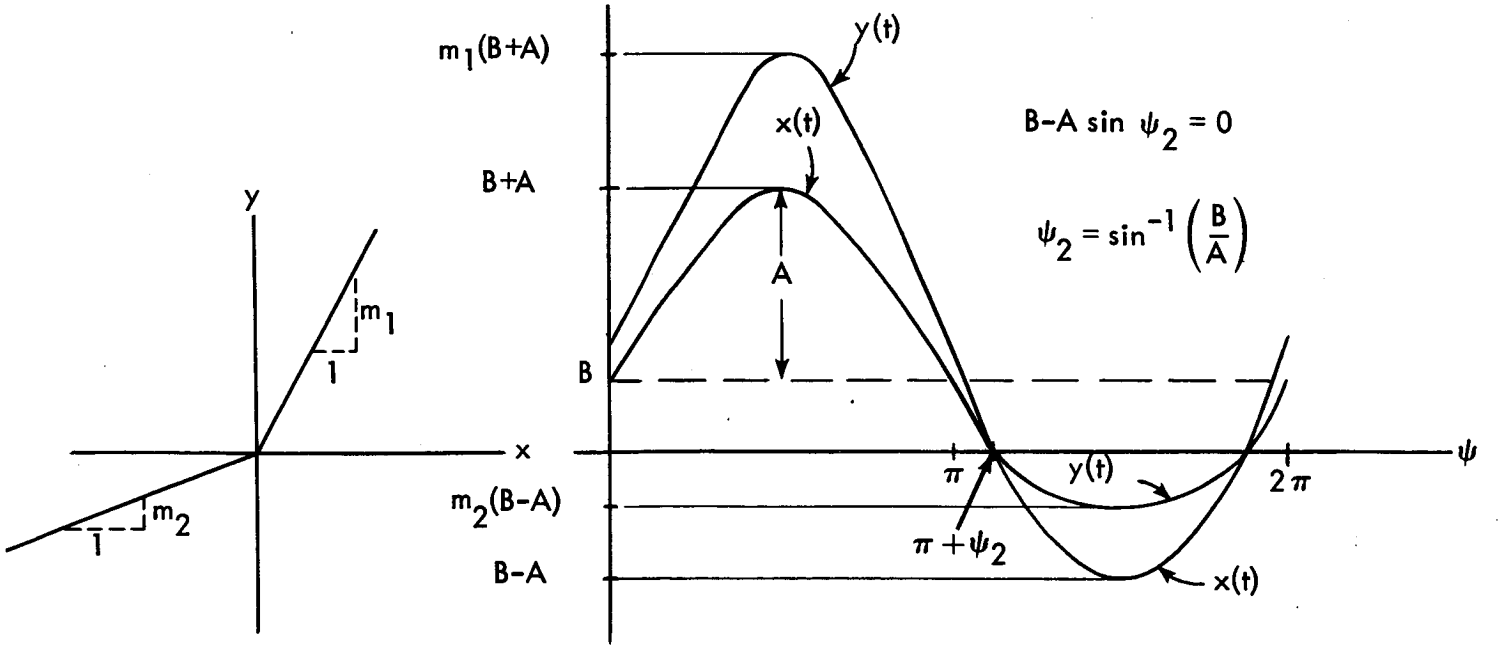

(b) Two-Segment Asymmetric Nonlinearity

Figure B-2. Input and Output Waveforms for Two Nonlinearities with Bias Plus Sinusoid Input.

APPENDIX C

GYRO FIGURE-OF-MERIT

C.1 Interpretation in Terms of System Attitude Errors

We will demonstrate that the figure-of-merit, J, expressed by

$$J = \tfrac{1}{2} \mathrm{tr}\,(\Delta C^T \Delta C)$$

is useful in describing system attitude error. It is assumed that the strap-down system performs well enough that the orientation described by the computed transformation matrix is in error by only a small angle. The direction cosine matrix contained in the computer will be designated C_c while the true system orientation will be represented by C. The matrix ΔC is defined by

$$C_c = C + \Delta C \qquad (C.1\text{-}1)$$

C is an orthogonal matrix. This quality specifies:

$$C^T C = I$$

Premultiplication of an arbitrary vector by C_c is equivalent to rotating that vector through what might generally be a large angle. Premultiplying the result by the transpose of C is equivalent to another rotation which, if C_c and C were equal, would return the vector to its original orientation. When the computer indicated transformation matrix is incorrect ($\Delta C \neq 0$), the net rotation of the vector can be represented by $\underline{\varphi}$, a vector constructed from the small angle rotations φ_x, φ_y, and φ_z about the x, y, and z axes. This situation is illustrated in Fig. 3.1-2. Because of the assumption of small angles, the product $C^T C_c$ can be approximated by

$$C^T C_c \tilde{=} \begin{bmatrix} 1 & -\varphi_z & \varphi_y \\ \varphi_z & 1 & -\varphi_x \\ -\varphi_y & \varphi_x & 1 \end{bmatrix}$$

Using the orthogonality condition and Eq. (C.1-1), we get

$$C^T \Delta C = \begin{bmatrix} 0 & -\varphi_z & \varphi_y \\ \varphi_z & 0 & -\varphi_x \\ -\varphi_y & \varphi_x & 0 \end{bmatrix}$$

Again because of the orthogonality condition,

$$(C^T \Delta C)^T (C^T \Delta C) = \Delta C^T \Delta C$$

$$= \begin{bmatrix} \varphi_y^2 + \varphi_z^2 & -\varphi_x \varphi_y & -\varphi_x \varphi_z \\ -\varphi_x \varphi_y & \varphi_x^2 + \varphi_z^2 & -\varphi_y \varphi_z \\ -\varphi_x \varphi_z & -\varphi_y \varphi_z & \varphi_x^2 + \varphi_y^2 \end{bmatrix}$$

From this we can see that

$$J = \varphi_x^2 + \varphi_y^2 + \varphi_z^2$$

The figure of merit chosen is thus equal to the square of the length of a small vector which represents the system orientation error.

C.2 Interpretation in Terms of Navigation Errors

The figure-of-merit,

$$J = \tfrac{1}{2}\,\mathrm{tr}(\Delta C^T \Delta C)$$

relating system attitude errors to gyro errors is also meaningful when the error in the transformed acceleration vector is considered.

The error in the transformed acceleration vector, $\underline{\Delta a}_r$, resulting from gyro errors is given by

$$\underline{\Delta a}_r = \Delta C\, \underline{a}_b$$

where $\underline{a}_b$ is the true acceleration vector in vehicle coordinates. The length of the error vector is given by

$$\underline{\Delta a}_r^T\, \underline{\Delta a}_r = \underline{a}_b^T\, \Delta C^T \Delta C\, \underline{a}_b \qquad \text{(C.2-1)}$$

Defining a new vector, $\underline{d}$ by

$$\underline{d} \triangleq \Delta C^T\, \Delta C\, \underline{a}_b,$$

Eq. (C.2-1) becomes the dot product

$$\underline{\Delta a}_r^T\, \underline{\Delta a}_r = \underline{a}_b \cdot \underline{d}$$

It is well known that

$$\underline{a}_b \cdot \underline{d} \le \| \underline{a}_b \| \quad \| \underline{d} \|$$

where the norm or length of the vectors is defined

$$\| \underline{d} \| = \left[\sum_i |d_i|^2 \right]^{\frac{1}{2}}$$

A consistent norm for a matrix A is defined by

$$\| A \| = \left[\sum_{i,j} |a_{ij}|^2 \right]^{\frac{1}{2}}$$

With the norms defined, it is known that:

$$\| d \| \leq \| \Delta C^T \Delta C \| \quad \| \underline{a}_b \|$$

It can easily be shown that

$$\| \Delta C^T \Delta C \| = \sqrt{2}\, J$$

Consequently, the upper bound on the length of the error vector of the transformed acceleration can be expressed by

$$\underline{\Delta a}_r^T \underline{\Delta a}_r \leq \sqrt{2}\, J \| \underline{a}_b \|^2 .$$

It can be seen that minimizing the figure-of-merit also minimizes this upper bound.

APPENDIX D

EFFECT OF GYRO ERRORS ON STRAPDOWN SYSTEM ERRORS

D.1 EQUATIONS FOR THE GROWTH OF THE FIGURE-OF-MERIT

In order to relate gyro output errors to the system-oriented measure of goodness we must describe the use made of gyro outputs to maintain a record of system attitude. The description of system attitude relative to a space-fixed set of coordinates is contained in a direction cosine matrix, C. It obeys the differential equation (Ref. 7):

$$\dot{C} = C\Omega \tag{D.1-1}$$

where Ω is a skew symmetric matrix constructed from the inertial rotation rate of the body, resolved into body axes:

$$\Omega = \begin{bmatrix} 0 & -\omega_z & \omega_y \\ \omega_z & 0 & -\omega_x \\ -\omega_y & \omega_x & 0 \end{bmatrix}$$

In the typical application, a digital computer is used to implement some form of the differential equation for C because of the accuracy and drift-free nature required of the computations. We choose as a model of the digital computer calculation the difference equation

$$C_{n+1} = C_n e^{\Delta\Theta_n} \tag{D.1-2}$$

where

$$\Delta\Theta_n \triangleq \int_{nT}^{(n+1)/T} \Omega(\tau)\, d\tau$$

This equation does not account for the non-commutativity of general rotations about the three body axes. However, commutativity error is a function of computer speed and the computation algorithm. We desire only to relate system attitude errors to gyro errors – independent of transformation algorithms or the transformation computer. Equation (D.1-2) permits us to relate small perturbations in $\Delta\Theta_n$ and the resulting error in the transformation matrix. It provides a first-order correct model of the error transmission for any algorithm and transformation computer.

Equation (D.1-2) is perturbed to arrive at a difference equation for ΔC.

$$\Delta C_{n+1} = \Delta C_n\, C_n^T\, C_{n+1} + C_{n+1}\, E_n + (\text{higher order terms in small quantities}) \qquad (D.1\text{-}3)$$

where E_n is the error in $\Delta\Theta_n$, viz:

$$E_n = \begin{bmatrix} 0 & -\int_{nT}^{(n+1)T} (\hat{\omega}_z - \omega_z)dt & \int_{nT}^{(n+1)T} (\hat{\omega}_y - \omega_y)dt \\ \int_{nT}^{(n+1)T} (\hat{\omega}_z - \omega_z)dt & 0 & -\int_{nT}^{(n+1)T} (\hat{\omega}_x - \omega_x)dt \\ -\int_{nT}^{(n+1)T} (\hat{\omega}_y - \omega_y)dt & \int_{nT}^{(n+1)T} (\hat{\omega}_x - \omega_x)dt & 0 \end{bmatrix}$$

That is, E_n is the gyro output error matrix. Using Eq. (D.1-3), the cost function, J, defined in Chapter 3 can be expressed in terms of a difference equation:

$$2J_{n+1} = 2J_n + 2\,\mathrm{tr}\,(C_{n+1}^T C_n \Delta C_n^T C_{n+1} E_n) + \mathrm{tr}\,(E_n^T E_n) \qquad \text{(D.1-4)}$$

With the assumption that $\Delta C_o = 0$, by repeatedly shifting indices in Eq. (D.1-3) and substituting into Eq. (D.1-4), ΔC is eliminated. Defining p_n as $2J_n$, we get:

$$p_{n+1} = p_n + 2\,\mathrm{tr} \sum_{j=1}^{n} C_{n+1}^T C_{n+1-j} E_{n-j}^T C_{n+1-j}^T C_{n+1} E_n + \mathrm{tr}\,(E_n^T E_n) \qquad \text{(D.1-5)}$$

Equation (D.1-5) is a difference equation expressing the propagation of the figure-of-merit as a function of the individual gyro errors. It results from retaining only second or lower order terms in these errors. It also involves all the direction cosine matrices from the start of calculation. No loss of generality results from taking C_o to be the identity matrix. In other words, the growth of the cost function is independent of the vehicle attitude at the start of computation. This reflects the non-directional nature of the measure-of-goodness chosen. No particular type of gyro is required for this expression to be valid. The only forcing terms are the errors in indicated attitude change about three orthogonal, vehicle-fixed axes. No sensor orientations within the vehicle are necessarily implied. Inspection of the terms of Eq. (D.1-5) reveals that no cross-products of gyro errors are included. Such terms do appear, however, if higher ordered products of error matrices are retained from Eq. (D.1-3). Since the skew symmetric property of the E matrix prevents any contribution to the trace of a third order product of error matrices, fourth order terms must be retained before gyro error cross-product contributions to system attitude error appear. This effect is discussed in Section D.3.

D.2 FIRST ORDER EFFECTS OF INDIVIDUAL GYRO ERRORS

If the vehicle is presumed to maintain a fixed attitude,

$$C_i = C_k \text{ for all } i, k$$

and Eq. (D.1-5) becomes

$$p_{n+1} = p_n + 2\,\mathrm{tr} \sum_{j=1}^{n} E_{n-j}^T E_n + \mathrm{tr}\,(E_n^T E_n) \qquad \text{(D.2-1)}$$

This equation relates the system attitude error to the gyro errors as expressed in the E matrices. Only the first order gyro error effects in the absence of vehicle motion are displayed. The last term on the right side is effectively twice the squared length of an error vector, that is

$$\mathrm{tr}\ (E_n^T E_n) = 2\ (e_{n_x}^2 + e_{n_y}^2 + e_{n_z}^2) \qquad \text{(D. 2-2)}$$

If the errors are stationary random variables and the mean value of J is sought, the equation can be written in terms of ensemble averages (denoted by the bar):

$$\bar{p}_{n+1} = \bar{p}_n + 2\,\mathrm{tr} \sum_{j=1}^{n} \overline{E_{n-j}^T E_n} + \mathrm{tr}\ \overline{(E_n^T E_n)} \qquad \text{(D. 2-3)}$$

In this case, Eq. (D. 2-2) can be written in terms of mean square errors along the three orthogonal body axes and the second term in Eq. (D. 2-3) is analogous to an autocorrelation function. In particular

$$\mathrm{tr}(E_{n-j}^T E_n) = 2\left(\varphi_{e_x e_x}(jT) + \varphi_{e_y e_y}(jT) + \varphi_{e_z e_z}(jT)\right) \qquad \text{(D. 2-4)}$$

It is apparent that the attitude error growth as expressed in Eq. (D. 2-1) is dependent on the autocorrelation properties of the gyro errors.

A differential equation for the growth of the system attitude error is developed in Appendix C of Ref. 19:

$$\dot{p}(t) = 2\,\mathrm{tr} \int_0^t D^T(t - \tau)\, D(t)\, d\tau \qquad \text{(D. 2-5)}$$

where continuous direction cosine matrix calculations are assumed and D is the matrix of angular rate indication errors analogous to the E matrix used above. Continuous calculations are a good approximation to the situation where the computation period, T, is small relative to the period of the gyro errors and to the duration of error growth being considered. Equation (D.2-5) can be used to demonstrate the system attitude error growth resulting from random individual gyro errors with particular correlation characteristics. Figure D.2-1 illustrates rms attitude error resulting from uncorrelated errors, random bias errors and in-phase sinusoidal errors in individual gyros. It can be seen that the system errors behave as the output of integrators whose inputs are the gyro errors.

D.3 EFFECT OF CORRELATION BETWEEN ERRORS IN PAIRS OF GYROS

Sizeable system attitude errors arise from the rectification of gyro errors in the direction cosine matrix calculation.* The most serious of these errors take the form of constant attitude drift rates which result from the erroneous indication or lack of indication of vehicle coning motion. It can be demonstrated that vehicle angular oscillations about pairs of orthogonal body-fixed axes or space-fixed axes produce constant angular rates about the third orthogonal axis. Any failure by the gyros to indicate this type of motion when it exists or any erroneous indication that such motion is taking place produces a system attitude drift rate.

*These errors are not necessarily unique with strapdown systems. The kinematics of an "ideal" platform are the same as those of an "ideal" transformation computation. However, the magnitude and correlation between gyro errors is different for the two systems.

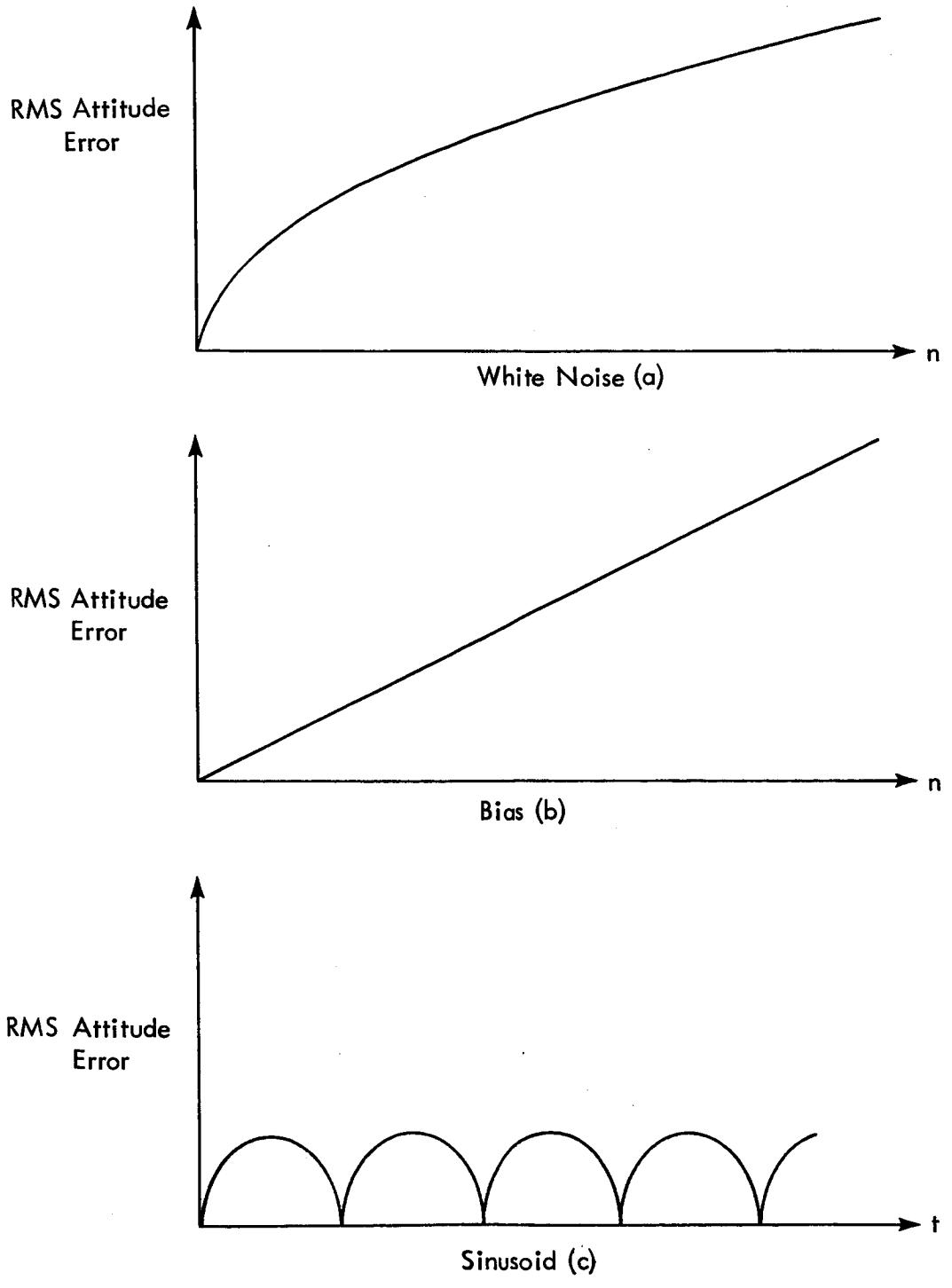

Figure D.2-1. Attitude Error Growth.

If we consider perfect implementation of the direction cosine matrix differential equation:

$$\dot{C} = C\Omega$$

and perfect vehicle angular rate indication by the gyros, no system attitude errors develop regardless of the vehicle motion. Strapdown system attitude errors arise from coning motion of the vehicle only if the differential equation for the transformation matrix is not implemented exactly (computer errors) or if the vehicle angular rates are not provided correctly (gyro errors). If vibratory vehicle motion exists and the gyros have unmatched phase lags attitude drift rate will occur (Ref. 9, Appendix G). If the phase lags are identical, the information is late in reaching the computer and the calculated direction cosine matrix lags behind the true transformation but no growing attitude error results. Quantization of rate information by a pulse restored gyro also provides a system attitude drift rate in the presence of coning motion.

Angular oscillations can occur about two body axes that generate a constant angular rate about the third axis and still cause the vehicle to return periodically to the same orientation. If the oscillations take place at a frequency above the gyro bandwidth only the constant rate will be sensed and the direction cosine matrix will indicate a growing change in orientation that constitutes a system attitude error. Consequently, if the oscillatory angular motion spectrum of the sensor package is significant at frequencies beyond the gyro bandwidth a potential system drift rate exists. The coning motion of the sensor package is therefore a consideration in designing gyro bandwidth.

Rectification of Oscillatory Gyro Errors and Body Motions – The retention of terms in Eq. (D.1-5) which describe vehicle motion illustrates the fact that the direction cosine calculations will rectify certain correlated

oscillatory gyro errors and body motions. The attitude drift rate results from a combination of true body motion and erroneously indicated body motion that appears as coning motion about two body fixed axes. This form of pseudo-coning is usually described as coming from gyro output axis angular acceleration errors because they have the necessary phase relative to oscillatory body motion. However, the computation rectification is more general and occurs for any gyro errors and body angular motions which are properly related. Section 3.3.2 of Ref. 19 shows that if the vehicle experiences an angular oscillation with amplitude a about one axis and if a false angular oscillation with amplitude b at the same frequency and having $\pi/2$ phase difference is indicated about another axis, a net system attitude error occurs about the third axis which causes the figure of merit to grow according to

$$p_n = \frac{a^2 b^2}{2} n^2$$

Equation (D.3-1) can be expressed in terms of a true angular rate oscillation with amplitude a' and an erroneous angular rate oscillation with amplitude b' as:

$$p(t) = \frac{(a')^2 (b')^2}{2\omega^2} t^2 \qquad \text{(D.3-2)}$$

where ω is the oscillation frequency. Using Eq. (D.3-2) to analyze output axis effect errors, a system attitude drift rate of 5.0 deg/hr is calculated for the parameters and environment presented in Section 2.5. While pseudo-coning errors due to in-phase oscillatory body motion and gyro errors can come from many sources, the output axis acceleration effect is clearly an important one.

Rectification of Oscillatory Gyro Errors – A pseudo-coning attitude drift rate can result from oscillatory gyro errors. To identify this effect in the difference equation for the figure-of-merit it is necessary to retain fourth order products of the error matrices and to evaluate triple summations.

Alternatively, pseudo-coning caused by oscillatory gyro errors can be easily demonstrated by considering the growth of the transformation error, ΔC, in the absence of vehicle angular motion. Taking C to be the identity matrix at all times and including two of the higher order terms from Eq. (D.1-3), we can write a difference equation for ΔC:

$$\Delta C_{n+1} = \Delta C_n \, (I + E_n) + E_n + \frac{(E_n)^2}{2} \qquad \text{(D.3-3)}$$

We postulate two out-of-phase oscillatory gyro error sequences such as those which can result from limit cycling of pulse rebalanced instruments:

$$e_z = 0, \; a, \; 0, \; -a, \; \ldots$$

$$e_y = b, \; 0, \; -b, \; 0, \; \ldots$$

The error matrices are a periodic sequence characterized by:

$$E_o = \begin{bmatrix} 0 & 0 & a \\ 0 & 0 & 0 \\ -a & 0 & 0 \end{bmatrix} \quad , \quad E_1 = \begin{bmatrix} 0 & -b & 0 \\ b & 0 & 0 \\ 0 & 0 & 0 \end{bmatrix}$$

$$E_2 = -E_o, \quad E_3 = -E_1, \quad E_4 = E_o, \text{ etc.}$$

Appendix C shows that the off-diagonal elements of ΔC represent the small misalignment angles φ_x, φ_y and φ_z

$$\Delta C \triangleq \begin{bmatrix} 0 & -\varphi_z & \varphi_y \\ \varphi_z & 0 & -\varphi_x \\ -\varphi_y & \varphi_x & 0 \end{bmatrix}$$

The gyro error sequence chosen provides an erroneous indication of out-of-phase oscillatory motion about two vehicle axes. The transformation computation cannot distinguish this from a similar true motion and should indicate a constant average angular rate about the third axis, x. Repeated substitution of the sequence of error matrices into Eq. (D.3-3) indicates an average growth in φ_x of ab every cycle, or:

$$\dot{\overline{\varphi}}_x = \frac{ab}{4T} \qquad \text{(D.3-4)}$$

It can be demonstrated that sinusoidal angular oscillations of the same frequency, ω, about two orthogonal body axes, with amplitudes a_1 and b_1, and having $\pi/2$ relative phase, produce an average angular rate about a third orthogonal axis given by

$$\text{actual coning rate} = \frac{a_1 b_1 \omega}{2} \qquad \text{(D.3-5)}$$

See Ref. 11, Appendix G. Taking a_1 and b_1 to be the first coefficients of the Fourier series expansions of e_y and e_z respectively.

$$a_1 = \frac{2b}{\pi}$$

$$b_1 = \frac{2a}{\pi}$$

and noting that (4T is the period)

$$\omega = \frac{2\pi}{4T}$$

this approximation to the coning rate is given by

$$\text{coning drift rate} \approx \frac{ab}{\pi T}$$

The difference between the pseudo-coning rate computed using Eq. (D.3-3) and the approximation above is small. The out-of-phase errors from two different gyros are combined in the direction cosine calculations to produce system attitude drift rate that approximates the coning rate given by Eq. (D.3-5).

It can be seen that the limit cycling nature of binary pulse rebalanced gyros can provide strapdown system errors through this mechanism. If oscillatory gyro output errors caused by limit cycles are permitted to enter the direction cosine matrix calculations, two gyros experiencing limit cycles with the same frequency and appropriate phase will generate a constant system drift rate. The size of this drift rate is explored in Section 4.2.

Gross Vehicle Rotation – All of the analysis in this appendix assumes a vehicle which does not change angular orientation. A modification of the results presented here to include the case of a rotating vehicle is given in Sections 3.4 and 3.5 of Ref. 19.

APPENDIX E

EFFECT OF SAMPLING ON REBALANCE LOOP MODING*

This appendix deals with the determination of limit cycle modes in sampled nonlinear rebalance loops, where the limit cycles tested have periods which are whole multiples of the sampling period. These are not the only limit cycles which may be possible in such systems, but experience with both real and simulated systems has shown them to be by far the most commonly-occuring modes.

The configuration of the system is shown in Fig. E-1. The binary element is shown as having possible hysteresis for reasons discussed in Section 2.4. A zero order hold is considered to follow the sampling switch. The linear part may include any number of continuous and discrete linear elements, and torquer dynamics can be assumed lumped in the linear part.

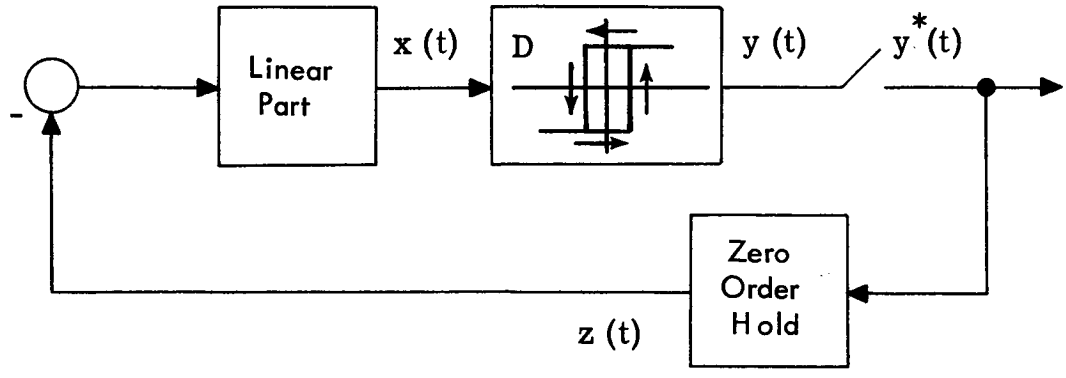

Figure E-1. Two-Level Relay Rebalance Loop Configuration

*The material in this Appendix follows Ref. 3, Section 9.1.

The Describing Function

One has free choice in deciding how much of the system to characterize with a describing function – so long as the nonlinear part is included. The analysis of this system is most like the analysis of continuous systems considered heretofore if one chooses to represent the effect of the nonlinearity, the sampling switch, and the zero order hold by a describing function. To this end, $x(t)$ is taken to be a sinusoid, unbiased to begin with, and the fundamental harmonic component of $z(t)$ is calculated. The frequencies we shall consider are whole fractions of the sampling frequency, $\omega_s = 2\pi/T$. Moreover, we shall center attention on the even fractions – 1/2, 1/4, 1/6, . . . – since these are the limit cycle modes one might expect to see in the present case where the linear part of the system includes a pole at the origin – an integration. As a result, $z(t)$ must be an unbiased function in any steady-state limit cycle with no input to the system. The drive signal into the linear part will then consist of a periodic cycle which includes an equal number of sampling periods of plus and minus drive. The only arrangement of these periods of plus and minus drive which is consistent with the sinusoid assumed as the input to the nonlinearity is n positive drive periods followed by n negative drive periods in the case of a cycle with period 2nT, where T is the sampling period. Such a cycle will be termed an n, n mode.

The input and output waveforms for the 2, 2 mode are shown in Fig. E-2. $x(t)$ is a sinusoid with period 4T and $z(t)$ is a square wave with that period. The output of the hold, $z(t)$, is shown lagging the output of the nonlinearity, $y(t)$, due to the fact that $y(t)$ is not in phase with the sampling points. The lag between the zero crossing of $y(t)$ and the next sampling point is not known a priori; it can take any value between 0 and T in time or 0 and π/n in phase angle. The amplitude of the fundamental harmonic of $z(t)$ is $(4/\pi)D$ and the phase lag of that component relative to $x(t)$ is $\sin^{-1} \delta/A + \varphi$ where φ is the sampling lag. The describing function for the chain of elements: nonlinearity, sampling switch, and hold, is then

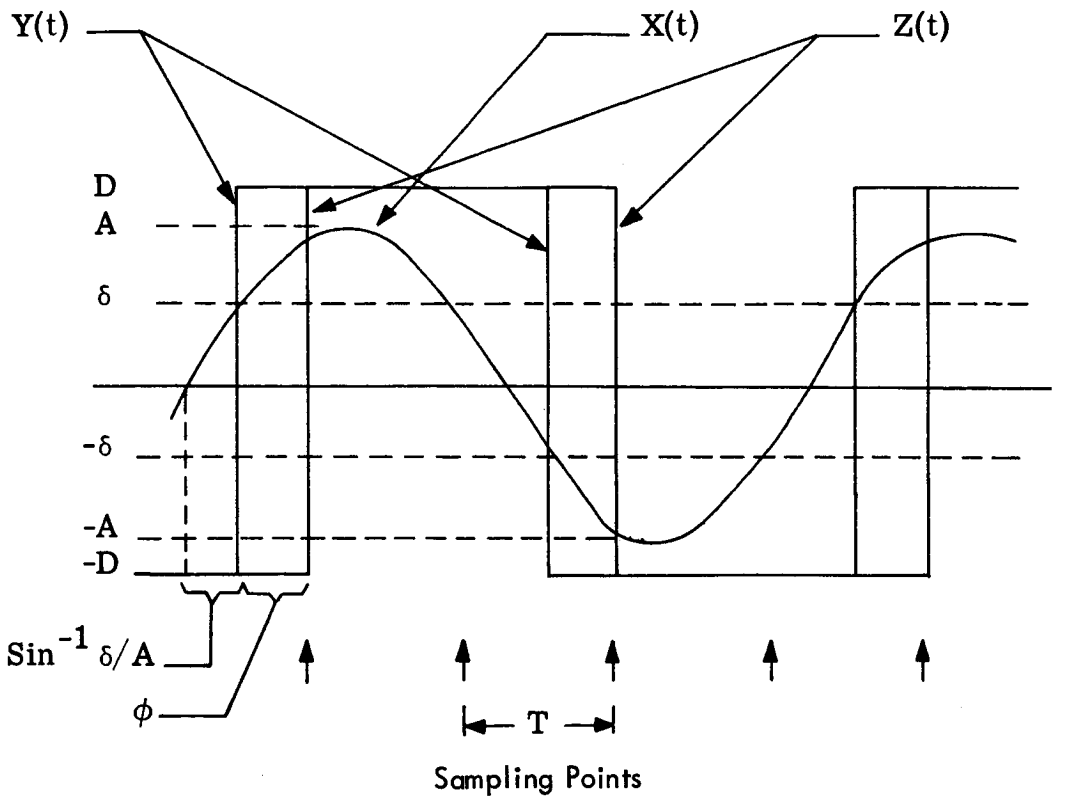

Figure E-2. Signal Waveforms for the 2,2 Mode

$$N(A, \varphi) = \frac{4D}{\pi A} \underline{/-\sin^{-1} \delta/A - \varphi} \qquad (0 < \varphi < \pi/n) \qquad (A > \delta) \qquad \text{(E-1)}$$

This expression holds for an n, n mode of any order.

The Linear Part

The remainder of the system, the linear part as shown in Fig. E-1, is characterized by its steady-state sinusoidal response at the frequency $(1/2n)\omega_s$. Since this is a continuous linear operator, the only requirement for applicability of describing function theory is that it attenuate the higher harmonics of z(t) sufficiently to return essentially the fundamental sinusoid to x(t).

Determination of Modes

Having a describing function, $N(A, \varphi)$, to characterize the nonlinear part, sampler, and hold, and a steady-state sinusoidal response function, $H(j\omega)$, to characterize the remaining linear part, the condition for the possible existence of a limit cycle mode is as always

$$1 + N(A, \varphi)\, H(j\omega) = 0 \qquad \text{(E-2)}$$

The gain-phase plot is a convenient means of displaying the solutions to this equation. Although only the frequencies $(1/2n)\,\omega_s$ are of interest, it is often useful – especially for the design of compensation – to plot the complete $H(j\omega)$ function. A typical curve is shown in Fig. E-3. Solutions of Eq. (E-2) are represented by intersections of this curve of $H(j\omega)$ with $-1/N(A, \varphi)$. $N(A, \varphi)$ in this case is defined only for the discrete set of frequencies $(1/2n)\omega_s$, and it depends both on A and n, the order of the mode. It is convenient to separate that part of N which depends only on A from that which depends on n for simplicity in plotting the function. Thus define

$$N'(A) = \frac{4D}{\pi A} \underline{/-\sin^{-1} \delta/A} \qquad \text{(E-3)}$$

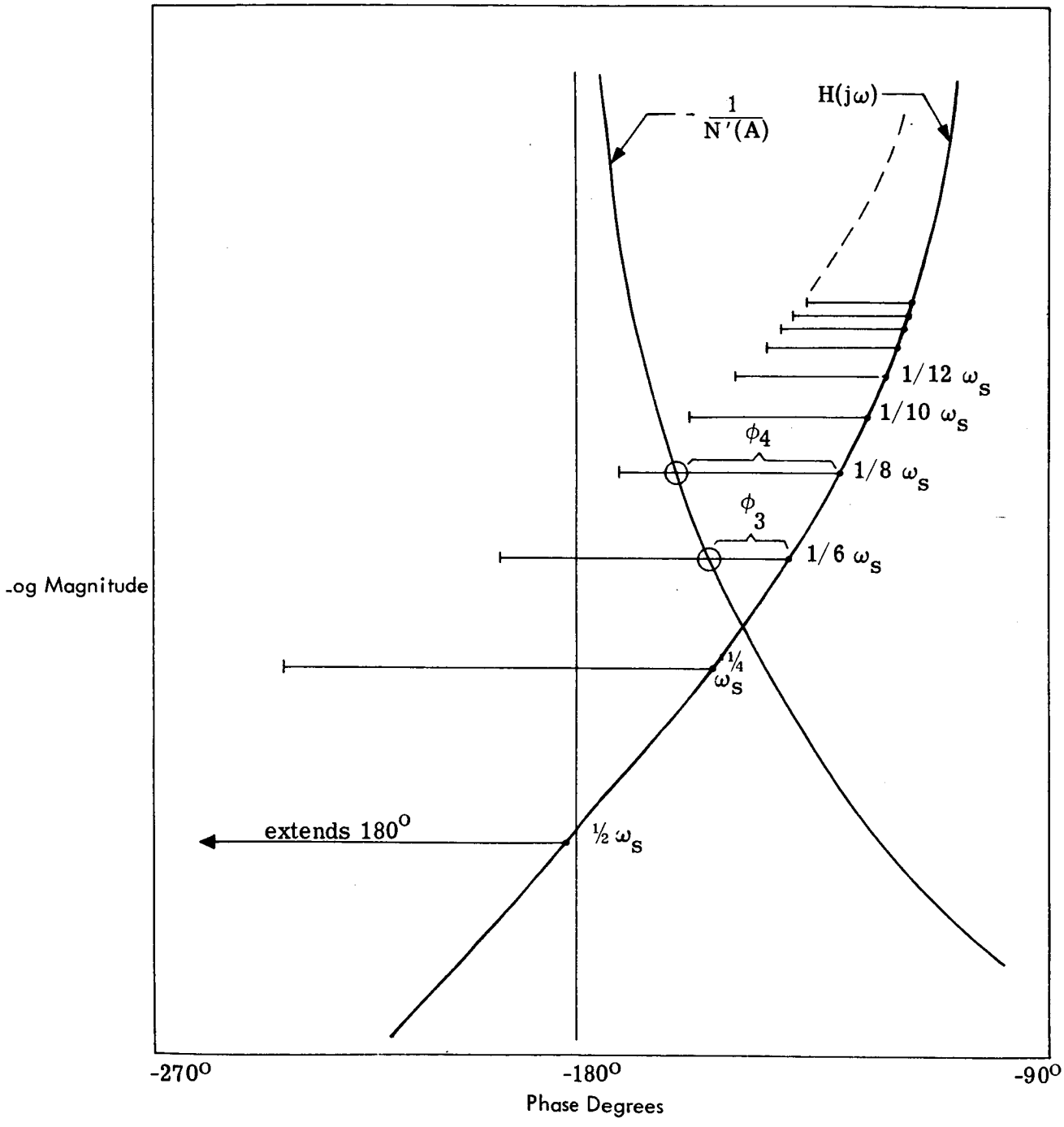

Figure E-3. Gain-Phase Plot for Sampled Rebalance Loop

which is the describing function given in Eq. (E-1) except for the sampling lag φ. This φ may take any value in the range $(0, \pi/n)$, and since this range depends on n – and thus ω – the bands of possible sampling lags can conveniently be shown as lines originating at the point of $H(j\omega)$ for each frequency and extending a distance corresponding to π/n. With the sampling lag accounted for separately in this manner, the describing function which is plotted, $-1/N'(A)$, is nothing more than the describing function for the two-level relay with hysteresis as it appears in continuous systems.

The completed plot, Fig. E-3, indicates all possible limit cycle modes. For the case shown, the only intersections of $H(j\omega)$ plus the sampling lag with $-1/N'(A)$ occur at the frequencies $1/6\ \omega_s$ and $1/8\ \omega_s$. Thus only the 3, 3 and 4, 4 modes are possible in this case. The higher frequency modes are not possible because the nonlinearity and linear part have too much phase lag even if the sampling action contributes none, and the lower frequency modes are not possible because even with the maximum possible sampling delay, the sinusoidal signal does not accumulate 360 degrees of phase lag around the loop. The intersections indicating the possible modes are circled in the figure. The frequency of each mode is indicated on the scale of $H(j\omega)$ at that point, the amplitude of each mode at the input to the nonlinearity is indicated on the scale of $-1/N'(A)$ at that point, and the phase lag due to the sampling delay in each mode is indicated by the phase difference between $H(j\omega)$ and $-1/N'(A)$ at those points.

Notice that for frequencies much smaller than the sampling frequency, the possible limit cycle frequencies become closely spaced and the maximum sampling lag is small. In this "low" frequency region the sampling has little effect on the behavior of the system. Hence the neglect of the sampling process in Section 2.4.

When more than one limit cycle mode is possible, the limit cycle which will be observed depends on the prior history of the system variables. If the modes are stable there is some region of initial conditions from which the system will settle into each mode. These regions are often much smaller for some

modes than for others. In any case, a system must be designed so all possible modes are acceptable. If one or more indicated modes are not acceptable, usually because the amplitude at some point in the system is too large, these modes must be eliminated by compensation.

Design of Compensation

In most instances the compensation required to improve those performance characteristics which can be evaluated by the use of describing functions is quite evident. So it is in this instance. If the 4, 4 mode as indicated on Fig. E-3 has an unacceptably large amplitude, it can be eliminated by providing at least $(45 - \varphi_4)$ degrees of phase lead at the frequency $1/8\ \omega_s$ somewhere around the loop. After such compensation, the 3,3 mode will still be possible, and in all likelihood one or both of the higher frequency modes as well. If the 3, 3 mode is to be eliminated also, the compensation is designed to provide at least $(60 - \varphi_3)$ degrees of lead at $1/6\ \omega_s$. The amplitudes of the remaining possible modes at various stations around the loop will differ with the location of the compensation, and this can be evaluated using just steady-state frequency response characteristics. The linear compensation can be implemented with either a continuous or discrete compensator.

Note that, in the absence of hysteresis, $\delta = 0$, and the curve of $-1/N'(A)$ extends along the entire phase = -180° line. Thus, the moding which occurs in this case is readily apparent from Fig. E-3. Discussion of compensation follows as above.

APPENDIX F

ANGULAR COMPLIANCE EFFECTS ON LIMIT CYCLES IN PULSE TORQUED GYROS

The use of a second order differential equation to describe the dynamic relation between float angle and applied torque in a single-degree-of-freedom gyro permits simple calculation of limit cycle characteristics. The effects considered in this dynamic model of the gyro float are only those of lumped rotor and gimbal inertia and linear fluid damping. Because the limit cycle float motion can be of high frequency it is desirable to investigate the possible effect of angular compliance between the rotor and gimbal. Angular flexure can generate sizeable error torques about the float output axis by coupling with the spin angular momentum. Consequently, the potential exists for significant modification of the torque-to-float angle transfer function used in determining gyro limit cycles.

Figure F-1 illustrates the effects essential for considering rotor-to-gimbal compliance. The rotor is connected to the gimbal along the gyro input (IA) and output (OA) axes by structural members with stiffness k_1 and k_2 respectively. No structural damping will be considered. Angular rotations of the rotor and gimbal with respect to an inertially fixed reference frame are represented as A_r and A_g with the appropriate subscript to show axis of rotation.

Summing moments on the rotor about the gyro input axis:

$$I_{ii_r} \ddot{A}_{r_i} = - k_1 (A_{r_i} - A_{g_i}) - H\dot{A}_{r_o} \qquad (F-1)$$

Summing moments about the gyro output axis:

$$I_{oo_r} \ddot{A}_{r_o} = -k_2 (A_{r_o} - A_{g_o}) + H\dot{A}_{r_i} \qquad \text{(F-2)}$$

Assuming that the gyro case and gimbal form an essentially rigid structure about the gyro input axis, A_{g_i} can be represented in Laplace Transform notation as the integral of the angular rate of the gyro about its input axis, ω_i:

$$A_{g_i} = \frac{\omega_i}{s} \qquad \text{(F-3)}$$

Similarly, A_{g_o} can be represented in terms of the angular rate about the output axis and the angle between the gyro case and gimbal, α_o:

$$A_{g_o} = \frac{\omega_o}{s} + \alpha_o \qquad \text{(F-4)}$$

Assuming equal rotor inertias and stiffness about the input and output axes, Eqs. (F-1) and (F-2) can be written in terms of the Laplace Transform operator, s, as a vector-matrix equation:

$$\begin{bmatrix} I_r s^2 + k & Hs \\ -Hs & I_r s^2 + k \end{bmatrix} \begin{bmatrix} A_{r_i} \\ A_{r_o} \end{bmatrix} = \begin{bmatrix} \frac{k}{s} \omega_i \\ k A_{g_o} \end{bmatrix} \qquad \text{(F-5)}$$

The rotor exerts a moment on the gimbal about the latter's output axis according to

$$\begin{matrix} \text{rotor moment} \\ \text{on gimbal} \end{matrix} = k (A_{r_o} - A_{g_o})$$

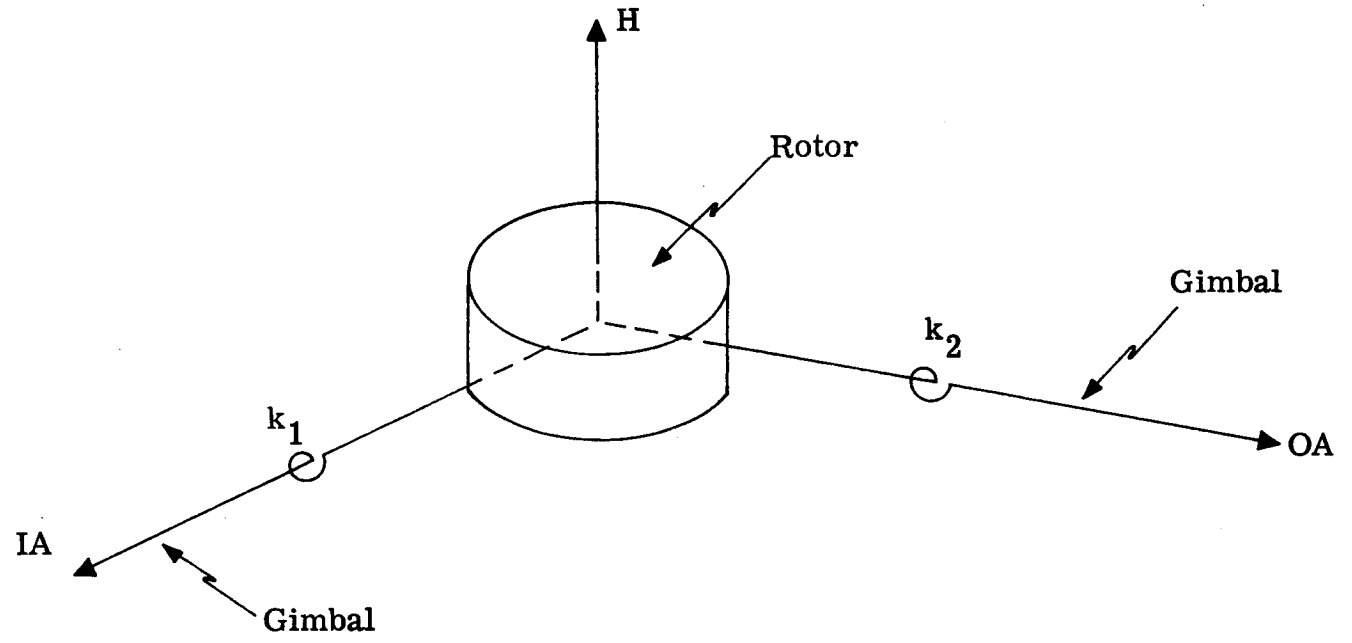

Figure F-1 Rotor-to-Gimbal Compliance

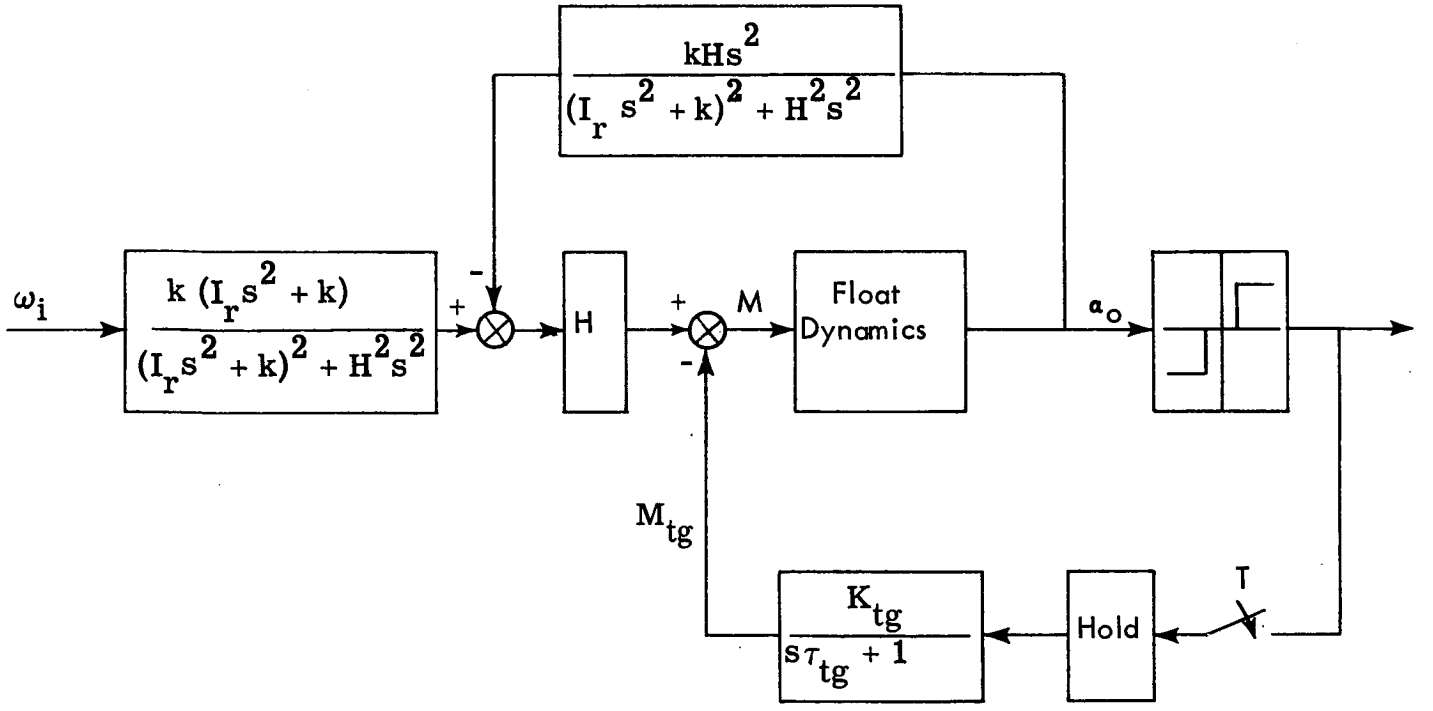

Figure F-2 Signal Flow D iagram Including Compliance Effects

Using Eq. (F-5)

$$\text{rotor moment on gimbal} = \frac{k^2 H \omega_i}{(Is^2 + k)^2 + H^2 s^2} - \frac{ks^2 (I^2 s^2 + kI + H^2) A_{g_o}}{(Is^2 + k)^2 + H^2 s^2} \qquad (F-6)$$

For limit cycle analysis only quantities which are state variables in the closed nonlinear loop are considered. Only the second term in Eq. (F-6) is of interest and the variable A_{g_o} is represented by its component, α_o. A signal flow diagram of the pulse torqued gyro including compliance effects is shown in Fig. F-2. The torque generator is represented as a first order lag with time constant τ_{tg}. In order to determine limit cycle characteristics it is necessary to obtain the linear transfer function relating α_o to the torque generator output, M_{tg}. This is determined from the closed loop transfer function of the linear feedback loop shown in Fig. F-3, where the float dynamics are represented according to

$$\text{float dynamics} = \frac{1/I_{oo_g}}{s(s + 1/\tau_f)}$$

$$\tau_f = \frac{I_{oo_g}}{C}$$

Defining:

$$\omega_g \triangleq \frac{H}{I_r}$$

$$\omega_n^2 \triangleq \frac{k}{I_r} \qquad (F-7)$$

the transfer function for the loop shown in Fig. F-3 is

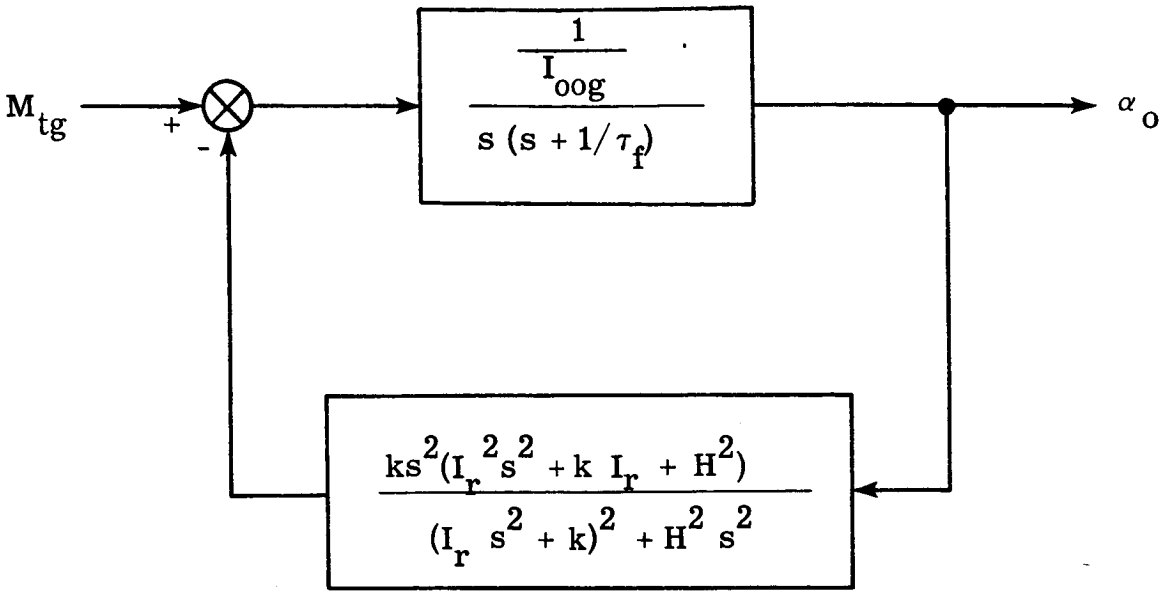

Figure F-3 Transfer Loop Between Torque Generator Output and Float Angle

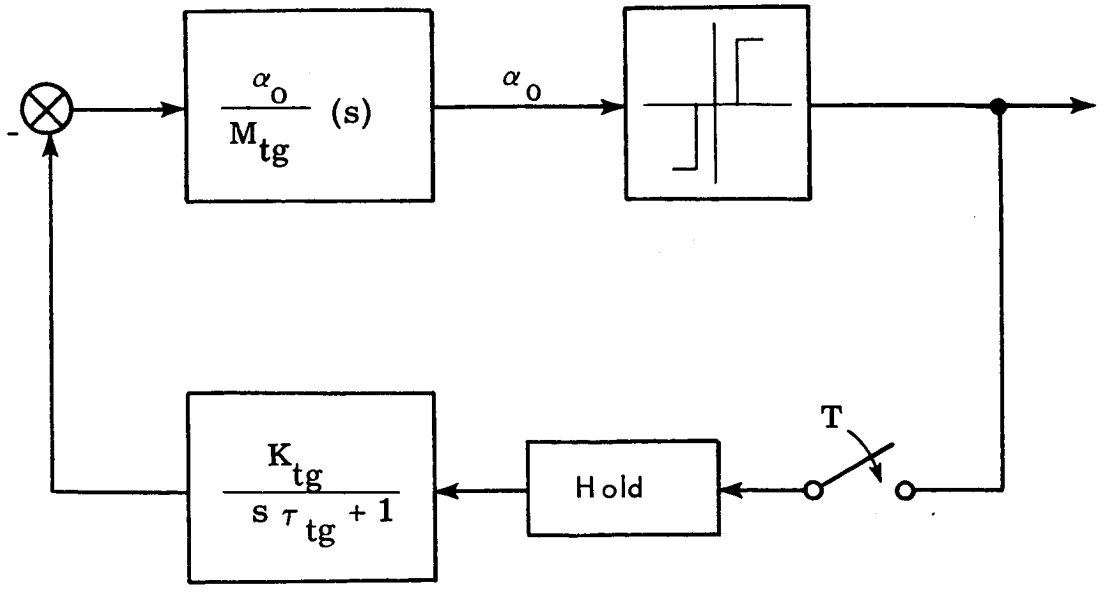

Figure F-4 Loop for Limit Cycle Analysis When Angular Compliance is Considered

$$\frac{\alpha_o}{M_{t_g}}(s) = \frac{s^4 + (2\omega_n^2 + \omega_g^2)s^2 + \omega_n^4}{\left\{ I_{oo_g} s^5 + \frac{I_{oo_g}}{\tau_f} s^4 + \left[I_{oo_g}(2\omega_n^2 + \omega_g^2) + k \right] s^3 + \frac{I_{oo_g}}{\tau_f}(2\omega_n^2 + \omega_g^2)s^2 + \left[\omega_n^4 I_{oo_g} + k\omega_n^2 + k\omega_g^2 \right] s + \frac{I_{oo_g}}{\tau_f}\omega_n^4 \right\}} \quad \text{(F-8)}$$

The nonlinear loop which provides the basis for determining the gyro limit cycle when angular compliance effects are considered is shown in Fig. F-4. A rectangular gain-phase plot for the linear portion of this loop is given in Fig. F-5. The characteristics shown are for the gyro parameters presented in Section 2.5 with $C = 8 \times 10^5$ dyne-cm-sec, $\tau_{tg} = 50$ μsec and a compliance natural frequency of 400 Hz. For comparison the gain-phase relation that results when compliance effects are ignored is also plotted in Fig. F-5. For the pulse torqued gyro the quantity $-1/N_A$ lies entirely on the -180 deg phase line. The two gain-phase characteristics (with and without compliance) are identical in the high and low frequency ranges but the consideration of compliance results in a more complex behavior in the midfrequency range. The dashed gain-phase line crosses the $-1/N_A$ line at three points where the solid (no compliance) line crosses only once. It is evident that in any detailed determination of a gyro limit cycle, compliance effects must be considered.

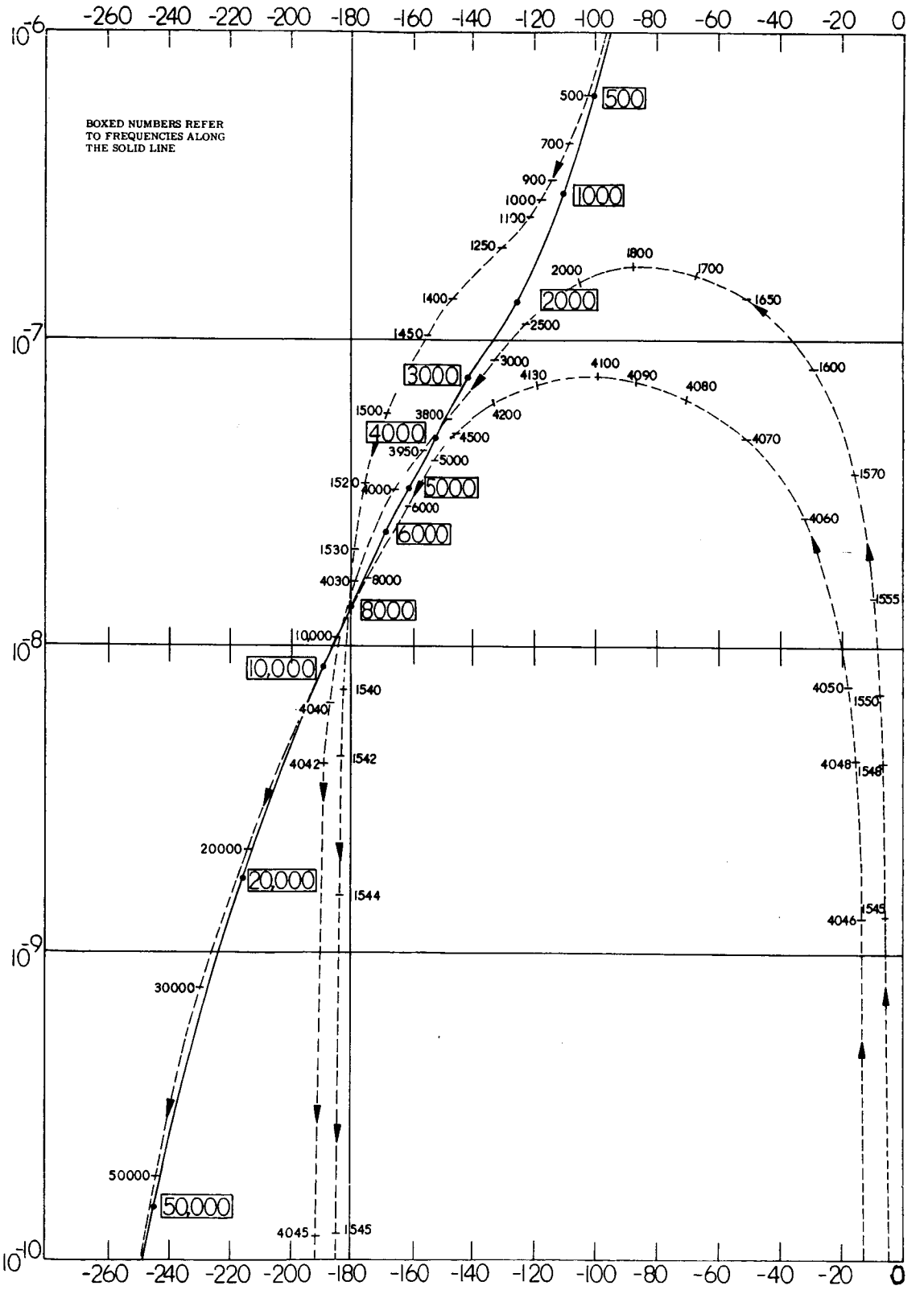

Figure F-5 Gain-Phase Plot Showing Compliance Effects.

APPENDIX G

THE EFFECT OF CORRELATION PERIOD T′ ON SYSTEM ATTITUDE ERROR GROWTH

Calculation of the mean square change in system attitude error over one correlation period, T′, which results from integration of individual gyro errors follows from:

$$\delta(i) = \int_{t_i}^{t_i+T'} \dot{\delta}(i, \tau)\, d\tau$$

$$\overline{\left[\delta(i)\right]^2} = \int_{t_i}^{t_i+T'} d\tau_1 \int_{t_i}^{t_i+T'} d\tau_2\, \overline{\dot{\delta}(i, \tau_1)\, \dot{\delta}(i, \tau_2)} \qquad \text{(G-1)}$$

Noting that, for stationary functions $\dot{\delta}$:

$$\overline{\dot{\delta}(i, \tau_1)\, \dot{\delta}(i, \tau_2)} = \varphi_{\dot{\delta}\dot{\delta}}(\tau_2 - \tau_1)$$

and making the change of variable

$$\tau_3 = \tau_2 - \tau_1$$

Eq. (G-1) can be written as

$$\overline{\delta^2} = \int_{t_i}^{t_i+T'} d\tau_1 \int_{t_i-\tau_1}^{t_i+T'-\tau_1} d\tau_3 \, \varphi_{\dot{\delta}\dot{\delta}}(\tau_3) \qquad \text{(G-2)}$$

The area of integration is illustrated in Fig. G-1.

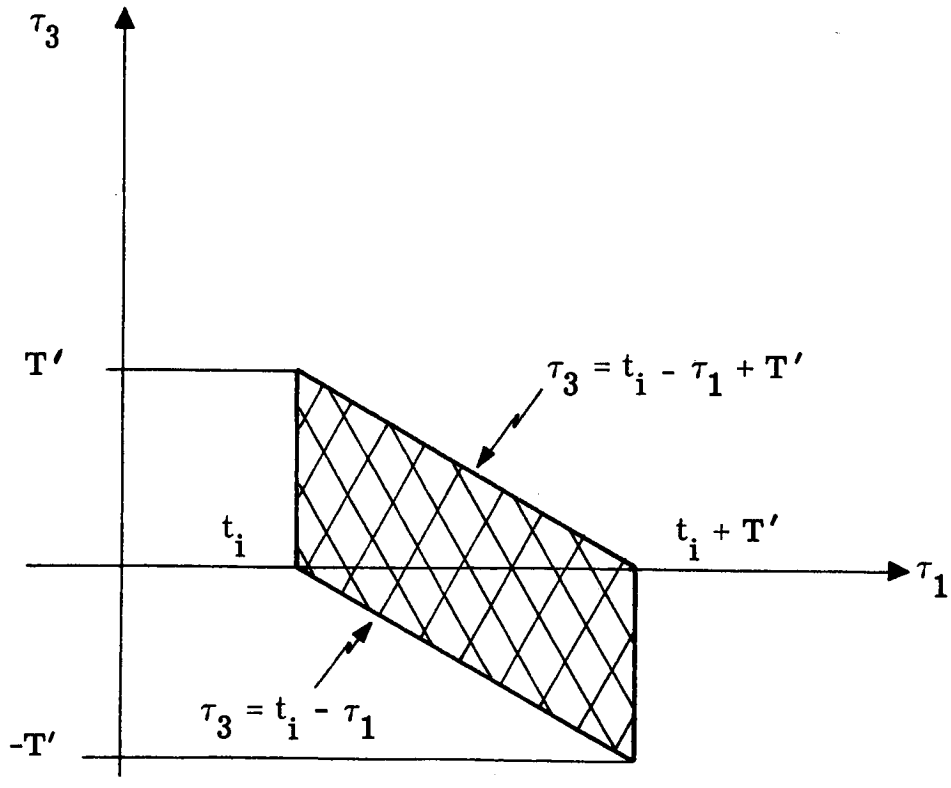

Figure G-1. Area of Integration

Integration can occur over the two triangles separately:

$$\overline{\delta^2} = \int_0^{T'} d\tau_3 \int_{t_i}^{t_i+T'-\tau_3} d\tau_1 \, \varphi_{\dot{\delta}\dot{\delta}}(\tau_3)$$

$$+ \int_{-T'}^{0} d\tau_3 \int_{t_i-\tau_3}^{t_i+T'} d\tau_1 \, \varphi_{\dot{\delta}\dot{\delta}}(\tau_3)$$

$$= 2 \int_0^{T'} d\rho \, (T' - \rho) \, \varphi_{\dot{\delta}\dot{\delta}}(\rho) \qquad \text{(G-3)}$$

We assume the spectral density of the random angular motion vector ω is constant out to the vicinity of a frequency ν_c and decreases rapidly thereafter. In addition, the gyro is presumed to have a bandwidth in excess of ν_c (in order to prevent vehicle coning motion from going undetected).

Consequently, in the example of spin-input crosscoupling cited in Section 5.1, the error rate $\dot{\delta}(i)$ is given by

$$\dot{\delta}(i, t) = K_1(i) \, K_2 \, \omega^2(t) \qquad \text{(G-4)}$$

If both $K_1(i)$ and $\omega(t)$ are stationary, independent zero mean random quantities and K_2 is constant:

$$\varphi_{\dot{\delta}\dot{\delta}}(\tau) = \overline{\dot{\delta}(i, t) \, \dot{\delta}(i, t+\tau)}$$

$$= \overline{K_1^2} \, K_2^2 \, \varphi_{\omega^2\omega^2}(\tau) \qquad \text{(G-5)}$$

If ω is assumed to have a Gaussian amplitude distribution, $\varphi_{\omega^2\omega^2}(\tau)$ can be expressed in terms of the autocorrelation function and mean square value of ω (see p. 94 of Ref. 13):

$$\varphi_{\omega^2\omega^2}(\tau) = \sigma_\omega^4 + 2\left[\varphi_{\omega\omega}(\tau)\right]^2 \qquad \text{(G-6)}$$

From the earlier description of the spectral density function of $\omega(t)$, $\varphi_{\omega\omega}(\tau)$ can be expressed in terms of ν_c:

$$\varphi_{\omega\omega}(\tau) \cong \sigma_\omega^2 \, e^{-\nu_c|\tau|} \qquad \text{(G-7)}$$

Combining Eqs. (G-3), (G-5), (G-6) and (G-7) and integrating, the mean square value of δ is found to be:

$$\overline{\delta^2} = \overline{K^2}\,\sigma_w^4\left[(T')^2 + \frac{2T'}{\nu_c} + \frac{e^{-2\nu_c T'} - 1}{(\nu_c)^2}\right] \qquad \text{(G-8)}$$

A few calculations reveal that, for the practical range of ν_c, the first term in Eq. (G-8) dominates if

$$\nu_c T' \geq 40 \qquad \text{(G-9)}$$

The boundary expressed by Eq. (G-9) is a hyperbola in the first quadrant of the ν_c, T' plane as illustrated in Fig. G-2. When this condition is satisfied the attitude error growth due to integration of individual gyro errors is essentially the same as that computed using Eq. (5.1-1).

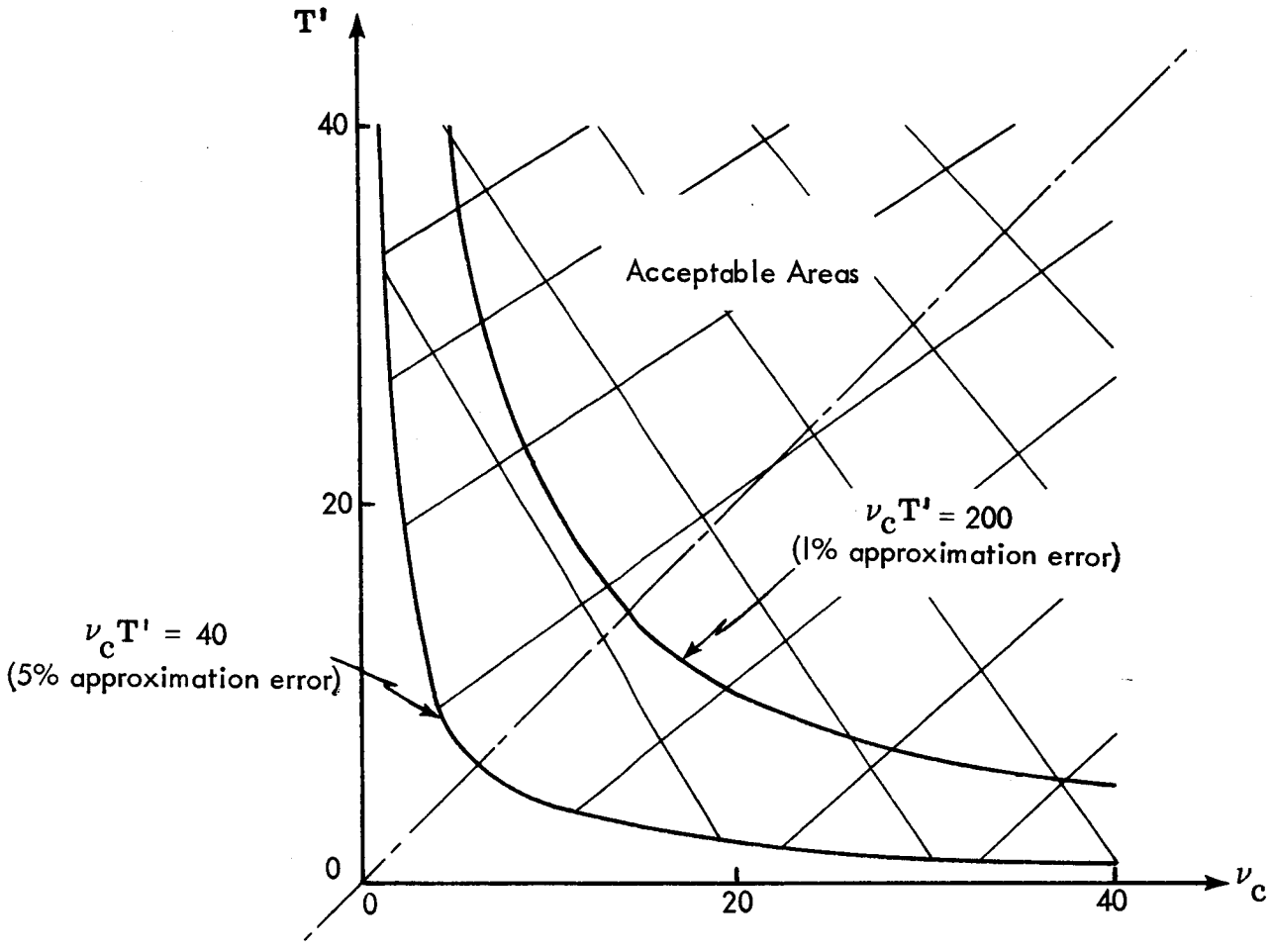

Figure G-2 Approximation Accuracy Limits